

THE UNIVERSITY OF HULL
FACULTY OF SCIENCE AND ENGINEERING
SCHOOL OF ENGINEERING

PhD Thesis

Atuman Samaila Joel

**STUDY OF PROCESS INTENSIFICATION FOR
POST-COMBUSTION CARBON CAPTURE BASED
ON CHEMICAL ABSORPTION THROUGH
MODELLING AND SIMULATION**

Supervisor: Prof Meihong Wang

April, 2016

This thesis is submitted in fulfilment of the requirements for a Doctor
of Philosophy (PhD) degree in Engineering

© University of Hull, 2016. All rights reserved. No part of this publication may
be reproduced without the a written permission of the copyright holder

The candidate confirms that the work submitted is his own, except where work which has formed part of jointly-authored publications has been included. The contribution of the candidate and the other authors to this work has been indicated below. The candidate confirms that appropriate credit has been given within the thesis where reference has been made to the work of others.

Part of the work in Chapters 1 and 2 of the thesis has appeared in publication as follows:

M. Wang, A. S. Joel, C. Ramshaw, D. Eimer, N. M. Musa, Process intensification for post-combustion CO₂ capture with chemical absorption: A critical review. Applied Energy 158(2015), 275-91

C. Ramshaw, D. Eimer and N. M. Musa contributions in the publication are not included in the thesis. M. Wang is my supervisor who acted in an advisory role, gave suggestions regarding the research direction and commented on the work.

The work in Chapter 4 of the thesis has appeared in publication as follows:

A. S. Joel, M. Wang, C. Ramshaw, E. Oko, Process analysis of intensified absorber for post-combustion CO₂ capture through modelling and simulation. International Journal of Greenhouse Gas Control 21(2014), 91–100.

A. S. Joel, M. Wang, C. Ramshaw, Modelling and simulation of intensified absorber for post-combustion CO₂ capture using different mass transfer correlations. Applied Thermal Engineering 74(2015), 47-53

M. Wang is my supervisors who acted in an advisory role, gave suggestions regarding the research direction and analysis methods and commented on the work. Contributions from C. Ramshaw and E. Oko in the publication are not included in the thesis.

The work in Chapter 5 of the thesis has appeared in publication as follows:

A. S. Joel, M. Wang, C. Ramshaw, Modelling and Simulation of Intensified Regenerator for Post-combustion CO₂ Capture based on Chemical Absorption. Applied Energy (2016) under review

M. Wang is my supervisor who acted in an advisory role, gave suggestions regarding the research direction and analysis methods and commented on the work.

This copy has been supplied on the understanding that it is copyright material and that no quotation from the thesis may be published without proper acknowledgement.

The right of Atuman Samaila JOEL to be identified as Author of this work has been asserted by him in accordance with the Copyright, Designs and Patents Act 1988.

Abstract

There have been a lot of questions on impact of greenhouse gas on changes in climate conditions regarding expected future dangers if mitigation measures are not put in place. Carbon dioxide emission from power sector is a major contributor of greenhouse gases. As a result, the sector is key target for deploying carbon abatement technologies such as carbon capture. Post-combustion capture (PCC) based on chemical absorption technology is one of the major capture approaches and the most matured of them. However, it is beset by some challenges such as high capital and operating costs due to required large sizes of packed columns and high solvent re-circulating rate. Through process intensification (PI) technology, the columns could be downsized by an order of magnitude without compromising their processing capacity. However, there have been limited studies on the techno-economics of PI-based technologies.

In this study, steady state models for standalone intensified absorber and stripper based on rotating packed bed (RPB) technology were developed and validated with experimental data from Newcastle University UK and Tsing Hua University Taiwan respectively. The models were developed in Aspen Plus® and dynamically linked with visual Fortran subroutines. Therefore, this is same as newly developed RPB models (i.e. absorber and stripper). To obtain more insights into the design and operation of standalone intensified absorber, standalone intensified stripper and close loop intensified PCC process, process analysis was carried out. Process analysis in standalone intensified absorber indicates that: (a) CO₂ capture level increases with increase in rotating speed. (b) Higher lean MEA inlet temperature leads to higher CO₂ capture level. (c) Increase in lean MEA concentration results in increase in CO₂ capture level. (d) Temperature bulge is not present in intensified absorber. (e) With fixed RPB equipment size and fixed Lean MEA flow rate, CO₂ capture level decreases with increase in flue gas flow rate. (f) At higher flue gas temperature (from 30 °C to 80 °C), the CO₂ capture level of the intensified absorber can be maintained. For standalone intensified stripper, the impact of rotor speed on the regeneration efficiency and energy were studied, the impact of reboiler temperature on the rate of CO₂ stripping was established and the impact of rich-MEA flow rate on regeneration energy and efficiency was determined.

From comparative assessment of conventional packed bed and RPB, it was found that a volume reduction factor of 12 and 10 times is possible for the absorber and stripper respectively.

The two validated models, together with model for heat exchanger were then linked together to form a closed loop intensified PCC process. Steady state model of the closed loop intensified PCC process was then used to perform process analysis on (i) the impact of liquid to gas (L/G) ratio on regeneration energy and CO₂ capture level, (ii) the impact of lean-MEA loading on regeneration energy and capture level (iii) capital and operating cost estimation for intensified PCC process were done, which shows a reduction in an investment cost compared to conventional PCC process.

The findings in this study showed that capital and operating costs can be reduced owing to its smaller size compared to conventional PCC process. Also cooling cost for flue gas and inter-cooling in the absorber can be saved since the RPB absorber can be operated at slightly elevated temperature of up to 80 °C without compromising the absorber performance and also since higher lean-MEA temperature and/or higher flue gas temperature shows little or no effect on the performance of the RPB. The newly proposed intensified PCC process PFD in the recommendation section of this thesis if successfully implemented can reduce operating and capital costs of PCC process. Finally, these insights can be useful for the design and operation of intensified PCC process.

Keywords: Process Intensification, Process Modelling and Simulation, Rotating Packed Bed, Post-combustion Carbon Capture, Chemical Absorption

Acknowledgements

My most profound gratitude goes to my supervisor Prof Meihong Wang for his constructive criticism in fine tuning the quality of this research work. Prof Meihong is more than just supervisor to me, He has been like a father that advises me on how to improve in the whole aspect of life outside PhD. Dr Ming Hou and Dr Chunfei Wu efforts in chairing my TAP meetings and their contributions and advice on how to improve my research quality is much appreciated. Useful discussion with Professor Chen Jian at Tsinghua University China is much appreciated. I would also want to appreciate the Admin staffs of the University of Hull whom in most cases are there for me it couldn't have been easy without their contributions. I couldn't find an appropriate word to express my gratitude to the University of Hull for the award of international fee waiver to perform this research. I also appreciate Natural Environment Research Council (NERC Reference: NE/H013865/2) for my maintenance grant and EU Marie Curie (FP7-PEOPLE-2013-IRSES) for funding my exchange programme at Tsinghua University, China and also completing remaining part of my maintenance grant. My employer in Nigeria, Abubakar Tafawa Balewa University Bauchi, I am most grateful for granting me study fellowship to undertake this research.

The Process and Energy System Engineering group staff, students and all my friends in Hull, you are such a big family I had the opportunity to work with. The jokes and encouragement from you guys is much appreciated.

To my beloved wife Mrs Briska Atuman and my son David your love for me has no bound, thank you for the excellent support shown. Keeping you people awake in the late hour and also not always giving you the attention you deserved, thank you for understanding with me even when I am tense with target that I have to meet. To my parents you are the inspiration of whatever I achieved in life, thank you for the good upbringing. To my brothers and sisters, I remain utterly appreciative for your support and love throughout the period of my study. I will not forget to mention the love and care from my In-laws, Mum thank you for the visit and taking care of our new born baby (David). Finally, I remain eternally grateful to God Almighty who gave me life, ability and good health to complete this research study.

Publications

Journal Papers

- [1] **A. S. Joel**, M. Wang, C. Ramshaw, E. Oko, Process analysis of intensified absorber for post-combustion CO₂ capture through modelling and simulation. *International Journal of Greenhouse Gas Control* 21(2014), 91–100.
- [2] **A. S. Joel**, M. Wang, C. Ramshaw, Modelling and simulation of intensified absorber for post-combustion CO₂ capture using different mass transfer correlations. *Applied Thermal Engineering* 74(2015), 47-53.
- [3] M. Wang, **A. S. Joel**, C. Ramshaw, D. Eimer, N. M. Musa, Process intensification for post-combustion CO₂ capture with chemical absorption: A critical review. *Applied Energy* 158(2015), 275-91
- [4] **A. S. Joel**, M. Wang, C. Ramshaw, Modelling and Simulation of Intensified Regenerator for Post-combustion CO₂ Capture based on Chemical Absorption. *Applied Energy* (2016) under review
- [5] E. Oko, M. Wang, **A. S. Joel**, C. Ramshaw, Review of current status of post-combustion CO₂ capture process based on chemical absorption. *International Journal of Coal Science and Technology* (2016) under review

Book Chapter

A. S. Joel, E. Oko, M. Wang, C. Ramshaw, J. G.M. Lee, K. WU, D. Kim, N. Shah, L. Ma, M. Pourkashanian, Application of rotating packed bed technology for intensified post-combustion CO₂ capture based on chemical absorption. In *Water-Food-Energy Nexus: Processes, Technologies and Challenges*, accepted for publication in Taylors and Francis Publishers

Conference Papers

- [1] **A. S. Joel**, M. Wang, C. Ramshaw, Analysis of intensified absorber operation for post-combustion CO₂ capture through modelling and simulation. *6th International Conference on Clean Coal Technologies, Thessaloniki Greece 12-16th May, 2013.*
- [2] **A. S. Joel**, M. Wang, Modelling and simulation of intensified regenerator for post-combustion CO₂ capture. *10th European Conference on Coal Research and its Applications, Hull UK. 15th-17th September 2014*
<http://www.coalresearchforum.org/eccria2014/Sessions%201A%20to%203A/3A2%20Joel%20Atuman.pdf>

Presentation

A. S. Joel, M. Wang, C. Ramshaw Process analysis of intensified absorber for CO₂ capture through modelling and simulation. *21st Process Intensification and Network (PIN) meeting in Newcastle University held on 23rd May, 2013.* <http://www.pinetwork.org/pubs/PIN21/joel.pdf>

Table of Contents

Abstract	iii
Acknowledgements	v
Publications	vi
Table of Contents	vii
List of Figures	xi
List of Tables	xiii
Nomenclature	xv
Abbreviations	xviii
Chapter 1 Introduction	1
1.1 CO ₂ Emissions and climate change.....	1
1.2 Different carbon capture approaches and CO ₂ separation technologies	2
1.2.1 CO ₂ separation technical options in the context of PCC	4
1.2.2 Current status of PCC using solvent and its commercial deployment.....	6
1.3 Introduction to PI and different PI technologies	8
1.4 Motivations to use PI in the context of PCC.....	14
1.5 Aim and objectives of the study	16
1.6 Scope of the PhD study	16
1.7 Research methodology and tools used for this study	17
1.7.1 Research methodology	17
1.7.2 Software tools used for the study	18
1.8 Outline of the thesis	18
Chapter 2 Literature review	20
2.1 RPB Absorber: Current status of experimental rigs and experimental studies	20
2.2 RPB stripper: Current status of experimental rigs and experimental studies	25
2.3 Intensified heat exchanger.....	25
2.3.1 Technologies available to choose	26
2.3.2 Recommendation for intensified heat exchanger for PCC application	30
2.4 Solvents for intensified carbon capture process	30
2.4.1 Factors to consider.....	30
2.4.2 Solvents used	32
2.4.3 Proprietary commercial solvents	35
2.4.4 Recommendations on solvent selection for PCC process.....	36
2.5 Current status of modelling and simulation of RPB absorber and stripper	36

2.2.1	Modelling/simulation of intensified absorber	36
2.2.2	Modelling/simulation of intensified stripper.....	36
2.2.3	Modelling and simulation of the whole plant.....	37
2.6	Summary	37
Chapter 3 Methodology for model development of intensified absorber and stripper		38
3.1	Modelling mass and heat transfer.....	38
3.2	Rate-based model development.....	39
3.2.1	Gas and liquid phase material balances	40
3.2.2	Gas and liquid phase energy balances	41
3.3	Physical property	41
3.3.1	Thermodynamic properties.....	41
3.3.2	Transport properties	42
3.4	Correlations suitable for RPB	43
3.4.1	Liquid phase mass transfer coefficient.....	43
3.4.2	Gas-side mass transfer coefficient.....	44
3.4.3	Total gas-liquid interfacial area	44
3.4.4	Liquid hold-up	45
3.4.5	Dry pressure drop expression	45
3.4.6	Motor power consumption by RPB absorber/stripper.....	46
3.5	Methods used to solve the system of differential equations	47
3.6	Implementation procedures	48
3.7	Summary	48
Chapter 4 Modelling, model validation and process analysis of standalone intensified absorber		50
4.1	Process description	50
4.2	Steady state modelling of intensified absorber	51
4.3	Steady state model validation of intensified absorber.....	52
4.3.1	Model validation based on experimental data from Jassim et al. [114]	52
4.3.2	Model validation based on Jassim et al. [114] experimental data comparing two sets of equations	58
4.4	Process analysis for intensified absorber	59
4.4.1	Effect of rotor speed on CO ₂ capture level.....	59
4.4.2	Effect of MEA concentration on CO ₂ capture level.....	62
4.4.3	Effect of flue gas flow rate on CO ₂ capture level.....	63
4.4.4	Effect of lean-MEA temperature on CO ₂ capture level	64
4.4.5	Effect of flue gas temperature on CO ₂ capture level	66
4.4.6	Temperature profile in RPB absorber.....	67

4.5	Comparison between intensified absorber and conventional absorber	69
4.5.1	Justification for case study	69
4.5.2	Setup of the case study.....	69
4.5.3	Results and discussions.....	70
4.6	Summary	71
Chapter 5 Modelling, model validation and process analysis of standalone intensified stripper		73
5.1	Process description	73
5.2	Steady state modelling of intensified stripper	74
5.3	Model validation of intensified stripper.....	74
5.3.1	Model validation based on experimental data from Jassim et al. [114]	74
5.3.2	Model validation based on experimental data from Cheng et al. [120].....	76
5.4	Process analysis for intensified regenerator	78
5.4.1	Effect of rich-MEA flow rate on regeneration efficiency.....	79
5.4.2	Effect of rich-MEA flow rate on regeneration energy.....	81
5.4.3	Effect of rotor speed on regeneration efficiency.....	85
5.4.4	Effect of rotor speed on regeneration energy.....	87
5.4.5	Effect of reboiler temperature on regeneration efficiency.....	88
5.4.5	Effect of reboiler temperature on regeneration energy.....	90
5.5	Comparison between intensified and conventional stripper.....	91
5.5.1	Justification for the case study	91
5.5.2	Setup of the case study.....	92
5.5.3	Results and discussion	92
5.6	Summary	93
Chapter 6 Process analysis, technical and economic assessment of intensified PCC process based on RPB technology.....		94
6.1	Process description	94
6.2	Process analysis on intensified PCC process.....	97
6.2.1	Impact of liquid to gas (L/G) ratio	97
6.2.2	Impact of lean-MEA loading	99
6.3	Technical performance comparison between intensified process and conventional process.....	101
6.3.1	Size reduction	101
6.3.2	Energy consumptions.....	101
6.4	Economic assessment.....	102
6.4.1	Capital cost estimations	102
6.4.2	Operating cost (OPEX) estimations	110
6.4.3	Annualized total cost (TOTEX).....	111

6.5	Summary	112
Chapter 7	Conclusions and recommendations for future study	114
7.1	Conclusions	114
7.1.1	Modelling of RPB column	114
7.1.2	Modelling, validation and process analysis of RPB absorber	114
7.1.3	Modelling, validation and process analysis of RPB stripper	115
7.1.4	Process analysis and costs estimation of intensified PCC process.....	115
7.2	Recommendations for future study.....	116
7.2.1	Scale-up study	116
7.2.2	Detailed technical and economic assessment for intensified PCC process ...	116
7.2.3	Detail analysis of energy consumed by RPB motor	116
7.2.4	Proposed Simplified PFD of intensified chemical absorption process for PCC 117	
References	119
Appendix A	Procedure for writing user defined subroutines.....	136
Appendix B	Cost estimation graphs and tables	139

List of Figures

Figure 1-1 World primary energy supply [3].....	2
Figure 1-2 Shares of global anthropogenic GHG, 2010 [3].....	2
Figure 1-3 Technical options for CO ₂ capture from coal-fired power plants [12].....	3
Figure 1-4 Process technologies for PCC [13].....	4
Figure 1-5 Process flow diagram of chemical absorption process for PCC [83]	7
Figure 1-6 Main benefits from process intensification [131].....	15
Figure 1-7 Summary of why PI for PCC [129].....	15
Figure 1-8 Overview of research methodology	17
Figure 2-1 Printed Circuit Heat Exchanger (Courtesy of Heatric Ltd): the big one at the back is shell-and-tube heat exchanger; while the small one in front is PCHE.	26
Figure 2-2 Summary of technology of PCHE, H2X, and FPHE (Courtesy of Heatric)	27
Figure 2-3 The Chart Marston Marbond compact heat exchanger (Courtesy Chart Marston Ltd.)	28
Figure 2-4 Spiral heat exchanger (courtesy of Alfa Laval) [158]	29
Figure 3-1 Two-film model for a differential packing segment	39
Figure 3-2 Methodology used in this thesis [115,116].....	48
Figure 4-1 Geometrical similarities and differences between RPB and conventional absorber [115].....	51
Figure 4-2 Effect of rotor speed on CO ₂ capture level at 56wt% MEA.....	61
Figure 4-3 Effect of rotor speed on CO ₂ capture level at 75wt% MEA.....	61
Figure 4-4 Effect of MEA concentrations on CO ₂ capture level	63
Figure 4-5 Effect of flue gas flow rate of CO ₂ capture level	64
Figure 4-6 Effect of lean-MEA temperature on CO ₂ capture level	66
Figure 4-7 Effect of flue gas temperature on CO ₂ capture level.....	67
Figure 4-8 Liquid temperature profile in RPB absorber at 25 °C lean MEA temperature	68
Figure 4-9 Liquid temperature profile in RPB absorber at 50 °C lean MEA temperature	68
Figure 5-1 Schematic diagram of a RPB regenerator [120].....	74
Figure 5-2 Effect of rich-MEA flow rate on regeneration efficiency (a) using Equation 5.1 (b) using Equation 5.2.....	80
Figure 5-3 Effect of rich-MEA flow rate on (a) Residence time (b) CO ₂ desorbed	80
Figure 5-4 Effect of rich-MEA flow rate on lean loading.....	81

Figure 5-5 Effect of rich-MEA flow rate on regeneration energy (a) without motor energy (b) with motor energy	82
Figure 5-6 Effect of rich-MEA flow rate on reboiler duty	83
Figure 5-7 Effect of Rich-MEA flow rate on (a) Heat of vaporisation (b) Sensible heat.....	84
Figure 5-8 Effect of Rich-MEA flow rate on heat of reversible reaction.....	84
Figure 5-9 Effect of Rich-MEA flow rate on (a) mass transfer rate (b) heat transfer rate	85
Figure 5-10 Effect of rotor speed on (a) regeneration efficiency (b) lean loading	86
Figure 5-11 Effect of rotor speed on (a) Residence time (b) CO ₂ desorbed	86
Figure 5-12 Effect of rotor speed on regeneration energy (a) without motor energy (b) with motor energy	88
Figure 5-13 Effect of rotor speed on reboiler duty	88
Figure 5-14 Effect of reboiler temperature on (a) regeneration efficiency (b) lean loading ..	89
Figure 5-15 Effect of reboiler temperature on amount of CO ₂ desorbed.....	89
Figure 5-16 Effect of reboiler temperature on regeneration energy (a) without motor energy (b) with motor energy.....	91
Figure 5-17 Effect of reboiler temperature on reboiler duty	91
Figure 6-1 Simplified PFD of intensified chemical absorption process for PCC using conventional reboiler and cross heat exchanger	96
Figure 6-2 Effect of L/G ratio on regeneration energy.....	99
Figure 6-3 Effect of L/G ratio on CO ₂ capture level.....	99
Figure 6-4 Effect of lean-MEA loading on regeneration energy	100
Figure 6-5 Effect of lean-MEA loading on CO ₂ capture level	101
Figure 7-1 Proposed simplified PFD of intensified chemical absorption process for PCC .	118
Figure A-0-1 Text file for creating DLOPT	136
Figure A-0-2 Correlation window for mass and heat transfer coefficient and interfacial area	137
Figure A-0-3 Holdup correlation window.....	138
Figure A-0-4 Run setting window.....	138
Figure B-0-1 Purchased costs for heat exchangers [224].....	139
Figure B-0-2Material factors for equipment in Table B-1 [224]	141

List of Tables

Table 1-1 Status of post-combustion CO ₂ capture development [15,21-28]	5
Table 1-2 Summary of different PI Technologies [90].....	9
Table 2-1 Summary of rig specifications for RPB absorber and findings using the rigs.....	21
Table 2-2 Summary of rig specifications and findings for RPB stripper	25
Table 2-3 Evaluation of solvent properties [162].....	32
Table 2-4 Performance of some proprietary commercial solvents [15].....	35
Table 3-1 Summary of the models in Aspen Plus [®] for transport properties calculations [201]	42
Table 4-1 Constants for power law expressions for the absorption of CO ₂ by MEA [186] ...	52
Table 4-2 Input process conditions at MEA concentration range of 53wt% to 57wt% [114,210].....	53
Table 4-3 Input process conditions at MEA concentration range of 72wt% to 78wt% [114,210].....	54
Table 4-4 Simulation results compared to the experimental data for Case 1 and Case 2 ...	55
Table 4-5 Simulation results compared to the experimental data for Case 3 and Case 4 ...	57
Table 4-6 Model correlation sets used for the modelling and simulations.....	58
Table 4-7 Simulation results with 2 different sets of correlations compared to the experimental data [105] for Case 1 Runs 1 and 3	59
Table 4-8 Simulation results with 2 different sets of correlations compared to the experimental data [105] for Case 3 Runs 1 and 3	59
Table 4-9 Process conditions for MEA concentration studies.....	62
Table 4-10 Process conditions for lean MEA temperature studies	65
Table 4-11 Process input conditions for conventional and RPB absorbers	70
Table 4-12 Comparison between conventional and RPB absorber	71
Table 5-1 RPB stripper packing specifications used by Jassim et al. [114]	75
Table 5-2 Input process conditions for Run 1 to Run 5 [114].....	75
Table 5-3 Simulation results compared to experimental data [114] for Run 1 to Run 5.....	76
Table 5-4 RPB stripper packing specifications used by Cheng et al [120].....	77
Table 5-5 Input process conditions for different reboiler temperatures [120].....	77
Table 5-6 Simulation results compared to experimental data [120]	77

Table 5-7 Process inputs	79
Table 5-8 Process conditions for Conventional and RPB regenerator.....	92
Table 5-9 Comparison between conventional and RPB stripper	93
Table 6-1 Design assumptions used for the design cases in this thesis	98
Table 6-2 Cost factors for the cost calculation for RPBs [225].....	107
Table 6-3 Cost factors for the cost calculation for pump.....	108
Table 6-4 Cost factors for the cost calculation for heat exchangers (CRHE, HX1, HX2, HX3)	109
Table 6-5 Investment costs for major units	110
Table 6-6 Operating cost estimation for intensified PCC process.....	111
Table B-1 Identification numbers for material factors for heat exchangers, process vessels, and pumps to be used with Figure B-2 [223]	139
Table B-2 Pressure factors for process equipment [223].....	142

Nomenclature

a	gas-liquid interfacial area (m^2/m^3)
A	cross sectional area (m^2)
$a_{g/l}$	gas-liquid interfacial area (m^2/m^3)
a_i	activity of species i in a solution
a_t	total specific surface area of packing (m^2/m^3)
a'_p	surface area of the 2 mm diameter bead per unit volume of the bead ($1/\text{m}$)
c	width of the square opening (mm)
C_{BM}	bare module price (€)
C_{al}	cost factor for alloy (-)
C_{CEPCI}	cost factor for cost digression (-)
C_{el}	costs for electrical power (€/kW/h)
C_{en}	cost factor for enclosure (-)
C_{ER}	currency exchange rate (€ $\text{\$}^{-1}$)
C_{IC}	investment costs (€)
C_i^l	concentration of component i
$C_{L/M}$	cost factor for reduction of material (-)
C_{L+M}	cost factor for labour and material (-)
Cp_i	is the heat capacity for component i
C_{OC}	operating costs (€/a)
C_{RS}	cost factor for high rotational speed (-)
C_{tax}	Cost factor for taxes (-)
C_{trans}	cost factor for transformation ratio of motor (-)
d	diameter of the stainless steel fibre (mm)
D	column diameter (m)
D_G	diffusivity coefficient of gas (m^2/s)
D_L	diffusivity coefficient of liquid (m^2/s)
E_j	activation energy (kJ/gmol)
F_{BM}	bare module factor (-)
F_m	material factor (-)

F_p	pressure factor (-)
G	superficial gas velocity (m/s)
g_c	gravitational acceleration or acceleration due to centrifugal field (m^2/s)
g_o	characteristic acceleration value ($100 m^2/s$)
G_{toe}	gigatoe
F	total molar flow rate
H	height of packing (m)
$h_{g/l}$	is the interfacial heat transfer coefficient
k_G	gas phase mass transfer coefficient (m/s)
K_G^a	overall gas phase mass transfer coefficient (1/s)
k_j^o	pre-exponential factor ($kmol/m^3.s$)
k_L	liquid phase mass transfer coefficient (m/s)
L	superficial mass velocity of liquid ($kg/m^2/s$)
P_{motor}	motor power (kilowatts)
Q_L	volumetric flow rate of liquid (m^3/s)
R	radial position (m)
R_c	gas constant ($J mol^{-1} K^{-1}$)
r_j	reaction rate for reaction j
r_i	inner radius of the packed bed (m)
r_o	outer radius of the packed bed (m)
r_s	radius of the stationary housing (m)
T	temperature (K)
U	superficial liquid velocity (m/s)
u_g	the gas velocity (m/s)
u_l	liquid velocity (m/s)
U_o	characteristic superficial liquid velocity (1cm/s)
\dot{V}	volume flow ($m^3 s^{-1}$)
V_i	volume inside the inner radius of the bed = $\pi r_i^2 Z$ (m^3)
V_o	volume between the outer radius of the bed and the stationary housing = $\pi(r_s^2 - r_o^2)Z$ (m^3)
V_t	total volume of the RPB = $\pi r_s^2 Z$ (m^3)
$y_{CO_2,in}$	mole fraction of CO_2 in inlet stream

$y_{CO_2,out}$ mole fraction of CO₂ in outlet stream
 Z axial height of the packing (m)

Greek letters

α_{ij} reaction order of species i in reaction j
 ε bed porosity
 $\epsilon_L, \varepsilon_L$ liquid holdup
 ε_g gas holdup
 ΔH_{vap} is the heat of vaporisation of H₂O
 ΔP_{RPB} dry pressure drop in RPB
 μ viscosity (Pa.s)
 ρ_L liquid density (kg/m³)
 ρ_G gas density (kg/m³)
 σ liquid surface tension (N/m)
 σ_c critical surface tension (N/m)
 σ_w surface tension of water (kg/s²)
 ν_L kinematic viscosity of the liquid (m²/s)
 ν_o characteristic kinematic viscosity (m²/s)
 ν_G kinematic gas viscosity (m²/s)
 ω angular velocity (rad/s)

Dimensionless groups

Fr_L liquid Froude number ($U^2 a_t / g_c$)
 Gr_G gas Grashof number ($d_p^3 g_c / \nu_G^2$)
 Gr_L liquid Grashof number ($d_p^3 g_c / \nu_L^2$)
 Re_G gas Reynolds number ($G / a_t \nu_G$)
 Re_L liquid Reynolds number ($U / a_t \nu_L$)
 Sc_G gas Schmidt number (ν_g / D_G)
 Sc_L liquid Schmidt number (ν_L / D_L)
 We_L liquid Webber number ($U^2 \rho_L / a_t \sigma$)
 φ theoretical probability of liquid uncaptured by fibers ($c^2 / (d + c)^2$)

Abbreviations

CAPEX	Capital Expenditure
CCGT	Combined Cycle Gas Turbine
CCP	Carbon Capture Project
CCS	Carbon Capture and Storage
CFD	Computational Fluid Dynamics
COP21	21 st Conference of Parties
ELECNRTL	Electrolyte-Non-Random-Two-Liquid
FOB	Free-On-Board
GPU	Gas Permeance Units
GHG	Green-House Gas
ICCS	Integrated Carbon Capture and Storage
IEA	International Energy Agency
IPCC	Intergovernmental Panel on Climate Change
LHV	Lower Heating Value
MEA	Monoethanolamine
MHI	Mitsubishi Heavy Industries
MTR	Membrane Technology and Research
MWe	Megawatt electrical
OPEX	Operational Expenditure
PCC	Post-Combustion Capture
PFD	Process Flow Diagram
PI	Process Intensification
PPM	Part Per Million
RPB	Rotating Packed Bed
TOTEX	Annualized total cost
UK	United Kingdom
WMO	World Metrological Organisation

Chapter 1 Introduction

In this chapter, CO₂ emissions and climate change are presented in Section 1.1. Section 1.2 highlights different capture approaches and CO₂ separation technologies. Process intensification (PI) and PI technologies are introduced in Section 1.3. Motivations for carrying out this research are presented in Section 1.4. Aim and objectives of this research study are presented in Section 1.5. The scope of the PhD research is presented in Section 1.6. The research methodology and tools used for the research are highlighted in Section 1.7. Finally, the structure of this thesis report is outline in Section 1.8.

1.1 CO₂ Emissions and climate change

Global energy demand is expected to continue to raise due to increasing world population and emergence of new economic powerhouse namely the BRICs nations (i.e. Brazil, Russia, India and China) [1]. Dependence on renewable energy alone such as solar, wind and tidal power to meet the projected demand is not feasible due to their intermittent and diffuse nature, except the geothermal renewable energy source which is not widely accessible [2]. Therefore, fossil fuel remains the most attractive options for meeting future energy demands.

According to IEA 2015 report, global total primary energy supply increased by almost 150% between 1971 and 2013, showing high dependence on fossil fuels (**Figure 1-1**) [3]. Globally, most fossil fuel fired electricity production is from coal (63%), followed by natural gas (29%) and oil (9%) [4]. For instance, about 85.5% of coal (produced and imported) was used for electricity generation in the UK in 2011[5]. However, combustion of fossil fuels (e.g. petroleum, coal and natural gas) accounts for the majority of CO₂ emissions. **Figure 1-2** shows the global share of anthropogenic GHG, with CO₂ contributing to 90% of the total. Statistics from World Metrological Organisation (WMO) showed that the amount of CO₂ in the atmosphere reached 393.1 ppm in 2012. The WMO report also showed that the amount of CO₂ in the atmosphere has increased on average by 2 ppm per year for the past 10 years. Recent report by CO₂-Earth [6] shows that as at 14 March 2016 CO₂ atmospheric

concentration stood at 404.47 ppm, this increased atmospheric concentration of CO₂ affects the radiative balance of the earth surface [7].

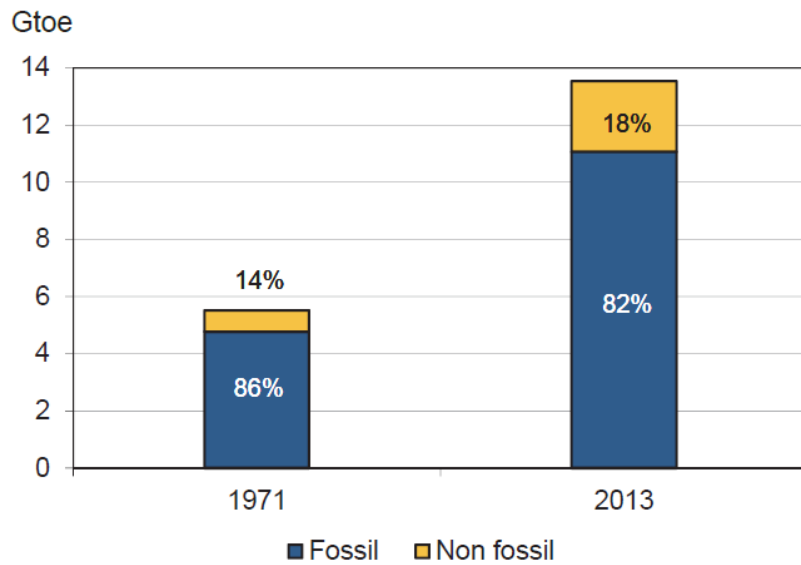


Figure 1-1 World primary energy supply [3]

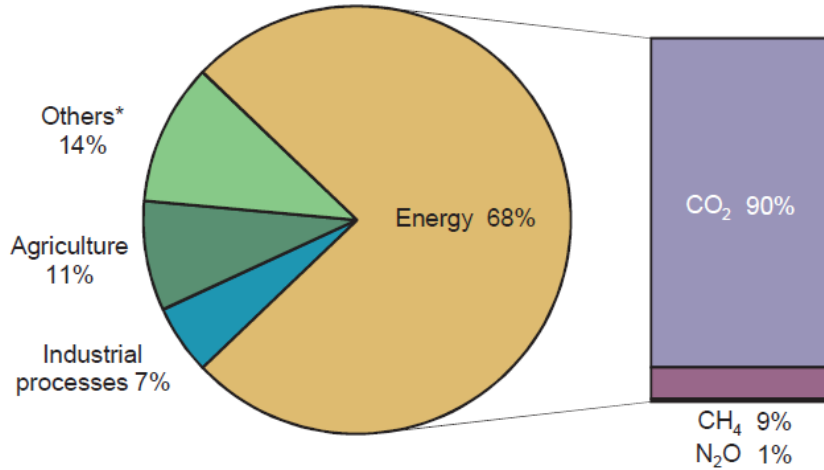


Figure 1-2 Shares of global anthropogenic GHG, 2010 [3]

1.2 Different carbon capture approaches and CO₂ separation technologies

The recent 21st Conference of Parties (COP21) in Paris in December 2015 which has 190 member nations reached an agreement to “*hold the increase in the global*

average temperature to well below 2°C above pre-industrial levels and to pursue efforts to limit the temperature increase to 1.5 °C above pre-industrial levels” by 2050 [8]. This has buttressed the Intergovernmental panel on climate change (IPCC) [9] ambitious goal to reduce CO₂ emission by 50% in 2050 as compared to the level of 2005. To achieve these targets, decarbonisation of world’s energy system is necessary. In order to achieve the required emission reductions in the most cost-effective manner, carbon capture and storage (CCS) will need to contribute around one-fifth of total reductions in emissions by 2050 [10].

CCS consists of three basic stages: (a) separation of CO₂; (b) CO₂ transportation and (c) CO₂ storage. There are three major approaches for CCS: post-combustion capture, pre-combustion capture and oxy-fuel process as shown in **Figure 1-3** [11]. The CO₂ separation technologies have been highlighted in **Figure 1-4**.

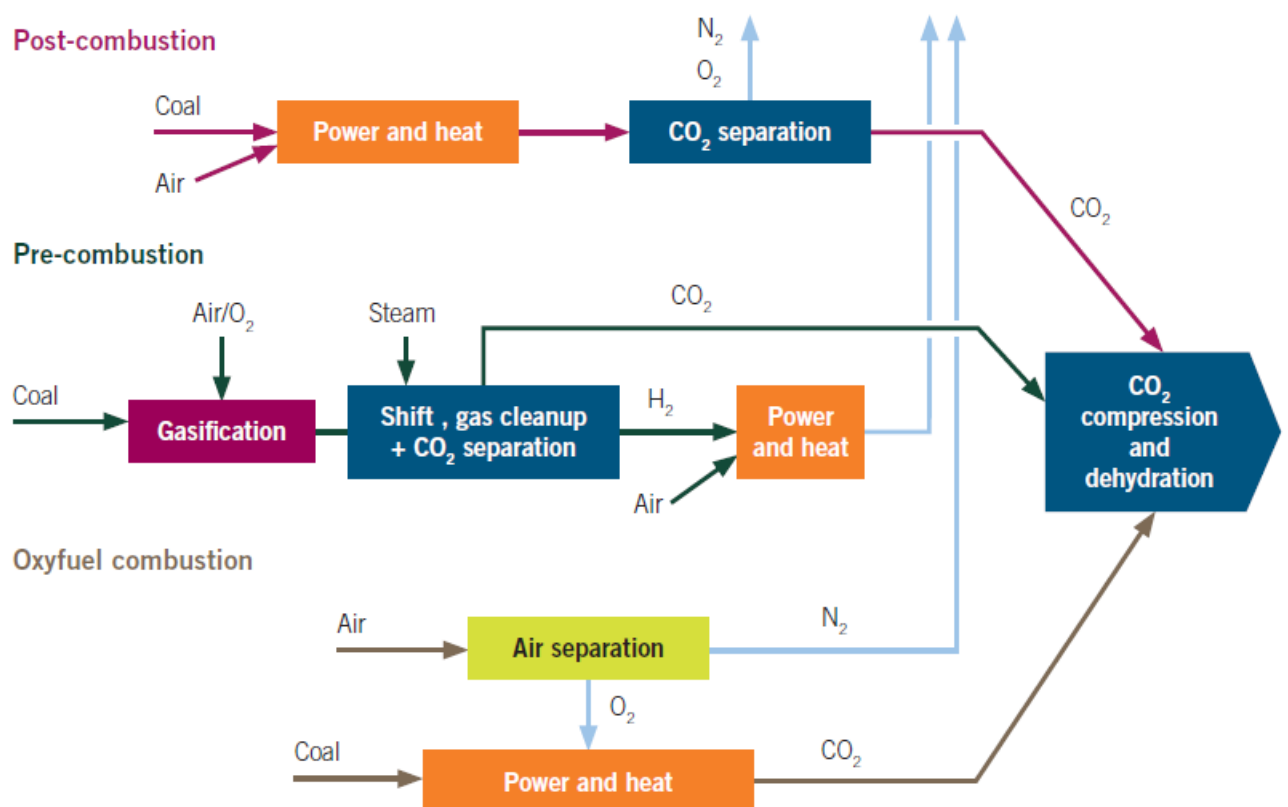


Figure 1-3 Technical options for CO₂ capture from coal-fired power plants [12].

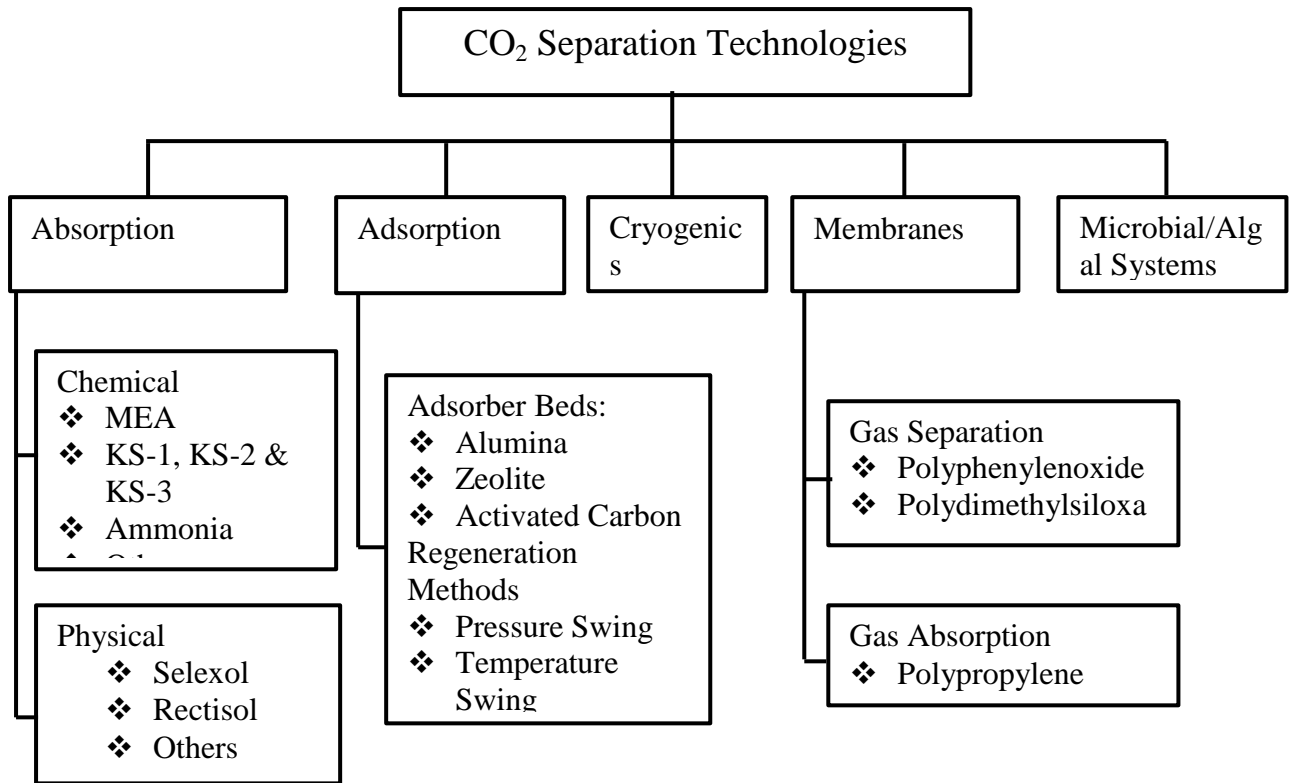


Figure 1-4 Process technologies for PCC [13]

1.2.1 CO₂ separation technical options in the context of PCC

Review studies on PCC technologies at various stages of development were reported in Abanades *et al.* [14], Goto *et al.* [15]. The technological readiness for different CO₂ capture technologies in the context of PCC including chemical looping, calcium looping, PCC using solvent, PCC using adsorbent and PCC using membrane has been reported in their studies. The most matured process is PCC using solvent [14,16].

However, PCC using solvent process has several drawbacks including: (1) low CO₂ loading capacity; (2) high equipment corrosion rate; (3) amine degradation by SO₂, NO₂, and O₂ in the flue gases which induces a high solvent makeup rate; (4) high energy consumption during solvent regeneration; (5) large equipment size [17-20] (in whole PCC process, absorber and stripper account for 55% and 17% of the total equipment purchase cost respectively for treating flue gas from 600 MWe coal fired power plant with 90% capture efficiency [21]). Table 1-1 gives its performance indicators and status for chemical absorption compared to adsorption and membrane technologies.

Table 1-1 Status of post-combustion CO₂ capture development [15,21-28]

	Absorbent	Adsorbent	Membrane
Commercial usage in chemical process industries	High	Moderate	Low/Niche
Operational confidence	High	High, but complex	Low to moderate
Primary source of energy penalty	Solvent Regeneration (thermal)	Solid sorbent Regeneration (thermal/vacuum)	Compression on feed and/or vacuum on permeate
Regeneration energy (MJ/kg-CO ₂)	2.2 – 6	0.5 – 3.12	0.5 – 6
Thermal efficiency penalty (%)	8.2 – 14	5.4 – 9.0	6.4 – 8.5
Development trends	New solvent, thermal integration	New sorbent, process configuration	New membrane, process configuration

Chemically modified adsorbents have proved to be applicable for PCC process because of large CO₂ adsorption capacity, high adsorption and desorption rates, high tolerance to moisture, and high selectivity towards CO₂ over other gases [29]. In terms of regeneration energy, Zhao *et al.* [30] reported that solid sorbent does not have any obvious advantage over the matured MEA process in terms of energy consumption in the first design (i.e. two reactor used, one for adsorption and the other for regeneration). But the novel (second) design (i.e. using three reactors, one for adsorption, one for regeneration and another one for formation of K₂CO₃.1.5H₂O), the regeneration energy can be reduced by utilizing the waste heat from the process, however this design is difficult to control because the reactors operate at different pressures. A lot of researchers have focused on new adsorbent development, process optimization, and equipment innovation [31-55].

Study by Abanades *et al.* [14] indicates that membrane process for PCC is at almost the same level of technological readiness as adsorption. Therefore, more studies in this area are needed in order to get detailed technical performance at large scale

conditions. Many researchers have developed new membranes that offer better performance in term of selectivity. The recent key projects developing membranes and modules for CO₂ capture include Membrane Technology and Research (MTR) in the USA, NanoGLOWA in Germany, the carbon capture project (CCP) and the CO₂CRC in Australia [14]. Membranes process for PCC is beneficial because of relatively small footprint, no phase change, simple mechanical system, steady-state operating conditions (usually), easy scale-up and flexibility [56-58]. The major challenge for membranes comes from the potential fouling of the membrane surfaces from particulate matter, uncertainty about the performance and cost of large-scale efficient vacuum pumps and compressors required for PCC, and the ability to integrate the process into a power plant. Technological outlook of membrane system is reported in Abanades et al. [14] and suggested that for the technology to be competitive with other PCC technology, the membrane needs to be of high CO₂ permeance (around 1000 gas permeance units (GPU) to be economical.

1.2.2 Current status of PCC using solvent and its commercial deployment

Significant progress have been made in commercial deployment of PCC using chemical solvent, but before discussing the stage of the progresses, process flow diagram (PFD) of the technology will be described for understanding of this process.

Figure 1-5 shows a simplified PFD for PCC process with chemical solvent. Flue gas from CO₂ sources such as power plant is first cooled down to a favourable temperature for absorptions (e.g. 40 to 50 °C) using the flue gas cooler. The flue gas is then sent into absorber using the flue gas blower. The flue gas is contacted counter-currently with lean solvent solution inside the absorber. The solvent chemically absorbs CO₂ in the flue gas. This leaves a treated gas stream of lower CO₂ content. The solvent solution (now higher in CO₂ loading, therefore called rich solvent) is regenerated in the stripper. CO₂ from the top of the stripper is compressed and transported while the lean (regenerated) solvent solution is returned to the absorber passing through a cross heat exchanger to recover heat with rich solvent from the absorber.

The successes recorded in the use of PCC based on chemical absorption process for fossil fuel-fired power plants is related the large amount of research that had taken place in that area. Dugas [59] carried out pilot plant experimental studies of PCC in the context of fossil fuel-fired power plants. Mangalapally *et al.* [60-63]

reported pilot plant studies of PCC for natural gas-fired power plant. Lawal *et al.* [17,64-66], Biliyok *et al.* [1], Kvamsdal *et al.* [67-70], MacDowell and Shah [71-73], MacDowell *et al.* [74], Lucquiaud *et al.* [75,76], Errey *et al.* [77], Agbonghae *et al.* [20,78] carried out steady state and dynamic modelling of CO₂ absorption for PCC using solvents for fossil-fuel fired power plants. Asendrych *et al.* [79], Sebastia-Saez *et al.* [80], Raynal *et al.* [81], Raynal and Royon-Lebeaud [82] studied PCC for fossil fuel fired power plant using CFD.

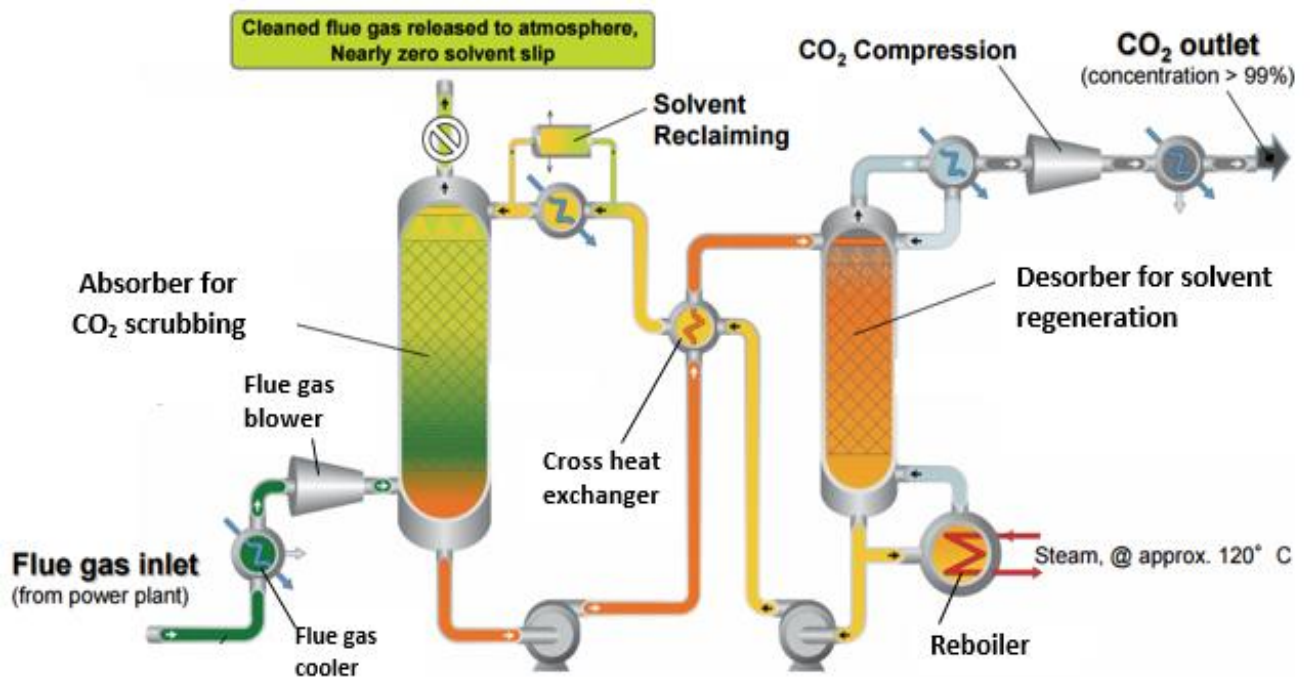


Figure 1-5 Process flow diagram of chemical absorption process for PCC [83]

Commercial deployment of PCC using chemical solvent technology indicates the high level of maturity of the technology. SaskPower's Boundary Dam Integrated Carbon Capture and Storage (ICCS) Demonstration Project (that came online on 2nd October, 2014) in Canada captures over one million metric tons of CO₂ per year, reflecting a 90% CO₂ capture rate for the 139 MWe coal-fired unit. This is the first commercial CCS plant in the world [84],

The demonstration plant of Southern Company's 25 MWe Plant Barry CCS project in Alabama, USA using Mitsubishi Heavy Industries (MHI) technology has been operational since Jun. 2011 and it reached full-scale capture of 500 tonnes a day in September 2012 [85].

Petra Nova/NRG 240 MWe W.A. Parish project using the MHI technology is the largest commercial PCC using solvent project in the world. It is located in southwest of Houston, Texas, USA. It is installed on an existing coal-fired power plant and is expected to be operational in 2016 [86]. The plant is expected to capture 1.6 million tons of CO₂ annually for use in enhanced oil recovery (EOR) at mature oil fields in the Gulf Coast region [86]


1.3 Introduction to PI and different PI technologies

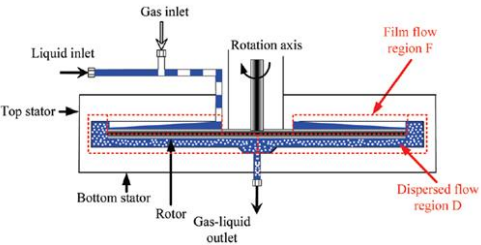
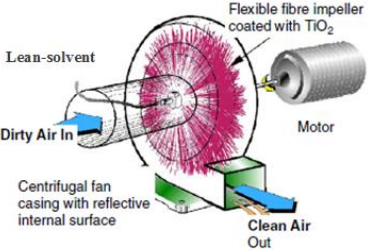
Ramshaw [87] defined PI as a strategy for making dramatic reductions in the size of a chemical plant so as to reach a given production objective. According to Stankiewicz and Moulijn [88], Ramshaw's definition is quite narrow, describing PI exclusively in terms of the reduction in plant or equipment size.

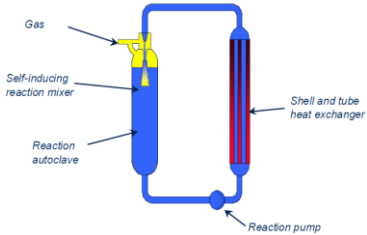
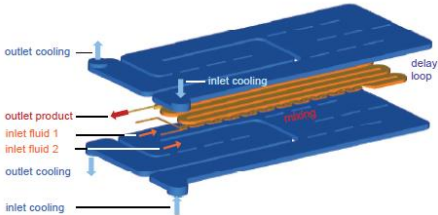
Reay et al. [89] defined PI as: *“Any engineering development that leads to a substantially smaller, cleaner, safer and more energy efficient technology.”* Reay et al. [89] definition is an improvement of Stankiewicz and Moulijn [88] definition by including the term “safer”. Reay et al. [89] view safety as an important driver in motivating businesses to seriously consider PI technologies. There are general approaches to PI with the aim of improving process performance [90]: (a) Reducing equipment size using an intensified field (e.g. centrifugal, electrical, microwave); (b) Simplifying processes by integrating multiple process tasks in a single item of equipment; (c) Reducing equipment size by reducing its scale of structure. PI technologies differ in functions and areas of application. Some will be very good at intensifying mass transfer (e.g. rotating packed bed (RPB)), whilst others are good at intensifying heat transfer (e.g. printed circuit heat exchangers)

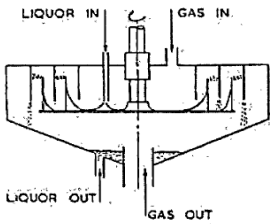
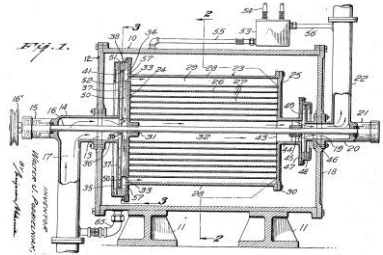
There are several PI technologies which are considered suitable for a particular system applications. **Table 1-2** describes different PI equipment's, mechanism by which intensification takes place, their present area of application and their suitability and limitation for CO₂ capture applications.

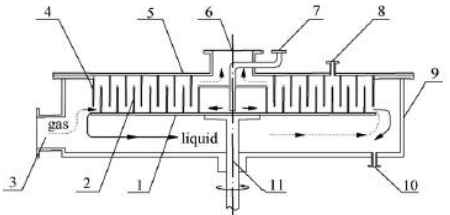
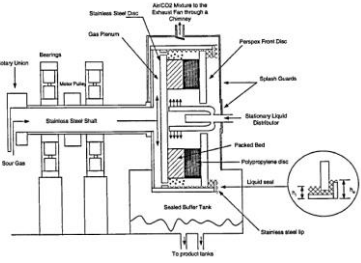
Table 1-2 Summary of different PI Technologies [90]

PI Equipment	Description	Mechanism for Intensification	Area of application at present	Suitability to CO ₂ capture	Limitation
<p>Static mixer</p>	<p>A static mixer or motionless mixer is a device inserted into a housing or pipeline with the objective of manipulating fluid streams. Different designs are available, typically consisting of plates or baffles positioned in precise angles in order to direct flow, increase turbulence and achieve mixing and reactions [91].</p> 	<p>Static mixer functions to divide, recombine, accelerate / decelerate, spread, swirl or form layers of fluid streams as they pass through the mixer. mixture components are brought into intimate contact thereby enhancing reaction processes [91]</p>	<p>Mostly this equipment is used for liquid system. e.g. Waste water treatment process (Formose treatment) [92]</p>	<p>Because of its high mass transfer capability, this can be used for CO₂ capture by combining the flue gas stream and the solvent stream. At the exit, a flash drum can be used to separate the treated gas and the rich solvent.</p>	<p>The challenge would be the high volume of flue gas to be treated (For example, 500 MWe coal-fired power plant releases 8,000 tonnes/day of pure CO₂). Also the length will be too long to treat such a huge volume of flue gas.</p>

<p>Spinning disc</p>	<p>Spinning disc reactor consists of a cylindrical housing with a rotating disc in the middle between the top and bottom plates of the cylinder, the rotating disc is connected to a motor [93-95]</p> 	<p>Gas and liquid are fed together through the inlet in the centre of the top stator, close to the rotating axis. A liquid film is present on top of the rotor, and a gas-liquid bubbly dispersion is located between the rotor and the bottom stator. The combined film flow on the rotor and the dispersed flow in the remainder part of rotor-stator reactor lead to higher gas-liquid mass transfer rate [93].</p>	<p>It is used for gas-liquid and liquid-solid mass transfer process such as desorption of oxygen from oxygen saturated water, polymerization, crystallization [93-98].</p>	<p>It has the potential for CO₂ absorption, either as an absorber because of its high mass transfer capability or as a stripper because of its high heat transfer ability. It can also be used as a reboiler.</p>	<p>It may result in additional unit such as flash drum to separate the rich solvent from treated gas stream since the flow is co-current. It also lack large surface per unit volume compared to RPB</p>
<p>Mop fan</p>	<p>Mop fan is a device that uses flexible fibre needle impeller instead of blade impeller within a centrifugal fan casing. The flexible fibre needle impeller is connected to a motor [99]</p> 	<p>Dirty air enters the mop through its centre contacting the solvent which is sprayed on the fibre needle impeller. The rotating mop leads to increase in interfacial area for capture.</p>	<p>Mop fan is used for removal of air-borne particulates [100]</p>	<p>The system uses a flexible fibre needle impeller (mop fan) device to increase the heat and mass transfer in the absorber for CO₂ capture [99-101].</p>	<p>Huge volume of flue gas to be treated from power plants means there needs to be many mop fans for CO₂ capture. It may also result in additional unit such as flash drum to separate the rich solvent from treated gas stream since the flow might be co-current.</p>

<p>Loop reactor</p>	<p>Advanced BUSS Loop[®] reactor is made up of a reaction vessel, a circulation pump, a heat exchanger with a high performance gas/liquid ejector to achieve high mass transfer rates [102].</p> 	<p>A gas-liquid ejector consists of four main sections. Optional swirl device, nozzle that provides a high velocity jet of fluid to create suction of the gas in the gas suction chamber and entrain gas into the ejector. Liquid jet attaches itself to the mixing tube wall resulting in a rapid dissipation of kinetic energy. This creates an intensive mixing where the high turbulence produces a fine dispersion of bubbles [102].</p>	<p>Loop reactor is used for hydrogenation, phosgenation, alkylation, amination, carbonylation, oxidation and other gas-liquid reactions [102,103].</p>	<p>Because of high mass transfer and heat transfer it may be applicable to CO₂ capture [102-104].</p>	<p>Design modification will be required for it to be use for CO₂ capture also huge volume of flue gas that will be treated is another challenge</p>
<p>Microreactor</p>	<p>Schematic representation of a 2nd generation microreactor based on a plate design for performing mixing, gaining volume (e.g. to increase residence time) and integrating heat exchange [105].</p> 	<p>There are many designs for Microreactor, but the plate design offers an advantage of good mixing, longer residence time and better temperature control using cooling or heating plate [105]. Two fluid streams flow co-currently into the reactor where there are static mixers inside the reactor to enhance mixing before the final product comes out.</p>	<p>The technology is mostly applied to fine chemical and pharmaceutical industries for production specialized drugs and hazardous chemicals [105-107].</p>	<p>Because of high mass transfer and heat transfer, and its ability to operate at controlled temperature, it has good potential for CO₂ capture [106,107].</p>	<p>The expected challenge of using this technology for carbon capture is the huge volume of flue gas to be treated.</p>
<p>Chamber's centrifugal absorber</p>	<p>This centrifugal absorber was introduced by Chambers and Wall in 1954. The lower plate is rotating while the upper plate is static.</p>	<p>The rotation of the lower plate makes the liquid coming into the chamber to splash as it is thrown</p>	<p>It is used for CO₂ capture as reported by Chambers and</p>	<p>With more modifications in design (to</p>	<p>Maximum CO₂ recovery was reported to be 85%,</p>

	<p>Mass transfer occurs in the intermesh of concentric rings as the lean solvent contact the flue gas. No packing was utilized [108].</p> 	<p>out while the flue gas contact the liquid counter-currently leading to mass transfer in the concentric regions of the absorber [108].</p>	<p>Wall [108].</p>	<p>incorporate packing in its bed so as to increase surface area of contact) and construction material (e.g. corrosion resistance materials), it can be used for CO₂ capture.</p>	<p>this is below the standard for CO₂ capture above 90%.</p>
<p>Podbieiniak's deodorizer</p>	<p>The contactor is basically a cylindrical rotor mounted on a shaft with contacting material [109].</p> 	<p>Gas and liquid meet counter-currently with the help of contacting material as the contactor rotates [109].</p>	<p>Used for stripping out odour and flavour substances from triglyceride oil using steam [109].</p>	<p>Has the potential for CO₂ capture especially as stripper.</p>	<p>Design modification will be needed when using it for CO₂ capture.</p>
<p>Rotating Zigzag bed</p>	<p>The RZB is characterized by a rotor coaxially combining a rotating disc with a stationary disc [110-112].</p>	<p>In the interior of rotor, the gas flows along a zigzag path and the liquid experiences repeated dispersion and agglomeration. There are two types of gas-liquid contact. The first step is cross-current contact of two phases when the liquid is thrown by the rotational baffles. The second step</p>	<p>RZB can function without liquid distributors, eliminate one dynamic-seal, and easily accommodate and accomplish intermediate feeds</p>	<p>It has the potential for CO₂ absorption because of its high mass transfer capability [110-112].</p>	<p>Energy cost is much higher than RPB, because the kinetic energy of the liquid from the liquid acceleration under the centrifugal force disappear when the liquid as droplets</p>

	 <p>1-rotational disc 2-rotational baffle 3-gas inlet 4-stationary baffle 5-stationary disc 6-gas outlet 7-liquid inlet 8-intermediate feed 9-rotor casing 10-liquid outlet 11-rotating shaft</p>	<p>is counter-current contact of two phases when the liquid falls down along the stationary baffles [110,111].</p>	<p>in continuous distillation processes [110-112].</p>		<p>impact on the wall of the stationary baffle with high velocity [113].</p>
<p>Rotating Packed Bed</p>	<p>The HiGee machine was constructed using a doughnut-shaped rotor, which is mounted on a shaft, and filled with high specific area packing [114]</p> 	<p>This technology takes advantage of centrifugal fields as stimulants for process intensification. Increasing the centrifugal acceleration improves the slip velocity, which in turn improves the flooding characteristics and interfacial shear stress, and consequently boosts the mass transfer coefficient [114].</p>	<p>Many studies such as Jassim <i>et al.</i>, [114], Joel <i>et al.</i>, [115,116], Cheng and Tan [117], Cheng et al., [118], Cheng and Tan [119] showed its application to CO₂ capture was successful.</p>	<p>RPB has the potential for CO₂ capture [114-117,119-124].</p>	<p>No known limitation to CO₂ capture</p>

1.4 Motivations to use PI in the context of PCC

Having discussed previously the milestone recorded (i.e. commercial deployment) in the use of conventional PCC technology for CO₂ capture, it comes with some challenges such as big size of the processing units and large solvent re-circulation rate. It was reported that a 500 MWe supercritical coal fired power plant operating at 46% efficiency (LHV basis) releases over 8,000 tonnes of pure CO₂ per day which is huge volume [125]. The use of PCC using chemical solvents based on the conventional technology (i.e. using packed tower) to capture such amount of CO₂ will require very large columns. Dynamic modelling and simulation studies of a 500 MWe sub-critical coal-fired power plant by Lawal et al. [17] showed that two absorbers with a packing height of 17m and 9m in diameter will be needed to separate CO₂ from the flue gas. Agbonghae et al. [20] reported that two absorbers and one stripper will be required for a 400 MWe gas fired combined cycle gas turbine (CCGT) power plant. The two absorbers having packing height 19.06 m and 11.93 m in diameter while the stripper has packing height 28.15 m and 6.76 m in diameter. These huge packed columns translate into high capital and operating costs. A significant amount of steam from power plants has to be used for solvent regeneration. This translates into high thermal efficiency penalty. It is reported that 3.2 to 4.5 MJ energy is required to capture per kg of CO₂ using 30 wt% MEA solvent [17,68,72,126,127]. On the other hand, through PI techniques there could be significant reductions in equipments sizes and energy consumption, hence lower capital cost [114-116,120,128], and improved process dynamics. The benefits of using PI technology are highlighted in **Figure 1-6**.

Other motivations for using PI technology for PCC have been highlighted in **Figure 1-7**: (a) Enhanced mass transfer due to better gas-liquid interactions. Biliyok et al. [1]

reported CO₂ capture using 30 wt% MEA concentration in a conventional packed tower and found that the process is mass transfer controlled [114,129] (b) Improved mass transfer due to micromixing in process where resistance lies in the liquid phase [130].

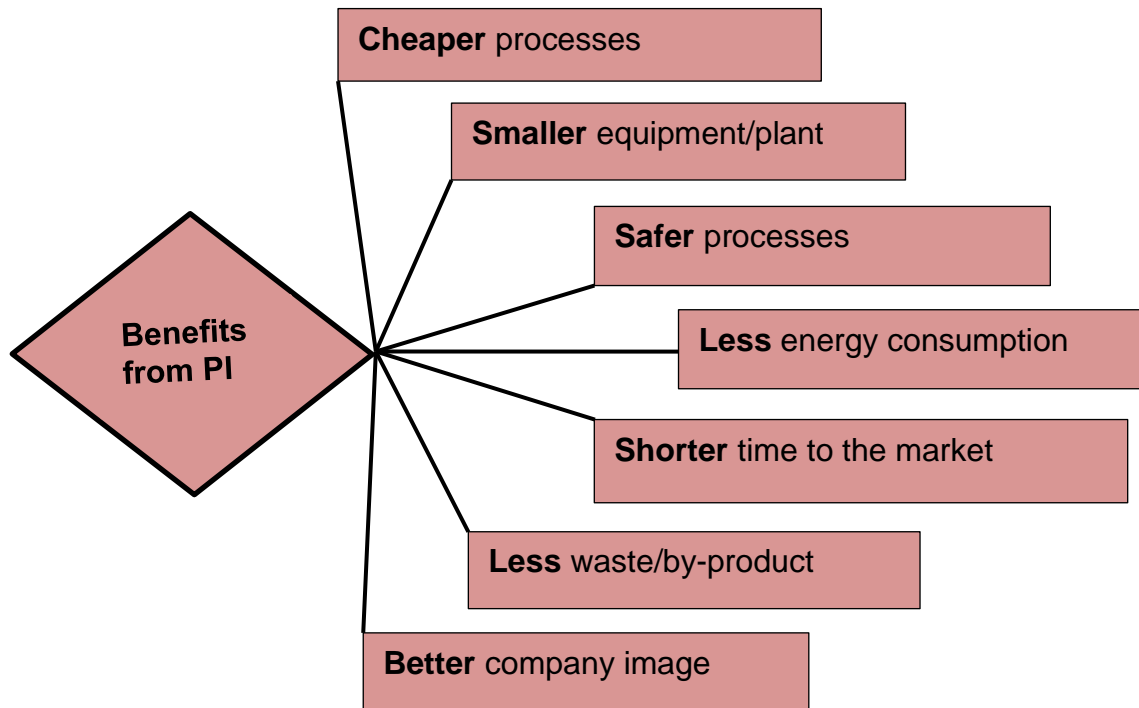


Figure 1-6 Main benefits from process intensification [131]

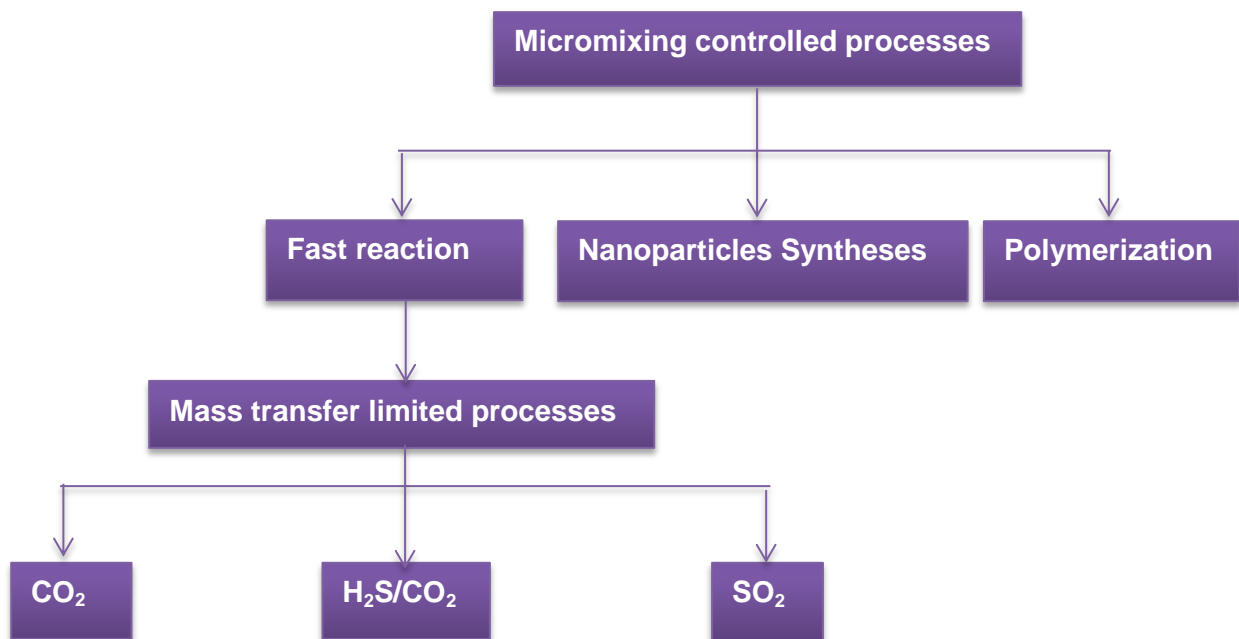


Figure 1-7 Summary of why PI for PCC [129]

1.5 Aim and objectives of the study

The thesis is aimed at developing a steady state model of intensified carbon capture process based on RPB technology using MEA solvent in the context of flue gas from CCGT power plant, and carrying out technical/economic analysis in comparison with conventional process based on packed column technology.

This aim can be achieved through the following objectives:

- Comprehensive and detailed review of literatures on the PI technology using RPBs in order to identify the knowledge gaps that could be filled with this research.
- Modelling, validation and analysis of standalone intensified absorber
- Modelling, validation and analysis of standalone intensified stripper
- Modelling and analysis of intensified PCC process with conventional cross heat exchanger and reboiler
- Technical and economical assessment of intensified PCC process compared to conventional PCC process

1.6 Scope of the PhD study

Modelling and analysis of intensified PCC process is presented in the thesis. The study looks at modelling, model validation and process analysis of standalone absorber and stripper before connecting them to form the whole intensified PCC process including conventional reboiler and cross heat exchanger. Validation of the whole intensified PCC process was not possible because there is no experimental data for such process in open domain. The study is limited to PCC based on chemical absorption using aqueous monoethanolamine. Only flue gas from CCGT power plant is considered in this study, but no modelling work was done for the CCGT power plant itself. The study was performed with steady state modelling only since the focus is to carry out technical and economic performance assessment of intensified PCC process compared to conventional PCC process.

1.7 Research methodology and tools used for this study

1.7.1 Research methodology

Figure 1-8 shows the methodology used for this thesis. Models for the standalone intensified absorber and stripper were validated respectively based on experimental data obtained from Newcastle University United Kingdom [114]. Also data for intensified stripper from National Tsing Hua University Taiwan [120] was used for the stripper model validation. Since there is no experimental data available for the closed loop intensified PCC process, the model was validated separately as standalone absorber and standalone stripper.

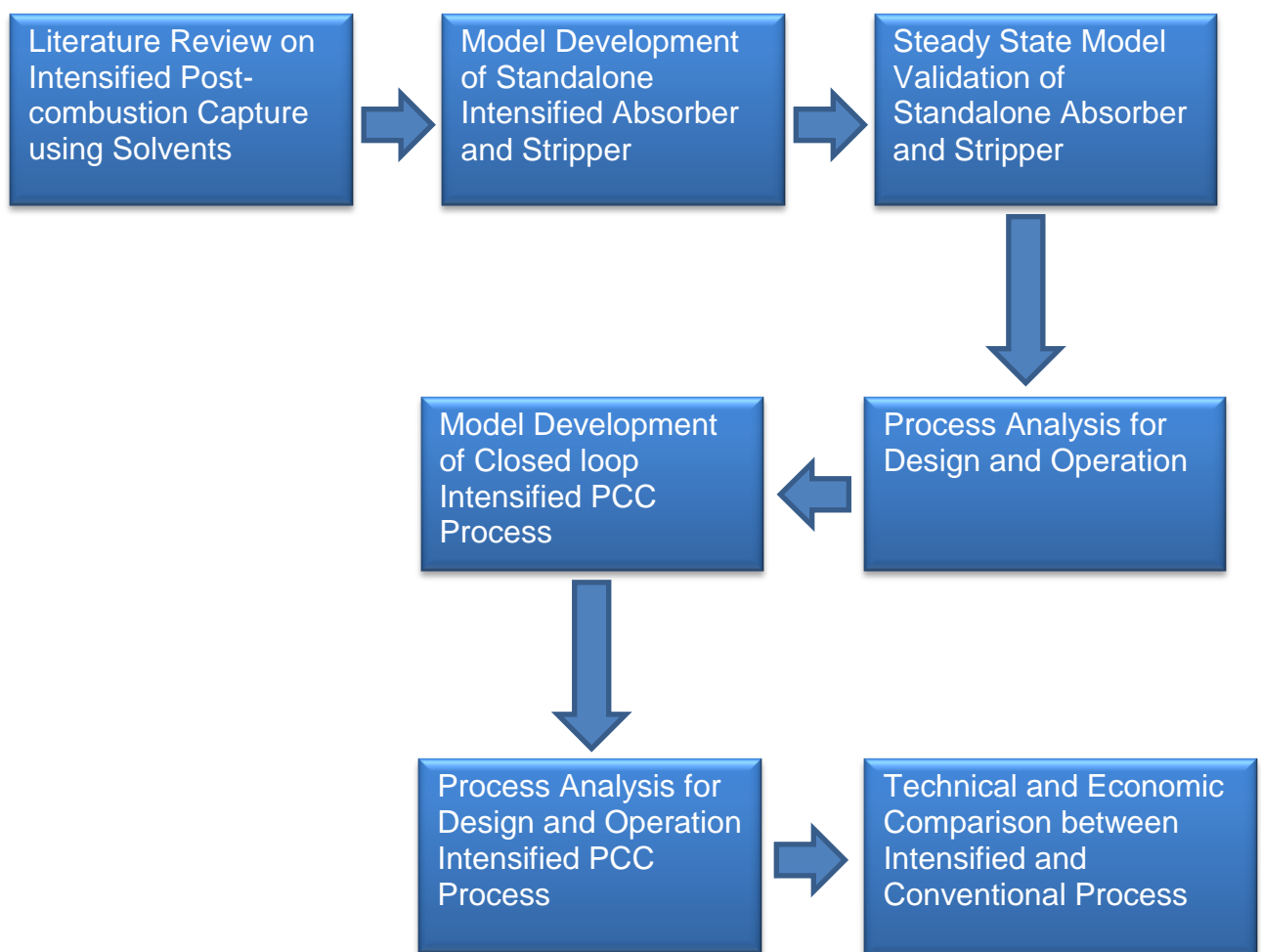


Figure 1-8 Overview of research methodology

1.7.2 Software tools used for the study

1.7.2.1 *Aspen Engineering suite*

Aspen Plus[®] as one of the application software in Aspen Engineering suite is used for this research. Aspen Plus[®] is a process modelling and simulation tool that includes model libraries of various unit operations. In addition, it is equipped with a relatively large physical property database via Aspen properties[®]. This application has the ability to be dynamically linked with intel[®] visual Fortran as explained in **Appendix A**

1.7.2.2 *Intel[®] Visual Fortran*

Fortran is derived from **Formulation Translating System**. It is regarded as general purpose, imperative programming language that is suitable for numerical computation and scientific computing. It is called intel[®] visual Fortran when installed on Windows. Intel[®] visual Fortran compiler has the potential of dynamically linking with Aspen Plus[®] as explained in **Appendix A**.

1.8 Outline of the thesis

This research report contains seven chapters including this chapter (**Chapter 1**).

Chapter 2 focuses on the current status of experimental rigs and experimental studies of RPB absorber and stripper. Different intensified heat exchanger technologies and their suitability for intensified PCC process are discussed. Solvent has a significant influence on the performance of PI process because of its short residence time required. Finally current research activities on modelling and simulation of RPB absorber and stripper are discussed.

In **Chapter 3**, Methodology for model development of the intensified absorber and stripper is presented. These include the physical properties, suitable modelling equations, implementation procedure and finally summary.

Modelling, model validation and process analysis of standalone intensified absorber is presented in **Chapter 4**. This chapter also has comparative studies on conventional and intensified absorber based on size reduction.

In **Chapter 5** modelling, model validation and process analysis of standalone intensified stripper is presented. The model is validated based on two set of experimental data from Newcastle University UK and Tsing Hua University Taiwan.

Also comparison between conventional stripper and intensified stripper is also presented in the chapter.

In **Chapter 6**, process analysis, technical and economic assessments of intensified PCC process are presented. Studies on impact L/G ratio and lean loading on intensified PCC performance are presented. Size reduction, energy consumptions and costs estimation of the plant are also presented.

Finally, conclusions were drawn and recommendations for future work for this thesis were presented in **Chapter 7**

Chapter 2 Literature review

This chapter presents a review on the current status of experimental rigs and experiment studies across the world for RPB absorber in Section 2.1 and RPB stripper in Section 2.2. A review on intensified heat exchanger is presented in Section 2.3. Solvents for intensified PCC process are recommended in Section 2.4. Highlight on current status of modelling and simulation of intensified PCC process is presented in Section 2.5. Finally summary of the review is in Section 2.6.

2.1 RPB Absorber: Current status of experimental rigs and experimental studies

The use of RPB for PCC based on chemical absorption has been explored by a number of research institutions. **Table 2-1** gives a summary of rig specifications for different institutions across the world and their major findings. The rig at Newcastle University UK has a diameter of 1 m and bed thickness of 0.05 m.

Table 2-1 Summary of rig specifications for RPB absorber and findings using the rigs

Institutions	Rig specification	Operating conditions	Results
Newcastle University, UK	Rig 1 geometry: $d_i = 0.156\text{ m}$, $d_o = 0.398\text{ m}$ $h = 0.025\text{ m}$ Packing type: expamet surface area: $2132\text{ m}^2/\text{m}^3$ Void fraction: 0.76	aqueous MEA solutions flowrate (a) 0.35 kg/s (b) 0.66 kg/s MEA concentrations of 30wt%, 55wt%, 75wt% and 100wt%. flue gas flow rate 2.86 kmol/hr	The effect of lean amine temperature, rotor speed, and MEA concentrations were investigated [114].
	Rig 2 geometry: $d_i = 0.190\text{ m}$, $d_o = 1.000\text{ m}$ $h = 0.050\text{ m}$ Packing type: Expamet and stainless wire mesh	Water is used as the solvent for hydrodynamic study in the RPB	The following were some of the target for the research study [132]. (a) Power consumption (b) Pressure drop (c) Liquid distribution
Beijing University of Chemical Technology (BUCT), China	Rig 1 geometry: $d_i = 0.080\text{ m}$ $d_o = 0.200\text{ m}$ $h = 0.031\text{ m}$ Packing type: stainless wire mesh surface area: $870\text{ m}^2/\text{m}^3$ void fraction: 0.95	Benfield solution (DEA-promoted hot potassium carbonate). Mass fraction of K_2CO_3 and DEA in aqueous absorbent was 27% and 4%, rotating speed of 1,300 rpm, liquid flow rate of 79.70 Lh^{-1} , gas flow rate of 0.481 molmin^{-1} , inlet CO_2 concentration of 4.10 mol% and temperature of 356 K	Yi <i>et al.</i> [133] studied effect of rotating speeds, liquid flow rates, gas flow rates and temperatures in RPB, with Benfield solution as the absorbent. End effect was identified in the study which means mass transfer is more at the inlet of the RPB.

	<p>Rig 2 geometry:</p> $d_i = 0.156 \text{ m}$ $d_o = 0.306 \text{ m}$ $h = 0.050 \text{ m}$ <p>Packing type: stainless wire mesh surface area: $500 \text{ m}^2/\text{m}^3$ void fraction: 0.96</p>	<p>NaOH solution at 20–30 °C in the range of 40–120 L/h flow rate and flue gas containing CO₂ and N₂ at flow rate range of 800–12 000 L/h</p>	<p>Luo <i>et al.</i> [134,135] study effective interfacial area and liquid side mass transfer coefficient, in a RPB equipped with blades. Mass transfer rate improve by 8 to 68% compared to conventional RPB without packing.</p>
	<p>Rig 3 geometry:</p> $d_i = 0.020 \text{ m}$ $d_o = 0.060 \text{ m}$ $h = 0.020 \text{ m}$ <p>Packing type: stainless wire mesh, surface area: $850 \text{ m}^2/\text{m}^3$ void fraction: 0.90</p>	<p>The ionic liquid (1-n-butyl-3-methylimidazolium hexafluorophosphate) gas flow rate, 0.6 – 1 L/min, liquid flow rate, 29.2 - 102.2 mL/min</p>	<p>Zhang <i>et al.</i> [136] found that liquid side volumetric mass transfer coefficient for RPB has been improved to around $3.9 \times 10^{-2} \text{ s}^{-1}$ compared with $1.9 \times 10^{-3} \text{ s}^{-1}$ for the conventional packed column under the same operating conditions</p>
<p>Taiwan (National Tsing Hua University, Chang Gung University and Chung Yuan University)</p>	<p>Rig 1 geometry:</p> $d_i = 0.076 \text{ m}$ $d_o = 0.160 \text{ m}$ $h = 0.02 \text{ m}$ <p>Packing type: stainless wire mesh surface area: $803 \text{ m}^2/\text{m}^3$</p>	<p>Flue gas stream containing 10 vol% CO₂. Four different aqueous solutions (DETA solvent, MEA solvent, DETA mixed with PZ, and MEA mixed with PZ). Gas flow rate 30 and 60 L/min. liquid flow rate 50 and 100 mL/min</p>	<p>Yu <i>et al.</i> [137], Tan and Chen [138] Overall mass transfer coefficient ($K_G a$) and HTU corresponding to the most appropriate operating conditions in RPB were found to be higher</p>

	void fraction: 0.96		than 5.8 s^{-1} and lower than 1.0 cm [119]. However HTU is around 40 cm for conventional PCC process
	<p>Rig 2 geometry:</p> $d_i = 0.048 \text{ m}$ $d_o = 0.088 \text{ m}$ $h = 0.120, 0.09, 0.06, 0.03 \text{ m}$ <p>Packing type: stainless wire mesh surface area: 855, 873, 879, 830 m^2/m^3; void fraction of 0.95</p>	<p>$\text{CO}_2\text{-N}_2$ stream containing 10 vol% CO_2. Gas flow rate was varied from 10 to 70 L/min and the liquid flow rate was varied from 0.2 to 0.5 L/min. Three different solvent were used (i) aqueous MEA solution (ii) mixed solvent PZ and MEA (iii) mixed solvent AMP and MEA.</p>	<p>Lin <i>et al.</i> [139] and Lin and Chen [140] reported RPB absorber with flue gas and lean solvent moving in cross flow. Cross flow RPB takes advantage of lower pressure drop and also has mass transfer efficiency comparable to counter-current – flow RPB</p>
India (India Institute of Technology (IIT) Kanpur)	<p>Rig geometry:</p> $d_i = 0.240 \text{ m}$ $d_o = 0.480 \text{ m}$ $h = 0.420 \text{ m}$ <p>Packing type: Ni-Cr metal foam specific surface area: 2500 m^2/m^3 void fraction = 0.9</p>	<p>Gas composition 98 mol% CH_4; 2 mol% CO_2 gas flow rate 2490 kmol h^{-1}, liquid flow rate 3038 kmol h^{-1} (30 wt% DEA)</p>	<p>Agarwal <i>et al.</i> [141], shows that there is good performance in gas phase control processes by enhancing volumetric mass transfer coefficient on the gas side to about 35 – 280 times compared to those of packed columns, the liquid side volumetric mass transfer</p>

			coefficient enhances in the range of 25 – 250 times compared to the packed column [142]
Iran (Process Intensification Research Lab., Chemical Engineering Department, Yasouj University)	<p>Rig geometry:</p> $d_i = 0.06 \text{ m}$ $d_o = 0.12 \text{ m}$ $h = 0.04 \text{ m}$ <p>Packing type: (a) Stainless steel wire mesh (b) Aluminium expamet specific surface area: (a) 1800 m²/m³ (b) 1300 m²/m³ void fraction = (a) 0.9 (b) 0.9</p>	Inlet gas stream contain 5000 ppm CO ₂ concentration. Gas and liquid flow rate were from 10 – 40 L/min and 0.2 – 0.8 L/min respectively. Rotor speed range 400 – 1600 rpm.	Rahimi and Mosleh [143] study height of transfer unit (HTU) of RPB using two different type of packing. The effect of rotational speed, gas flow rate, liquid flow rate and MEA concentration on HTU were studied. HTU values for CO ₂ capture were within 2.4 ~ 4 cm depending on the rotational speed, gas and liquid flow rates, and solution concentration

2.2 RPB stripper: Current status of experimental rigs and experimental studies

There are only two published studies on intensified stripper using the RPB. **Table 2-2** summarizes the rig specifications and their findings (Newcastle University in the UK and National Tsing Hua University in Taiwan). In both groups, the reboiler is the same as that of conventional packed column (i.e. still quite big in size).

Table 2-2 Summary of rig specifications and findings for RPB stripper

Institutions	Rig specification	Process variables	Findings
Newcastle University, UK	Rig geometry: $d_i = 0.156\ m$ $d_o = 0.398\ m$ $h = 0.025\ m$ Packing type: expamet surface area: 2132 m^2/m^3 Void fraction: 0.76	Three rich solvent MEA concentration (i.e. 30 wt%, 54 wt% and 60 wt%) was used. Solvent flow rate range from 0.2 kg/s to 0.6 kg/s	Conventional packed column was compared with RPB under similar performance and it was found that the height and diameter has reduction factor of 8.4 and 11.3 respectively [114].
National Tsing Hua University, Hsinchu, Taiwan	Rig geometry: $d_i = 0.076\ m$ $d_o = 0.160\ m$ $h = 0.020\ m$ Packing type: wire mesh surface area: 803 m^2/m^3 Void fraction: 0.96	Two solvents were used (1) blended 20 wt% DETA + 10 wt% PZ aqueous solution (2) 30 wt% MEA aqueous solution. Rich solvent flow rate 400 mL/min	Back pressure regulator was introduced in order to operate the stripper at higher temperature and pressure. The result shows that specific energy consumption with RPB is less than conventional packed column [120].

2.3 Intensified heat exchanger

In conventional PCC process, there is a cross heat exchanger. This is huge in volume. In addition to this, the piping surrounding the cross heat exchanger has high footprint. Therefore, the cross heat exchanger should be intensified so as to have smaller footprint, high heat transfer rate and possibly combining units function.

2.3.1 Technologies available to choose

2.3.1.1 Printed Circuit Heat Exchanger (PCHE)

The PCHE was invented in 1980 in Australia and applied to refrigerators in 1985 by Heatric (UK) [144]. The PCHE is a high-integrity plate type compact heat exchanger in which fluid flow channels are produced by chemical etching on flat metal plates. Etched plates are stacked to produce single block by diffusion bonding [144-147].

Because of the compactness provided by PCHE design, the volume of PCHEs are typically 4–6 times smaller and lighter than conventional shell-and-tube heat exchangers designed for the same thermal duty and pressure drop as shown in **Figure 2-1** [148,149]. Low pressure drop in PCHE can be found based on design (i.e. air-foil fin PCHE and zigzag channel PCHE). Kim *et al.* [146] compared air-foil fin PCHE and zigzag channel PCHE which have the same heat transfer performance but the pressure drop of airfoil fin PCHE is one-twentieth of zigzag PCHE. PCHE effectiveness was reported to be more than 98% and can operate at maximum allowable pressure of 600 bar and more than 800 °C maximum operating temperature (limited by material of construction). PCHE has multi-fluid capability (intensification achieved by reducing the number of exchanger units) [149]. Heatric Ltd [150] reported that PCHE has lower capital and operating cost compared to shell and tube heat exchanger due to reduced amount of coolant required (i.e. reducing by about 55%).



Figure 2-1 Printed Circuit Heat Exchanger (Courtesy of Heatric Ltd): the big one at the back is shell-and-tube heat exchanger; while the small one in front is PCHE.

2.3.1.2 Formed Plate Heat Exchanger (FPHE)

The FPHE uses the same concept as various fin plate heat exchangers, but adds the advantage of replacing the brazing process (i.e. lower operation temperature and there is grain formation) with the diffusion-bonding process. This is shown in **Figure 2-2**. Heatric Ltd reported that FPHE has bigger channels size (about 3mm x 3mm) than the PCHE, this leads to lower pressure drop than PCHE [149]. FPHE has effectiveness of more than 98%. Maximum allowable pressure for FPHE is 200 bar and can operate at higher temperature of up to 800 °C, it has multi-fluid capability (Intensification by reducing number exchanger units)[149].

2.3.1.3 Hybrid Heat Exchanger (H²X)

H²X technology developed by Heatric Ltd combines the etched plates and the formed fins to form what is known as Hybrid Heat Exchanger [149]. The heat exchanger takes some of the advantages offered by PCHE and FPHE. H²X has bigger hydraulic diameter than PCHE because of the presence of FPHE and can also withstand higher pressure than FPHE because of the advantage offered by the presence of PCHE. Typical hydraulic diameter of PCHE is in the range of 0.1 mm to 3 mm while that of FPHE is in the range of 1.2 mm to 3.3 mm [149].

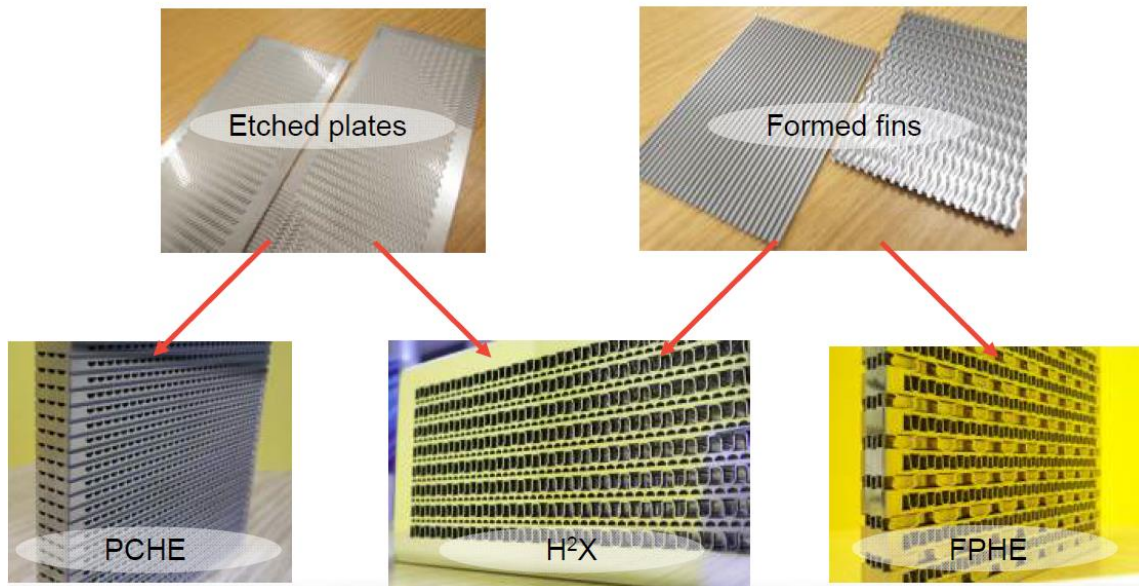


Figure 2-2 Summary of technology of PCHE, H²X, and FPHE (Courtesy of Heatric)

2.3.1.4 The Marbond heat exchanger

The manufacturing procedures of Marbond heat exchanger are similar to those of the PCHE. It is made of slotted flat plates which have been chemically etched through. The plate pack is then diffusion-bonded together [151,152]. Unlike PCHE the Marbond heat exchanger is

designed with several thinner, slotted plates and typically stacked together to form a single sub-stream, thus giving the potential for very low hydraulic diameters [151]. **Figure 2-3** shows an inside view of the Marbond heat exchanger. In some applications, it has a substantially higher area density than the PCHE. For example, a doubling of porosity, other factors being equal, results in a halving of the volume for a given surface area [153]. The challenge is that Marbond heat exchanger has high pressure drop. Compared to plate heat exchanger, Marbond heat exchanger pressure drop can increase up to 50% at high mixing intensities [154]

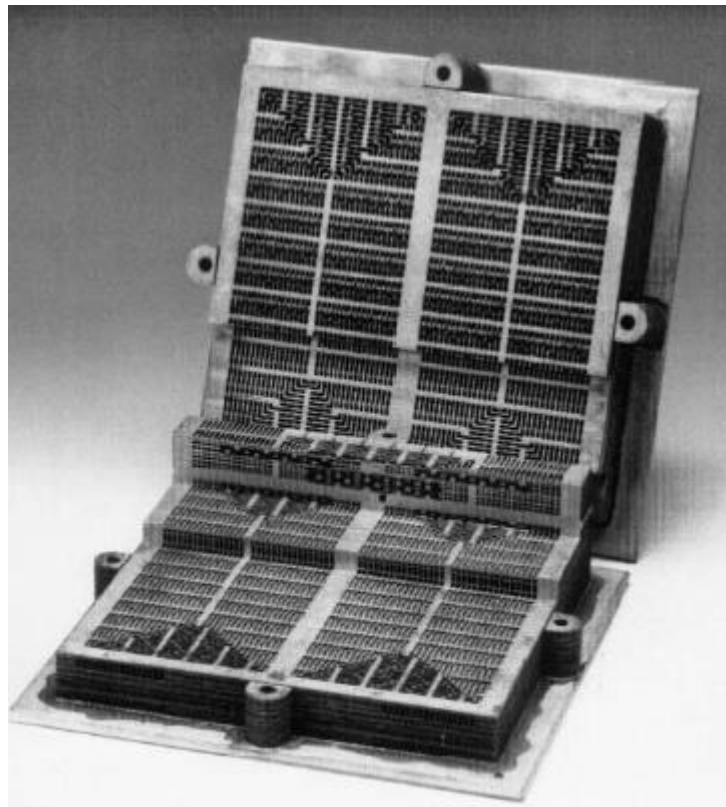


Figure 2-3 The Chart Marston Marbond compact heat exchanger (Courtesy Chart Marston Ltd.)

2.3.1.5 *Spiral heat exchanger (SHE)*

SHE refers to a helical tube configuration. The term refers to a circular heat exchanger with two long metal strips of plate rolled together to form a pair of concentric spiral channels of rectangular cross-section, one for each fluid. The passages can be either smooth or corrugated, in some cases studs are welded onto one side of each strip to fix the spacing between the plates, to provide mechanical strength and to induce turbulence that increases heat transfer [155].

The internal void volume is lower (less than 60%) than in a shell-and-tube heat exchanger [155], and this yields a compact and space-saving construction that can be readily integrated in any plant and reduces installation costs. The heat transfer surface ranges from 0.05 m² for refrigeration applications up to about 500 m² with a maximum shell diameter of 1.8 m and the sheet metal thickness range is 1.8–4 mm for industrial processes [156]. The surface area requirement is about 20% lower than that for a shell-and-tube unit for the same heat duty [155]. SHEs are often used in the heating of high viscosity and dirty fluids. SHE exhibits lower tendency to fouling, this is because when fouling start to build-up the flow area decreases and since entire flow must pass through it this lead to increase in the local flow velocity thereby causing scrubbing effect that flushes away any accumulated deposit that forms, also because of the turbulence nature of the flow both spiral flow and continuous curving passages occurs with no room for fouling growth [157]

Maintenance (i.e. cleaning) for SHE is not difficult, because all the heat transfer surfaces are readily accessible by simply removing the heads [157]. Figure 2-4 shows typical Alfa Laval Spiral heat exchanger internal fluid flows.



Figure 2-4 Spiral heat exchanger (courtesy of Alfa Laval) [158]

2.3.2 Recommendation for intensified heat exchanger for PCC application

To make a decision on best intensified heat exchanger to be used for PCC application, many factors need to be considered. Some of them are listed as follows [148]: (a) Operating pressure limits; (b) Thermal performance (also known as the effectiveness of the heat exchanger); (c) Expected working temperature range; (d) Product mix to be used in the exchanger (liquid-to-liquid or gas-to-gas); (e) Pressure drop desired across the expected heat exchanger; (f) The expected fluid flow capacities over both sides of the heat exchanger; (g) Method of cleaning employed, maintenance and repair issues associated with heat exchanger; (h) Materials required for construction; (i) Ease of expansion of exchanger when it becomes necessary; (j) The cost of the heat exchanger .

Compromise would therefore have to be made in most cases when selecting a heat exchanger. For instance, cost of the exchanger is a paramount factor, but it should not be the determining factor. If just for a cheaper heat exchanger, certain desired performance demands of the heat exchanger would have to be forfeited.

The author believe that the PCHE and the Marbond heat exchanger look promising for use in intensified PCC process because of its many benefits such as high efficiency (>98%), Compactness to improve controllability and economics, weight saving, high temperature and retrofit options [149,151,152]. PCHE has been reported to have additional advantage of being multi-fluid, meaning it can be used for preheating of rich-MEA stream and also as a condenser for CO₂ – stream.

2.4 Solvents for intensified carbon capture process

There are extensive studies in solvent selection from both academia and industry trying to identify alternative solvents for conventional PCC process. There are studies on PI using different solvents [114-116,133-137,139,140,159-161].

2.4.1 Factors to consider

Factors to consider when conducting solvent screening for conventional PCC process and intensified PCC process is similar to some extent but the major difference comes from residence time of solvent in both technologies. In intensified PCC process, the residence time is relatively short (less than 10% of the conventional PCC process). Therefore the factors to consider are: (1) CO₂ absorption reaction kinetics, (2) CO₂ absorption capacity, (3) heat of absorption, (4) solvent toxicity, (5) solvent volatility, (6) solvent corrosivity, (7)

solvent degradation, (8) solvent foaming, (9) solvent viscosity, (10) solvent surface tension and (11) cost.

(1) CO₂ reaction kinetics: This determines the rate at which CO₂ will be captured. Fast reaction kinetics are essential for intensified PCC processes since the residence time is very short.

(2) CO₂ absorption capacity: This is related to the solvent flow rate required and the sensible heat requirement. Higher CO₂ absorption capacity would require lower solvent flow rate and subsequent less regeneration energy demand.

(3) Heat of absorption: This would be an important factor affecting reboiler heat duty. Lower heat of absorption will require less regeneration energy input to reverse the chemical reaction and release absorbed CO₂.

(4) Solvent stability, operational issues and environmental impact: These are the other factors to be evaluated when selecting solvents. Solvent degradation (which may be controlled by having high chemical and thermal stability) and corrosion will increase operation and maintenance (O&M) costs due to high solvent make up rate and shorter equipment lifetime. Higher solvent viscosity would increase the pump work in circulating the solvent between the absorber and regenerator. Cost and availability of potential solvents in commercial scale could contribute to limitations of the process feasibility. Environmental impacts such as solvent toxicity and volatility deserve serious attention when judging the potential of a solvent since causing secondary pollution while capturing CO₂ is not a scenario the public would be willing to consider.

Other solvent characteristics such as surface tension and foaming tendency are also important factors to consider when judging a solvent's potential. **Table 2-3** gives evaluation of solvent properties based on relative importance on a scale of 0 to 10, with 10 being the most important property and 0 the least important property [162]. These may provide insights for solvent selection in intensified PCC process.

Table 2-3 Evaluation of solvent properties [162]

Property	Importance	Potential Show-stopper	Evaluation Methods
Reaction kinetics	10	Yes	Literature, wetted-wall column(WWC)
Absorption capacity	10	Maybe	Calculation from VLE and Chemical reactions
Heat of absorption	10	Yes	Literature, Calorimetry Measurement, Calculation from VLE
Toxicity	6	Yes	Literature/material safety data sheet(MSDS)
Volatility	4	Yes	Literature
Corrosivity	6	Maybe	Literature, Laboratory Test
Degradation	6	Yes	Literature, Laboratory Test
Foaming	4	Maybe	Literature
Viscosity	4	Yes	Literature, Pilot Test
Surface tension	6	Maybe	Literature
Cost	2	Maybe	Vendor

2.4.2 Solvents used

Different solvents were used for intensified PCC process by different research groups. Some researchers use one solvent while others mix solvents so as to benefit from the properties each solvent offers.

2.4.2.1 Alkanolamine

The use of MEA for CO₂ capture in RPB was reported in Jassim *et al.* [114]. MEA has high reactivity but is rapidly replaced by more efficient solvents because of its corrosive nature, toxicity and high heat of reaction with CO₂. Diethanolamine (DEA) reacts more slowly with CO₂. As a result, it is not good for intensified PCC process. Methyldiethanolamine (MDEA) has become an important alkanolamine because of its low energy requirement, high capacity and high stability but has the disadvantage of low rate of reaction with CO₂. Lin *et*

al., [139] presented a study on the evaluation of various alkanolamine solutions for CO₂ removal in cross-flow RPB. The reaction rate of these solvents with CO₂ followed the order of Piperazine (PZ) > MEA > 2-amino-2-methyl-1-propanol (AMP).

Yu *et al.* [137] reported study on CO₂ capture by alkanolamine solutions containing diethylenetriamine (DETA) and PZ in RPB. They found that the CO₂ capture efficiency of DETA in terms of overall mass transfer coefficient $K_G a$ and HTU was superior to that of MEA in RPB. This is because DETA possesses higher CO₂ absorption capacity and reaction rate with CO₂ than MEA. Higher boiling point and lower vapour pressure of DETA will lead to lower energy requirement and less loss of solvent in stripper compared with MEA, suggesting DETA as a promising solvent to substitute MEA for CO₂ capture. The mixed solution DETA + PZ exhibited higher CO₂ capture efficiency than DETA indicating PZ was a great promoter for capturing CO₂. This was because the promoter PZ possesses higher reaction rate with CO₂ than DETA [137].

2.4.2.2 NaOH

Munjaj *et al.* [163] reported the use of NaOH for absorption of CO₂. Their study shows that the gas-liquid mass transfer could be improved. Lin *et al.* [164] compared the overall volumetric mass-transfer coefficient ($K_G a$) of RPB for different solvents (i.e. NaOH, MEA and AMP) and found that $K_G a$ values for the CO₂-MEA system were approximately 2-5 times higher than those for the CO₂-AMP system also $K_G a$ values for MEA were at least 20% higher than those for NaOH at the same operating conditions. Therefore rate of reaction for CO₂ capture in RPB follows the order MEA > NaOH > AMP [165]. But AMP has higher absorption capacity than MEA. Lin and Chen [81], Luo *et al.* [135] studied chemisorption's of CO₂ using NaOH in RPB. They found that NaOH has the potential for use as solvent in RPB, but one of the major challenges is the formation of stable salt which make solvent regeneration difficult. Comparing NaOH with MEA and AMP, it was found to have superior CO₂ absorption capacities and inferior mass transfer rates [166].

2.4.2.3 Ionic liquid (1-n-butyl-3-methylimidazolium hexafluorophosphate)

The use of ionic liquids for CO₂ capture is gaining interest due to their unique characteristics (i.e. thermal stabilities, negligible vapour pressures up to their thermal decomposition points, tunable physicochemical properties and high CO₂ solubility) [136,167]. However, ionic liquids have high viscosity with poor fluidities. A significant limitation for large-scale application of a continuous CO₂ capture process for conventional packed columns by ionic liquid is the high resistance to mass transfer and consequently low gas – liquid mass

transfer rate due to the high viscosity. As reported in Chen *et al.* [124], the dependence of volumetric mass transfer coefficient ($k_L a$) on liquid viscosity in RPB is less than that of packed column, this is because the rotation leads to droplet and thinner film layer thereby increasing the wetted area of the packing while in conventional packed column the wetted area decreases at high viscosity leading to decrease in mass transfer.

2.4.2.4 Potassium Carbonate (K_2CO_3)

The use of K_2CO_3 is receiving great attention because of its high CO_2 absorption capacity. Firstly, K_2CO_3 is a more efficient solvent for CO_2 than either MEA or DEA [168]. This means that for a given amount of solvent, K_2CO_3 can absorb more than the other two solvents. In addition, the cost of this solvent is lower because less is needed and K_2CO_3 is cheaper [168]. Secondly, with K_2CO_3 , the cross heat exchanger is eliminated as the stripper runs at lower temperature than the absorber [168]. Lastly K_2CO_3 is not volatile, which means minimal losses of the solvent with the exit gas occur. Since K_2CO_3 is not prone to the degradation reactions associated with MEA, there is no loss of solvent associated with degradation [169]. However one of the major drawbacks of using K_2CO_3 in RPB is its low rate of reaction. This necessitated the need for promoter so as to increase its rate of reaction. Kothandaraman *et al.* [169] reported regeneration energy (without energy recuperation) of 3.2 MJ/kg for K_2CO_3 when treating flue gas (12 vol% CO_2).

2.4.2.5 Benfield solution (Amine-promoted hot K_2CO_3 solution)

Amine-promoted hot K_2CO_3 solution, which is called Benfield solution, is used in Benfield process [170]. The amine promoter could significantly enhance the reaction rate while the carbonate–bicarbonate buffer offers advantages of large capacity for CO_2 capture and ease of regeneration [133,170]. Pilot plant studies by Field *et al.* [171] shows that hot-carbonate system is particularly effective for removing CO_2 , especially when present at high partial pressure. Steam consumption is one-third to one-half that of ethanolamine. Therefore, Benfield Process is known as an economic and efficient way of removing large quantities of CO_2 from flue gases and can be effectively used in RPB [133].

2.4.2.6 Piperazine (PZ)

PZ is a diamine solvent whereby one amine group is involved in a fast reaction with CO_2 to form the carbamate while the other amine absorbs the released proton [172]. PZ reacts rapidly with CO_2 and thus has attracted interest for usage in CO_2 capture, particularly as a reaction rate promoter for CO_2 absorption in carbonate and tertiary amine solutions

[159,172-175]. Chemical reactions which describe the absorption of CO₂ in PZ solutions are more complex than MEA [172,173].

Reaction rate between CO₂ and aqueous PZ solution is high [159,173-175]. However, the absorption has to take place at high temperatures because its solubility in water is limited [174]. Freeman *et al.* [173] suggested the use of concentrated PZ solution for CO₂ capture because of its effective resistant to oxygen degradation and thermal degradation. Despite its high reactivity with CO₂, it has some challenges such as limited solubility in water, more volatile than MEA and also more corrosive than MEA

2.4.3 Proprietary commercial solvents

To avoid high thermal efficiency penalty due to high regeneration energy, new solvents were developed and commercialised. Econamine FG+ is MEA-based solvent with proprietary inhibitors [176,177]. Sander and Mariz [176] reported resultant solution circulation factor (m³ solvent per m³ Econamine FG+ solvent) for Econamine FG+ solvent as 1 while 18wt% MEA solvent has 1.7. The Kansai Electric power Co. and Mitsubishi Heavy Industries, Ltd. have developed new aqueous solutions of sterically-hindered amines designated as KS-1, KS-2 and KS-3 [178-180]. The world's largest commercial PCC plant (Petra Nova/NRG 240 MWe W.A. Parish project) plan to use KS-1 solvent when commissioning in 2016 [86]. The first commercial CCS plant (SaskPower's Boundary Dam 139 MWe project) uses Consolv solvent [84], the solvent is based on tertiary amines, and includes a promoter to yield sufficient absorption rates for low pressure flue gas streams. H3 solvent is Hitachi's proprietary solvent formulation which has much lower regeneration energy compared with MEA [181]. Regeneration energy and thermal efficiency penalty for different proprietary commercial solvents were compared in **Table 2-4**.

Table 2-4 Performance of some proprietary commercial solvents [15]

Solvent	Regeneration Energy (GJ/t-CO ₂)	Efficiency penalty (%)	References
Econmaine FG+	3.12	9.2	IEAGHG [182]
KS-1	3.08	8.4	IEAGHG [182]
KS-2	3.0	9.3	Gibbins and Crane [183]
CANSOLV	2.33	8.2	Just [184], Shaw [185]
H3	2.8	7.8	Wu <i>et al.</i> [181], Stover <i>et al.</i> [186]

2.4.4 Recommendations on solvent selection for PCC process

Selection of solvents for CO₂ capture process is a very important design decision for both conventional and intensified PCC processes. Firstly, the residence time in the intensified PCC process is less than 10% of the conventional PCC process. Therefore solvent for intensified PCC process should have fast kinetics to capture CO₂. That is why most studies on RPB absorber uses primary or secondary alkanolamines due to their fast kinetics. Concentration of the solvent in RPB is usually high in order to have high reaction rate. High concentration solvent generally has high viscosity, which prevents its use in conventional PCC process. However, this is not a problem in RPB case. Secondly to ensure high CO₂ absorption capacity and rapid reaction kinetics, mixing solvents such as amine-promoted K₂CO₃ will play a significant role. Thirdly the regeneration energy of solvents should be low in addition to fast kinetics and high absorption capacity. Oexmann *et al.* [187] reported mixing MDEA and PZ gives lower regeneration energy of 2.52 GJ/t-CO₂. Lastly when an intensified PCC plant is to be built in a place not far from residential area, volatility of the solvent will have big impact on whether or not the project will be permitted.

2.5 Current status of modelling and simulation of RPB absorber and stripper

Process models validated against experimental data from small scale rigs can be used to scale up and predict the performance of RPB for PCC at commercial scales.

2.2.1 Modelling/simulation of intensified absorber

There are some studies in the open literature that discuss the modelling and simulation of an intensified absorber. The group in Taiwan modelled the RPB as a series of continuous stirred tank reactors (CSTR). Cheng and Tan [119] reported that five CSTRs with a contactor can achieve the set target for a given case through simulation study. The research group at University of Hull, UK reported modelling and simulation of RPB absorber using Aspen Plus[®] and visual FORTRAN [115,116]. Their key findings include: (a) the packing volume can be reduced 52 times and the absorber size can be reduced 12 times; (b) there is no temperature bulge, due to the heat released by CO₂ absorption, is observed inside the packing [115,116].

2.2.2 Modelling/simulation of intensified stripper

Experimental studies of intensified stripper were only reported in Jassim *et al.* [114] and Cheng *et al.* [120]. No modelling and simulation of intensified stripper for PCC process has been reported in open literature.

2.2.3 Modelling and simulation of the whole plant

No modelling or simulation studies of the whole intensified PCC process have been published in the open literature at the time of this study.

2.6 Summary

The review of the literatures shows that there are many experimental studies of RPB as an intensified absorber for carbon capture, but just two papers reported the use of RPB as an intensified stripper for carbon capture.

Modelling and simulation studies of intensified absorber was reported by just few research groups while no report of modelling and simulation of intensified stripper for PCC process.

A lot of studies have been done on experimental studies and modelling of intensified heat exchangers but its application to intensified carbon capture process is still not yet implemented.

Solvents for intensified PCC process application have been reported by few researches for RPB absorber but quantifying the regeneration energy implications in the RPB stripper is not yet studied.

No systematic study on modelling, simulation, technical and economic performance assessment of closed loop intensified capture process based on RPB technology reported in any open literature.

Chapter 3 Methodology for model development of intensified absorber and stripper

Chapter 3 presents the methodology used in modelling standalone intensified absorber and stripper. Section 3.1 describe the modelling of mass and heat transfer based on two film theory. In Section 3.2 rate based model development is highlighted to describe the material and the energy balances. Section 3.3 highlights the importance of physical properties in modelling intensified PCC process. Correlations suitable for intensified PCC process are presented in Section 3.4. The method use in solving the system of differential equations in the rate based model is highlighted in Section 3.5. Model development implementation procedure is highlighted in Section 3.6. Modelling of the intensified absorber and intensified stripper follows the same procedure, therefore modelling implementation procedure is use for both.

3.1 Modelling mass and heat transfer

The rate based model in the Aspen Plus[®] uses two film theory model. To describe such a process accurately, it is necessary to develop mathematical models taking into account the material balances, energy balances, mass transfer, heat transfer, phase equilibrium and summation equations. The influence of chemical reactions on mass transfer cannot be neglected. From **Figure 3-1**, the model will include ideally mixed vapour and liquid bulk phases and two film regions adjacent to the interface.

The two-film theory assumes that the liquid and vapour phases both consist of film and bulk regions. Heat and mass transfer resistances are assumed to be restricted to these laminar film regions [188]. The rest of the bulk liquid and vapour is assumed to have a uniform composition based on agitation. There is no convection in the film, and dissolved gases cross these regions by molecular diffusion alone [188]. The rate of mass transfer is affected by the film thickness, which in turn depends on the liquid agitation, geometry, and physical properties [188]. Although the model theory is not very realistic, its predictions are usually remarkably similar to those based on more sophisticated models [188,189].

Mass transfer in the two-film theory model could be described based on Fick's law or Maxwell-Stefan formulation. The Maxwell-Stefan formulation is well suited for modelling

mass transfer under these conditions but Fick's law is not suitable for this application because its assumptions are valid only for [190]:

- Binary mixtures or dilute components in a multicomponent mixture – chemical absorption of CO₂ in MEA is from a multicomponent mixture where CO₂ concentration may reach significant levels.
- Diffusion in the absence of electrostatic force fields – amine solvents are ionic and as such electrostatic force fields exist.

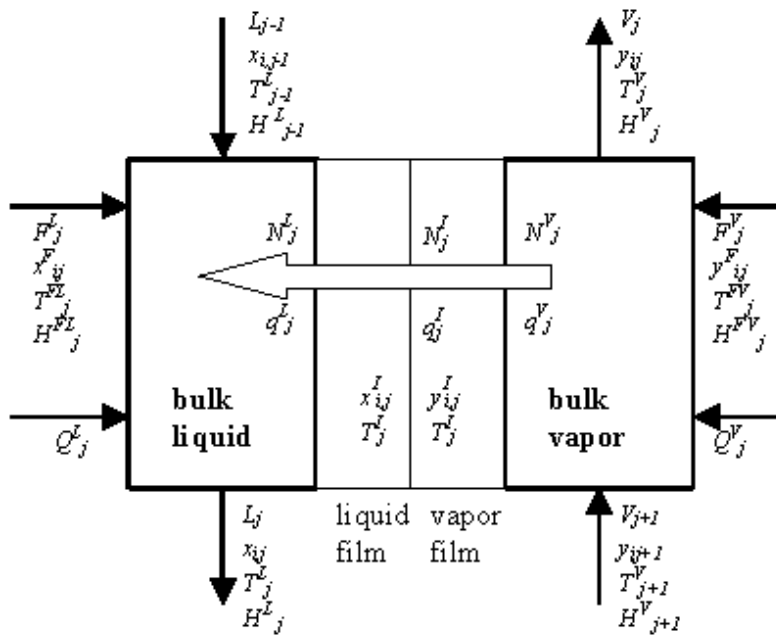


Figure 3-1 Two-film model for a differential packing segment

3.2 Rate-based model development

In the rate-based approach, actual rates of multi-component mass and heat transfer as well as chemical reactions are considered directly [191]. The process is described using the two-film theory and mass transfer rates are calculated using the Maxwell-Stefan formulation. Heat and mass transfer resistances are modelled in the liquid and vapour films.

The following assumptions were used in developing this steady state model:

- Linear pressure drop along the column.
- No accumulation in liquid and vapour films as well as in the bulk vapour.
- Phase equilibrium at interface between liquid and vapour films.

- Negligible solvent degradation.
- Assume that the difference between the outer and inner radius ($r_o - r_i$) in RPB is same as the height of column in conventional packed column.
- Gas and liquid flow only in the radial coordinate (i.e. axial height of the column in conventional packed bed)
- All reactions occurs in a liquid phase
- Negligible heat loss to the surroundings
- Ideal gas phase (due to low pressure)

3.2.1 Gas and liquid phase material balances

Mass balances for gas and liquid phase in the RPB are described by **Equations 3.1 and 3.2** [68].

Material balances for gas phase:

$$\varepsilon_g \frac{dC_i^g}{dt} = -C_i^g \frac{\partial u_g}{\partial r} - u_g \frac{\partial C_i^g}{\partial r} - a_{g/l} N_i \quad 3.1$$

Material balances for liquid phase:

$$\varepsilon_l \frac{dC_i^l}{dt} = -u_l \frac{\partial C_i^l}{\partial r} - a_{g/l} N_i \quad 3.2$$

Where ε_g and ε_L are the gas and liquid holdup, estimation of molar fluxes (N_i) for component i to and from liquid bulk is done in the liquid film model. $a_{g/l}$ is the gas-liquid interfacial area, C_i^l is the concentration of component i , u_g and u_l are the gas and liquid velocities, r is the radius of RPB. While the liquid velocity is constant, the gas velocity is calculated from the total mass balance for the gas phase:

$$\frac{dF_g}{dr} = -a_{g/l} A \sum N_i \quad 3.5$$

F is the total molar flow rate and A is the cross-sectional area given by $2\pi rZ$ where Z is the RPB axial height. It is assumed that ideal gas law is applicable. Therefore the total mass balance is given as:

$$\frac{du_g}{dr} = -\frac{u_g}{P} \frac{\partial P_g}{\partial r} + \frac{u_g}{T} \frac{\partial T_g}{\partial r} - \frac{a_{g/l}}{C_{tot}^g} \sum N_i \quad 3.4$$

3.2.2 Gas and liquid phase energy balances

Energy balances for gas phase:

$$\varepsilon_g \frac{dT_g}{dt} = -u_g \frac{\partial T_g}{\partial r} + \frac{a_{g/l}}{\sum(C_i C p_i)_g} h_{g/l} (T_l - T_g) \quad 3.5$$

Energy balances for liquid phase:

$$\varepsilon_l \frac{dT_l}{dt} = -u_l \frac{\partial T_l}{\partial r} - \frac{a_{g/l}}{\sum(C_i C p_i)_l} (h_{g/l} (T_l - T_g) - \Delta H_r N_{CO_2} - \Delta H_{vap} N_{H_2O}) \quad 3.6$$

Where Cp_i is the heat capacity for component i , $h_{g/l}$ is the interfacial heat transfer coefficient, ΔH_r is the heat of absorption (desorption) of CO_2 and ΔH_{vap} is the heat of vaporisation of H_2O .

Heat transferred between the two phases due to temperature differences is the first in the bracket of **Equation 3.6**, the second term represents the heat released due to CO_2 absorption and reaction in the aqueous MEA solution, the third term represents the heat released or absorbed due to H_2O condensation or vaporization.

3.3 Physical property

3.3.1 Thermodynamic properties

The design of gas treating processes, whether equilibrium-based or rate-based, fundamentally depends on the availability of an appropriate thermodynamic model that can accurately interpolate and extrapolate experimental thermodynamic data for the given system [192-194]. If process simulation is to be successful, then the availability of an appropriate thermodynamic model for the system of interest becomes critical and indispensable [193,195]. The thermodynamic model covers phase and chemical equilibria and heat of absorption.

Phase equilibria is attained when the chemical potential of each of the species is the same in all the phases present in a given system, in addition to uniform temperature and pressure [196]. It governs the distribution of molecular species between the vapour and liquid phases in an equilibrium mixture. Ionic species on the other hand are treated as non-volatile and therefore assumed to be present in the liquid phase only [192,197]. Chemical equilibrium governs the balance of ionic and molecular species in the liquid phase. It has a strong influence on the phase equilibria.

In the RPB model, the important thermodynamic properties namely fugacity coefficient and activity coefficient, Henry's constant, Heat of absorption, chemical equilibrium constant are calculated using correlations within eNRTL thermodynamic model in Aspen Properties[®] with modifications using VLE data for high solvent concentration (>30 wt% MEA) obtained from Aronu *et al* [198] and Mason and Dodge [199] bearing in mind that the correlations are based on 30 wt% or less MEA concentration

3.3.2 Transport properties

The transport properties include density, viscosity, surface tension, thermal conductivity, and binary diffusivity [200]. A summary of selected models in Aspen Plus[®] that can be used for transport properties calculations is given in **Table 3-1**. Validation of these models before using it for PI is important because PI is usually operated with higher concentration solvent.

Table 3-1 Summary of the models in Aspen Plus[®] for transport properties calculations [201]

Property	Gas Phase	Liquid Phase
Density	COSTALD model by Hankinson and Thomson [202]	Clarke density model
Viscosity	Chapman-Enskog model with Wilke approximation	Jones-Dole model
Surface tension		Onsager-Samaras model
Thermal conductivity	Stiel-Thodos model with Wassiljewa-Mason-Saxena mixing rule	Reidel model
Binary diffusivity	Dawson-Khoury-Kobayashi model	Nernst-Hartley model (for mixtures with electrolytes)
	Chapman-Enskog Wilke-Lee model	Wilke-Chang model (for molecular species)

3.4 Correlations suitable for RPB

3.4.1 Liquid phase mass transfer coefficient

Liquid phase mass transfer coefficient equation in an RPB was proposed by some researches such as Tung and Mah [203], Chen et al.[123] and Rajan et al. [142]. For the purpose of this study two different correlations were selected, the one proposed by Tung and Mah [203] and the one proposed by Chen et al [123].

Tung and Mah [203] correlation was developed based on penetration theory to describe the liquid mass transfer behaviour in the RPB (i.e. Equation 3.1).

$$\frac{k_L d_p}{D_L} = 0.919 \left(\frac{a_t}{a} \right)^{1/3} Sc_L^{1/2} Re_L^{2/3} Gr_L^{1/6} \quad (3.1)$$

where k_L is the mass transfer coefficient of liquid, d_p is the diameter of packing pore, D_L is the diffusion coefficient of liquid, a_t is the total specific surface area of packing, a is the gas-liquid interfacial area, Sc_L is the liquid Schmidt number, Re_L is the liquid Reynolds number and Gr_L is the liquid Grashof number.

In developing Equation 3.1 the following assumptions were made (a) Coriolis acceleration is assumed negligible (b) Effect of geometry of the packing material is negligible. This is why there is a need for an alternative correlation for liquid phase mass transfer coefficient.

Chen *et al.* [123] developed liquid phase mass transfer correlation considering end effect and packing geometry. The correlation was found to be valid for different sizes of the RPBs and for viscous Newtonian and non-Newtonian fluids. Because of these advantages, Equation 3.2 is suggested for use in calculating the liquid phase mass transfer coefficient, and also findings from Joel *et al.* [116] suggested the use of Equation 3.2 because of its smaller error prediction.

$$\frac{k_L a d_p}{D_L a_t} \left(1 - 0.93 \frac{V_o}{V_i} - 1.13 \frac{V_i}{V_t} \right) = 0.35 Sc_L^{0.5} Re_L^{0.17} Gr_L^{0.3} We_L^{0.3} \left(\frac{a_t}{a_p'} \right)^{-0.5} \left(\frac{\sigma_c}{\sigma_w} \right)^{0.14} \quad (3.2)$$

where V_i is the volume inside the inner radius of the bed, V_o is the volume between the outer radius of the bed and the stationary housing, V_t is the total volume of the RPB, We_L is the liquid Webber number, a'_p is the surface area of the 2 mm diameter bead per unit volume of the bead, σ_c is the critical surface tension and σ_w is the surface tension of water.

3.4.2 Gas-side mass transfer coefficient

Onda *et al.* [204] correlation for calculating gas-side mass transfer coefficient (Equation 3.3) developed for conventional packed column has been proposed to be valid for RPB [205]. Sandilya *et al.* [205] suggested that the gas rotates like a solid body in the rotor because of the drag force caused by the packing. Consequently the gas-side mass transfer coefficient is predicted to be similar to that in a conventional packed column. However this did not account for end effect and packing effect [206].

$$k_G = 2.0(a_t D_G) Re_G^{0.7} Sc_G^{1/3} (a_t d_p)^{-2} \quad (3.3)$$

where k_G is the gas phase mass transfer coefficient, D_G is the diffusivity coefficient of gas, Re_G is the gas Reynolds number and Sc_G is the gas Schmidt number.

Chen [206] presented local gas-side mass transfer coefficient correlation using two-film theory for RPB (Equation 3.4). Equation 3.4 for calculating the gas phase mass transfer coefficient was used in the model because it accounts for the effect of rotation of the RPB, end effect and packing geometry.

$$\frac{k_G a}{D_G a_t^2} \left(1 - 0.9 \frac{V_o}{V_t}\right) = 0.023 Re_G^{1.13} Re_L^{0.14} Gr_G^{0.31} We_L^{0.07} \left(\frac{a_t}{a'_p}\right)^{1.4} \quad (3.4)$$

Where Gr_G is the gas Grashof number

3.4.3 Total gas-liquid interfacial area

Total gas-liquid interfacial area correlation for conventional packed column was developed by Onda *et al.* [204] as shown in Equation 3.5. Equation 3.5 can be modified to account for the effect of rotation of the bed but because it is not originally designed for RPB Equation 3.6 is used which was developed by Luo *et al.* [134].

$$\frac{a}{a_t} = 1 - \exp \left[-1.45 \left(\frac{\sigma_c}{\sigma}\right)^{0.75} Re_L^{0.1} We_L^{0.2} Fr_L^{-0.05} \right] \quad (3.5)$$

where Fr_L is the liquid Froude number and σ liquid surface tension

Luo *et al.* [134] studied gas-liquid effective interfacial area in an RPB considering different packing geometry, accounting for the effect of fibre diameter and opening of the wire mesh.

$$\frac{a}{a_t} = 66510 Re_L^{-1.41} Fr_L^{-0.12} We_L^{1.21} \varphi^{-0.74} \quad (3.6)$$

where φ is the theoretical probability of liquid uncaptured by fibres

3.4.4 Liquid hold-up

Liquid holdup correlation used in this thesis is given by Burns *et al.* [207]. The correlation fit is based on resistance and response time. Their study shows that the liquid hold-up is approximately inversely proportional to the local packing radius and is largely independent of gas flow up to the flooding point and also liquid viscosity has only a weak influence on hold-up [207].

$$\epsilon_L = 0.039 \left(\frac{g_c}{g_o}\right)^{-0.5} \left(\frac{U}{U_o}\right)^{0.6} \left(\frac{v_L}{v_o}\right)^{0.22} \quad (3.7)$$

$$g_o = 100 \text{ m s}^{-2}, \quad U_o = 1 \text{ cm s}^{-1}, \quad v_o = 1 \text{ cS} = 10^{-6} \text{ m}^2 \text{ s}^{-1}$$

$$U = \frac{Q_L}{2\pi r Z} \quad (3.8)$$

where ϵ_L is the liquid holdup, g_c gravitational acceleration, g_o is the characteristic acceleration value, U is the superficial liquid velocity, U_o is the characteristic superficial liquid velocity, v_L is the kinematic viscosity of the liquid, v_o is the characteristic kinematic viscosity and Q_L liquid volumetric flow rate

3.4.5 Dry pressure drop expression

Semi-empirical dry pressure drop expression was given by Llerena-Chavez and Larachi [208]. The model correlation was developed based on Ergun-type semi-empirical relationships in which the gas-slip and radial acceleration effects, the laminar and inertial

drag effects and the centrifugal effect were aggregated additively to form the pressure drops correlation in the RPB.

$$\Delta P_{RPB} = \frac{150(1-\varepsilon)^2\mu}{d^2\varepsilon^3} \left(\frac{G}{2\pi Z}\right) \ln \frac{r_o}{r_i} + \frac{1.75(1-\varepsilon)\rho}{d\varepsilon^3} \left(\frac{G}{2\pi Z}\right)^2 \left(\frac{1}{r_i} - \frac{1}{r_o}\right) + \frac{1}{2}\rho\omega^2(r_o^2 - r_i^2) + F_c \quad (3.9)$$

where F_c is a corrective function given as:

$$F_c = \varepsilon(a - G + (b + \omega^c)G^2) \quad (3.10)$$

a, b, and c are fitting parameters given as:

$$a = -0.08 \text{ m}^3/\text{s} \quad b = 2000(\text{rpm})^c \quad c = 1.22$$

where ΔP_{RPB} is the dry pressure drop in RPB, ε is the bed porosity, G is the gas flow rate, μ is the viscosity,

3.4.6 Motor power consumption by RPB absorber/stripper

The amount of power consumed by motor for rotating RPB absorber and stripper is calculated using the correlation proposed by Singh *et al.* [209]. The correlation was used to account for all the frictional losses and also the power required for accelerating the liquid entering the packing bed to the rotational speed at the outer radius. It is important to note that frictional losses are highly dependent upon the design of the machine and cannot be predicted without advance knowledge of the design (i.e. type of bearings, direct or pulley drive, etc.) [209].

$$P_{motor} = 1.2 + 1.1 \times 10^{-3} \rho_L r_o^2 \omega^2 Q_L \quad (3.11)$$

Where P_{motor} is the motor power, Q_L is the volumetric flow rate of liquid and ω is the angular velocity

3.5 Methods used to solve the system of equations

In the rate based model, the full set of equations is solved using Newton's method, using the solution from the equilibrium-based mode as the initial guess [210]. The model simulation calculation is in two-part. First, an initialization calculation is performed using the equilibrium-based model to get initial guesses for the temperature, flow, and composition profiles [210]. Then the rate-based calculation is performed using the results of the initialization as initial guesses. A simple continuation/homotopy method is also used to allow smoother switching from equilibrium to rate-based solution [210].

Model derivatives are determined from coded analytic expressions or numerical method which is computed by finite differences [210]. Either of the two methods can be used for physical property derivatives calculation which can then be use for Newton-based calculations to solve the simultaneous nonlinear equations. The coded analytic expression is the most preferred solver for derivatives and it is set as default. The numerical method is useful when there is concern that analytic derivatives are causing convergence difficulties, also sometimes it can be used to validate the correctness of the analytical solution [210].

To reduce the size of the Jacobian, the mass transfer coefficients ($k_{i,k,j}$) are written in the form:

$$k_{i,k,j} = k_j^o D_{i,k,j}^{\alpha_j}$$

where k_j^o is a function of flow, temperature, composition, and many properties, but is independent of the components i and k . The k_j^o and α_j are the independent variables, one per stage, rather than the binary diffusivity and mass transfer coefficients, and these are the variables which user subroutines must return; Aspen Rate-Based calculates the binary mass transfer coefficients without including each one separately in the problem matrix. This reduces the size of the Jacobian drastically when there are a large number of components in the system [210].

Newton method calculation can be controlled be specifying [210] (i) maximum of newton iterations, (ii) maximum number of flowsheet evaluations, (iii) alternative tolerance on the manipulated variables, the iteration stops when the change in the scaled manipulated variable is less than X Tolerance, (iv) reduction factor which determines the number of Newton iterations used before calculating a new Jacobian (derivative) matrix, (v) number of iterations to reuse the Jacobian (derivative) matrix.

3.6 Implementation procedures

The procedure used in this thesis for modelling and simulation of the RPBs is shown in **Figure 3-2**.

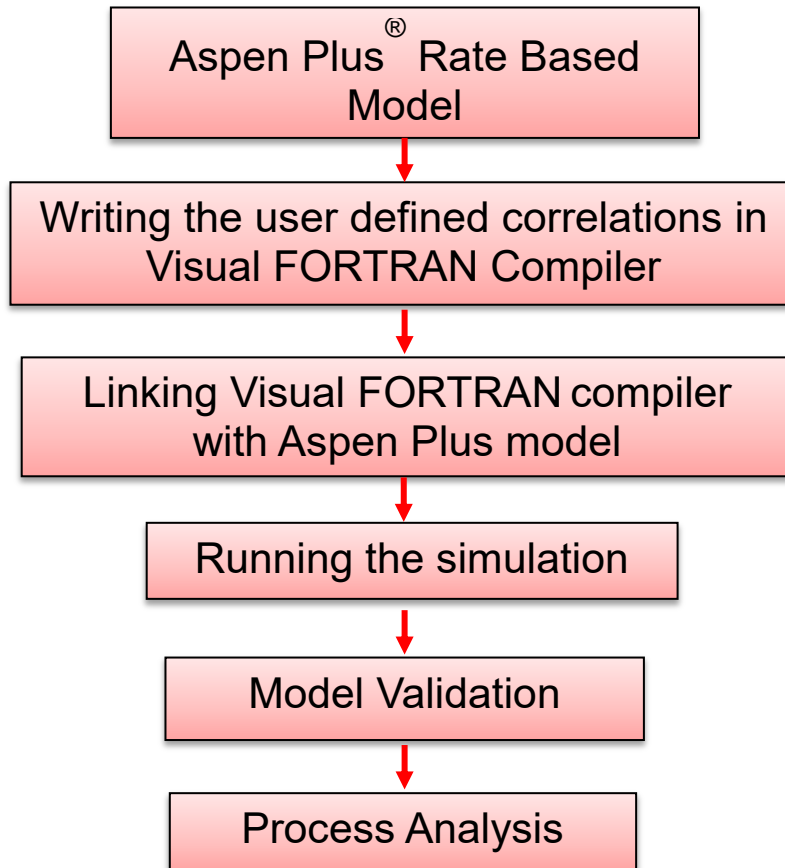


Figure 3-2 Methodology used in this thesis [115,116]

3.7 Summary

This chapter discussed methodology used for model development of the standalone intensified absorber and stripper. Model description of mass and heat transfer in RPB using two-film theory was done in Section 3.1. In Section 3.2 rate based modelling description was done to understand the material and energy balances in the RPBs model. Physical properties form the foundation for all simulation studies. Therefore, selection of the right property package is very important for a good model prediction. Physical properties which includes thermodynamic properties and transport properties were discussed in Section 3.3. Correlations for mass transfer coefficient, gas-liquid interfacial area and liquid holdup suitable for RPB models were discussed in Section 3.4. Further

study on the correlations will be discussed In Chapter 4, where two sets of correlations were grouped together and compared to each other in term of model prediction to see which sets is better and why they are better. Highlight on the method for solving the system of differential equations from mass and energy balances is discussed in Section 3.5. Model implementation procedure was presented in Section 3.3. The same implementation procedure was used for both standalone intensified absorber and standalone intensified stripper.

Chapter 4 Modelling, model validation and process analysis of standalone intensified absorber

In this Chapter, process description for intensified absorber is presented in Section 4.1. Section 4.2 describes the steady state modelling of the standalone intensified absorber. Section 4.3 presents steady state model validation based on experimental data from Newcastle University [114]. Process analysis of intensified absorber is presented in Section 4.4. In Section 4.5 comparative study between intensified absorber and conventional absorber was made. The chapter ends with summarizing the research findings in Section 4.6.

4.1 Process description

The geometrical similarities of RPB absorber and conventional absorber are illustrated in **Figure 4-1**. Lean-MEA solvent enters the RPB through the liquid distributor and the solvent is sprayed into the inner diameter of the RPB. The solvent is then distributed into the packing by centrifugal force. Flue gas is forced from the outer diameter into the inner diameter. Lean-MEA solvent and flue gas contact each other counter-currently in the packing where CO_2 will be absorbed by the lean-MEA solvent and the lean gas will move out of the RPB from the top. Rich-MEA solvent (i.e. rich in CO_2) will be collected at the bottom of the RPB absorber for further treatment.

In packed bed, the path for gas phase will go through length 'H' and residence time is mainly determined by the column height while in RPB, the gas path is from outer radius to inner radius. On the other hand, flue gas flowrate in conventional packed column can be determined by the diameter of the column. However in RPB, it is determined by the axial depth (h) of the RPB packing.

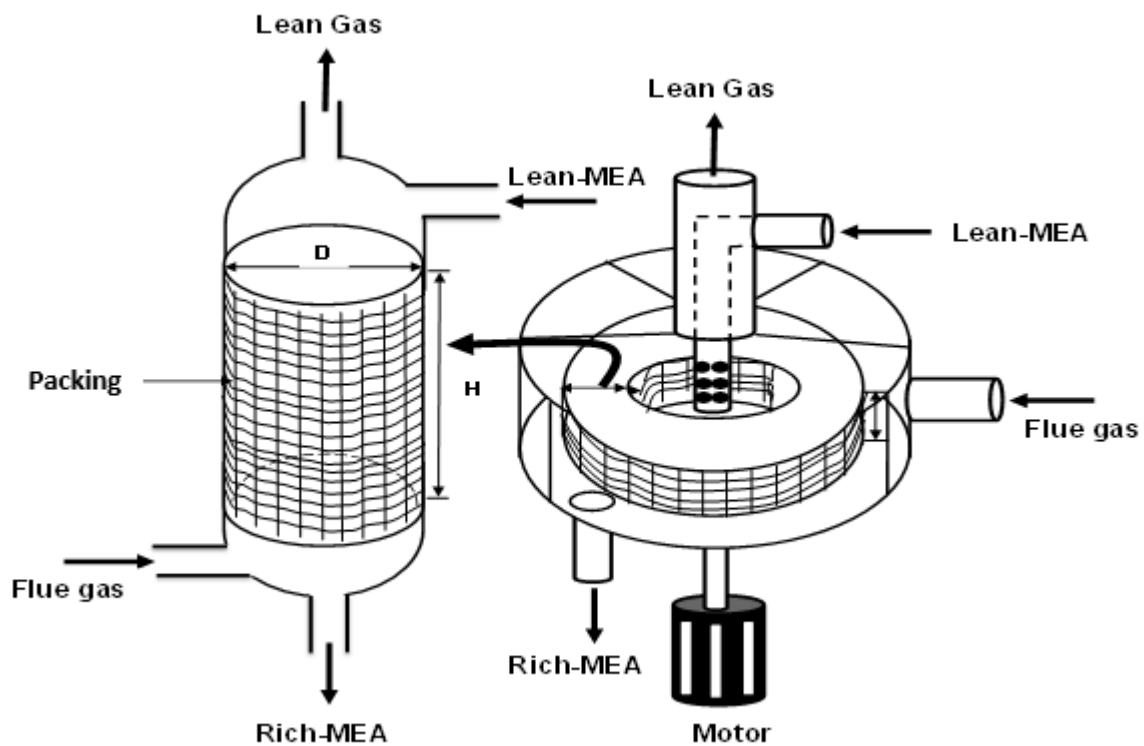


Figure 4-1 Geometrical similarities and differences between RPB and conventional absorber [115]

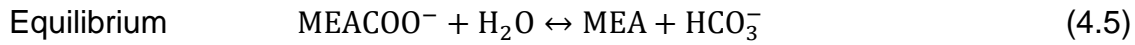
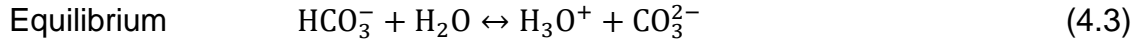
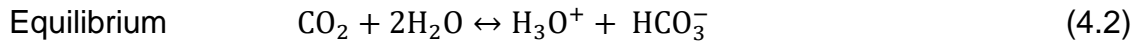
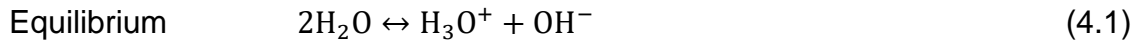
4.2 Steady state modelling of intensified absorber

Modelling of the intensified absorber using RPB was reported in Joel *et al.* [115,116]. The default mass/heat transfer correlations of the Aspen Plus[®] rate-based model were replaced with subroutines written in Intel[®] visual FORTRAN. The new model represents intensified absorber using RPB. Liquid phase mass transfer coefficient given by Chen *et al.* [123], gas-phase mass transfer coefficient given by Chen [206], interfacial area correlation estimated by Luo *et al.* [134], liquid hold-up correlation given by Burns *et al.* [207] and the dry pressure drop expression given by Llerena-Chavez and Larachi [208] are written in the Intel[®] visual FORTRAN for the dynamic linkage with the Aspen Plus[®] model.

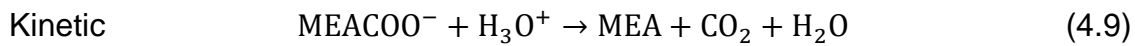
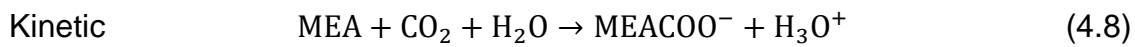
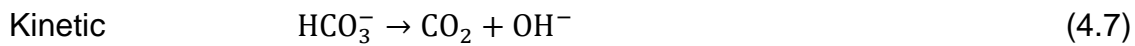
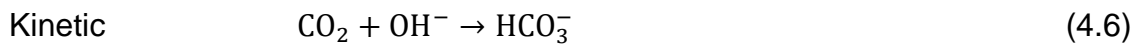
Physical property

To describe the vapour–liquid equilibrium, the chemical equilibrium and the physical properties, Joel *et al.* [115] selected the Electrolyte Non-Random-Two-Liquid (ElecNRTL) activity coefficient model in Aspen Plus[®]. The equilibrium constants for reactions in **Equations 4.1 – 4.5** are calculated from the standard Gibbs free energy change, the

equilibrium reactions are assumed to occur in the liquid film and kinetics reactions equations and parameters were obtained from AspenTech [201].



Kinetic reaction used for the calculation is specified by **Equations 4.6 – 4.9**.



Power law expressions are used for the rate-controlled reactions. The kinetic parameters for reactions in **Equations 4.6 – 4.9** are presented in **Table 4-1**

$$r_j = k_j^o \exp\left(-\frac{E_j}{R_c} \left[\frac{1}{T} - \frac{1}{298.15}\right]\right) \prod_{i=1}^N a_i^{\alpha_{ij}} \quad (4.10)$$

Table 4-1 Constants for power law expressions for the absorption of CO₂ by MEA [186]

Reaction No.	k_j^o	E_j , cal/mol
6	4.32e+13	13249
7	2.38e+13	29451
8	9.77e+13	9855.8
9	2.18e+13	14138.4

4.3 Steady state model validation of intensified absorber

4.3.1 Model validation based on experimental data from Jassim et al. [114]

The experimental data used for model validation was obtained from Jassim [211] and Jassim et al. [114]. From their experiments, two lean-MEA concentration (average 55 wt% and 75 wt%) were selected so as to fall within a reasonable range of MEA concentration to minimize the problem of corrosion and maximize CO₂ absorption rate. Two different lean-MEA flow rates were selected, one having the lean-MEA flow rate of 0.66 kg/s and

the other having lean-MEA flow rate of 0.35 kg/s. This is to achieve different liquid to gas (L/G) mass ratios. Four cases were considered.

Case 1: Lean-MEA flow rate of 0.66 kg/s and average MEA concentration of 55 wt%.

Case 2: Lean-MEA flow rate of 0.35 kg/s and average MEA concentration of 55 wt%.

Case 3: Lean-MEA flow rate of 0.66 kg/s and average MEA concentration of 75 wt%.

Case 4: Lean-MEA flow rate of 0.35 kg/s and average MEA concentration of 75 wt%.

Each of the four cases has four runs. The runs differ from each other by either lean-MEA temperature or rotor speed. Two different rotor speeds (600 rpm and 1000 rpm) were used.

Table 4-2 gives the input process conditions for Case 1 and Case 2 having average MEA concentration of 55 wt% while **Table 4-3** gives the input process conditions for Case 3 and Case 4 having average MEA concentration of 75 wt%.

RPB absorber packing is modelled with 7 RadFrac segments. Same simulation for 12 RadFrac segments were performed for same packing height and it was found that capture level difference was less than 1 %. Based on that all the validation studies were done with 7 RadFrac segments.

Table 4-2 Input process conditions at MEA concentration range of 53wt% to 57wt% [114,211]

Variable	Case 1				Case 2			
	Run 1	Run2	Run3	Run4	Run5	Run6	Run7	Run8
Rotor speed (RPM)	600	600	1000	1000	600	600	1000	1000
Lean temperature (°C)	39.6	20.7	40.1	20.9	39.5	22.3	39.6	22.6
Lean pressure (atm.)	1	1	1	1	1	1	1	1
Flue gas flow rate (kmol/hr)	2.87	2.87	2.87	2.87	2.87	2.87	2.87	2.87
CO ₂ composition in Flue gas (vol %)	4.71	4.60	4.48	4.45	4.43	4.47	4.35	4.09
Lean-MEA flow rate (kg/s)	0.66	0.66	0.66	0.66	0.35	0.35	0.35	0.35
Lean-MEA composition (wt %)								
H ₂ O	40.91	43.35	40.91	42.40	41.01	40.11	41.03	39.10
CO ₂	3.09	3.45	3.09	3.60	3.99	3.89	3.97	3.90
MEA	56.00	53.20	56.00	54.00	55.00	56.00	55.00	57.00

Table 4-3 Input process conditions at MEA concentration range of 72wt% to 78wt% [114,211]

Variable	Case 3				Case 4			
	Run 1	Run2	Run3	Run4	Run5	Run6	Run7	Run8
Rotor speed (RPM)	600	600	1000	1000	600	600	1000	1000
Lean temperature (°C)	41	21.4	40.2	20.7	40.8	22.1	39.4	20.6
Lean pressure (atm.)	1	1	1	1	1	1	1	1
Flue gas flow rate (kmol/hr)	2.87	2.87	2.87	2.87	2.87	2.87	2.87	2.87
CO ₂ composition in Flue gas (vol %)	4.40	4.36	4.36	4.29	3.55	4.38	4.38	4.53
Lean-MEA flow rate (kg/s)	0.66	0.66	0.66	0.66	0.35	0.35	0.35	0.35
Lean-MEA composition (wt %)								
H ₂ O	22.32	20.83	23.41	23.00	24.95	21.57	22.16	19.71
CO ₂	2.68	2.17	2.59	1.90	3.05	2.43	2.84	2.29
MEA	75.00	77.00	74.00	75.10	72.00	76.00	75.00	78.00

Table 4-4 Simulation results compared to the experimental data for Case 1 and Case 2

Variable7 c	Case 1											
	Run 1			Run 2			Run 3			Run 4		
	Expt.	model	Relative error (%)	Expt.	model	Relative error (%)	Expt.	model	Relative error (%)	Expt.	model	Relative error (%)
CO ₂ loading of Lean MEA, (mol CO ₂ /mol MEA)	0.0772	0.0772		0.0897	0.0897		0.0772	0.0772		0.0924	0.0924	
CO ₂ loading of Rich MEA, (mol CO ₂ /mol MEA)	0.0822	0.0830	1.0949	0.0951	0.0956	0.5257	0.0822	0.0828	0.8516	0.0955	0.0980	2.6178
Average Lean MEA/Rich MEA, (mol CO ₂ /mol MEA)	0.0797	0.0801	0.6273	0.0924	0.0926	0.2165	0.0797	0.0800	0.3764	0.0940	0.0952	1.2766
CO ₂ capture level (%)	94.9	93.56	0.8746	83	92.21	11.0964	95.4	94.06	1.4046	87.0	92.79	6.6552
CO ₂ penetration (%)	5.1	6.44		17	7.79		4.6	5.94		13.0	7.21	

Variable	Case 2											
	Run 5			Run 6			Run 7			Run 8		
	Expt.	Model	Relative error (%)	Expt.	Model	Relative error (%)	Expt.	Model	Relative error (%)	Expt.	Model	Relative error (%)
CO ₂ loading of Lean MEA, (mol CO ₂ /mol MEA)	0.1000	0.1000		0.0955	0.0955		0.0996	0.0996		0.0945	0.0945	
CO ₂ loading of Rich MEA, (mol CO ₂ /mol MEA)	0.1105	0.1106	0.0905	0.1044	0.1054	0.9579	0.1073	0.1096	2.1435	0.1021	0.1034	1.2733
Average Lean MEA/Rich MEA, (mol CO ₂ /mol MEA)	0.1053	0.1056	0.2849	0.1000	0.1005	0.5000	0.1035	0.1047	1.1594	0.0983	0.0989	0.6104
CO ₂ capture level (%)	87	90.03	3.4828	84.1	88.58	5.3270	89.9	90.78	0.9789	86.2	89.33	3.6311
CO ₂ penetration (%)	13	9.97		15.9	11.42		10.1	9.22		13.8	10.67	

Validation results were presented in terms of CO₂ capture level, CO₂ penetration and lean-MEA loading which are defined in **Equations 4.11, 4.12 and 4.13** respectively.

$$\text{CO}_2 \text{ capture level (\%)} = \left(\frac{y_{CO_2,in} - y_{CO_2,out}}{y_{CO_2,in}} \right) \times 100 \quad (4.11)$$

$$\text{CO}_2 \text{ penetration (\%)} = (1 - \text{CO}_2 \text{ capture level}) \quad (4.12)$$

$$\begin{aligned} \text{Loading} &= \frac{\text{Moles of all CO}_2 \text{ carrying species}}{\text{Moles of all MEA carrying species}} \\ &= \frac{[CO_2] + [HCO_3^-] + [CO_3^{2-}] + [MEACOO^-]}{[MEA] + [MEA^+] + [MEACOO^-]} \end{aligned} \quad (4.13)$$

where $y_{CO_2,in}$ is the mole fraction of CO₂ in inlet stream and $y_{CO_2,out}$ is the mole fraction of CO₂ in outlet stream.

In **Table 4-4**, the model predictions were compared to experimental data at the input conditions shown in **Table 4-2**. In all the runs considered for Cases 1 and 2, relative error of prediction for almost all the various variables assessed is less than 7% except in Case 1 Run 2 where the error prediction on CO₂ capture level is 11.0964%.

In **Table 4-5**, the simulation predictions were compared to experimental data at the input conditions shown in Table 4-3. The results for Case 3 and Case 4 show that for all runs the error prediction is less than 8% except Case 3 Run 2 where the error prediction on CO₂ capture level is 11.8883%.

The results show that the model developed using Aspen Plus[®] rate-based absorber model modified with new correlations suitable for RPB absorber is able to reasonably capture the behaviour of an intensified absorber using RPB. This is because Jassim *et al.* [114] reported that the CO₂ measurement in the gas sample has a reproducibility of ±0.6% and in the liquid sample CO₂ and MEA measurement has reproducibility of ±1.6% and ±1.4% respectively. Also error created as result of rotation can increase the CO₂ capture level error. Error prediction reported in **Table 4-4 and Table 4-5**, of less than 12% is acceptable. As a result, the model can be used to analyse typical RPB behaviour at different input conditions.

Table 4-5 Simulation results compared to the experimental data for Case 3 and Case 4

Variable	Case 3											
	Run 1			Run 2			Run 3			Run 4		
	Expt.	Model	Relative error (%)	Expt.	Model	Relative error (%)	Expt.	Model	Relative error (%)	Expt.	Model	Relative error (%)
CO ₂ loading of Lean-MEA, (mol CO ₂ /mol MEA)	0.0492	0.0492		0.0389	0.0389		0.0483	0.0483		0.0355	0.0355	
CO ₂ loading of Rich-MEA, (mol CO ₂ /mol MEA)	0.0531	0.0533	0.3766	0.0420	0.0428	1.9048	0.0505	0.0524	3.7624	0.0402	0.0395	1.7413
Average Lean-MEA/Rich-MEA, (mol CO ₂ /mol MEA)	0.0512	0.0512	0.0000	0.0405	0.0409	0.9877	0.0490	0.0503	2.6531	0.0379	0.0375	1.0554
CO ₂ capture level (%)	98.2	93.79	4.4908	84.2	94.21	11.8883	97.5	94.49	3.0872	91.2	93.20	2.1930
CO ₂ penetration (%)	1.8	6.21		15.8	5.79		2.5	5.51		8.8	6.80	

variable	Case 4											
	Run 5			Run 6			Run 7			Run 8		
	Expt.	Model	Relative error (%)	Expt.	Model	Relative error (%)	Expt.	Model	Relative error (%)	Expt.	Model	Relative error (%)
CO ₂ loading of Lean-MEA, (mol CO ₂ /mol MEA)	0.0582	0.0582		0.0443	0.0443		0.0523	0.0523		0.0407	0.0407	
CO ₂ loading of Rich-MEA, (mol CO ₂ /mol MEA)	0.0635	0.0645	1.5748	0.0495	0.0516	4.2424	0.0586	0.0598	2.0478	0.0477	0.0481	0.8386
Average Lean-MEA/Rich-MEA, (mol CO ₂ /mol MEA)	0.0609	0.0613	0.6568	0.0469	0.0480	2.3454	0.0555	0.0561	1.0695	0.0442	0.0444	0.4525
CO ₂ capture level (%)	98.0	90.82	7.3265	84.3	89.36	6.0024	98.1	91.78	6.4424	91	89.84	1.2747
CO ₂ penetration (%)	2.0	9.18		15.7	10.64		1.9	8.22		9	10.16	

4.3.2 Model validation based on Jassim et al. [114] experimental data comparing two sets of equations

For this study the experimental data used for model validation was also obtained from Jassim *et al.* [114]. Two sets of correlations were used for the validation. The sets of correlations are presented in **Table 4-6** and the input condition are shown in **Table 4-2 Case 1 Runs 1 and 3** and in **Table 4-3 Case 3 Runs 1 and 3**

Table 4-6 Model correlation sets used for the modelling and simulations

Correlations	Set 1	Set 2
Liquid-phase mass transfer coefficient	Tung and Mah[203]	Chen <i>et al.</i> [123]
Gas-phase mass transfer coefficient	Onda <i>et al.</i> [204]	Chen, [206]
Interfacial area	Onda <i>et al.</i> [204]	Luo <i>et al.</i> [134]
Liquid hold-up	Burns <i>et al.</i> [207]	Burns <i>et al.</i> [207]

Validation results were presented in terms of CO₂ capture level and CO₂ loading of lean-MEA evaluated in mole basis as defined in **Equations 4.11 and 4.13**

In **Table 4-7**, the model predictions were compared to experimental data for the two correlation sets in **Table 4-6** and for input conditions in **Table 4-2**. For **Case 1 Run 1** in **Table 4-2** (56 wt% MEA concentration and 600 rpm rotor speed) the CO₂ capture level using Set 1 correlation is 92.90% while using Set 2 correlation is 96.36%. For both sets of correlation the model reasonably predicts the experimental data with relative error of less than 3%

In **Table 4-8**, the simulation predictions were compared to the experimental data at the input conditions shown in Table 4-3. The error prediction of **Case 3 Runs 1 and 3** using Set 2 correlation gives better agreement with the experiment data, the reason for this could be from the liquid and gas phase mass transfer resistance where Chen et al. [123] and Chen [206] account for the effect of viscosity and packing geometry.

These results shows that the absorber model developed based on Aspen Plus[®] rate-based model modified for RPB with correlations implemented in visual FORTRAN is able to reasonably capture the behaviour of an RPB absorber. As a result, the model can be used to analyse typical RPB behaviour at different input conditions

Table 4-7 Simulation results with 2 different sets of correlations compared to the experimental data [105] for Case 1 Runs 1 and 3

Variable	Case 1 Run 1					Case 1 Run 3				
	Expt.	Set 1	Error 1	Set 2	Error 2	Expt.	Set 1	Error 1	Set 2	Error 2
CO ₂ loading of Lean MEA, (mol CO ₂ /mol MEA)	0.0772	0.0772		0.0772		0.0772	0.0772		0.0772	
CO ₂ loading of Rich MEA, (mol CO ₂ /mol MEA)	0.0828	0.0827	0.1208	0.0832	0.4831	0.0828	0.0825	0.3623	0.0827	0.1208
Average Lean MEA/Rich MEA, (mol CO ₂ /mol MEA)	0.0800	0.0800	0.0000	0.0801	0.1250	0.0800	0.0799	0.1250	0.0801	0.1250
CO ₂ capture level (%)	94.9	92.9	2.1075	96.65	1.8440	95.4	93.26	2.2432	96.95	1.6247

Table 4-8 Simulation results with 2 different sets of correlations compared to the experimental data [105] for Case 3 Runs 1 and 3

Variable	Case 3 Run 1					Case 3 Run 3				
	Expt.	Set 1	Error 1	Set 2	Error 2	Expt.	Set 1	Error 1	Set 2	Error 2
CO ₂ loading of Lean-MEA, (mol CO ₂ /mol MEA)	0.0492	0.0492		0.0492		0.0483	0.0483		0.0483	
CO ₂ loading of Rich-MEA, (mol CO ₂ /mol MEA)	0.0531	0.0530	0.1883	0.0531	0.0000	0.0510	0.0521	2.1569	0.0524	2.7451
Average Lean-MEA/Rich- MEA, (mol CO ₂ /mol MEA)	0.0512	0.0511	0.1953	0.0512	0.0000	0.0497	0.0502	1.0060	0.0503	1.2072
CO ₂ capture level (%)	98.20	93.28	5.0102	97.36	0.8554	97.50	93.57	4.0308	98.66	1.1897

4.4 Process analysis for intensified absorber

4.4.1 Effect of rotor speed on CO₂ capture level

4.4.1.1 Justification for case study

Energy requirement for an RPB depends on the rotor speed which in turn affects the capture level. As a result, it is important to understand the relationship that rotor speed bears with capture level so that the energy requirement for maintaining the speed can be maximized with respect to capture level.

4.4.1.2 Setup of the case study

To do this, the rotor speed was varied from 400 rpm to 1200 rpm. This range was chosen to cover the validated rotor speeds of 600 rpm and 1000 rpm. Two lean-MEA temperatures,

20.9 °C and 39.5°C, were chosen. This is needed to study the impact of the rotor speed at lower and higher temperature conditions. Again, two MEA concentrations were chosen to explore the impact of varying rotor speed on CO₂ capture level on two different MEA concentrations.

The case study setup input conditions are shown in **Case1 Run 1 of Table 4-2** for 56 wt% MEA concentration and **Case 3 Run 1 of Table 4-3** for 75 wt% MEA concentration. In both cases, rotor speed changes as 400 rpm, 600 rpm, 800 rpm, 1000 rpm and 1200 rpm. The analysis was implemented with Set 1 correlations.

4.4.1.3 *Results and discussions*

Figure 4-2 and Figure 4-3 show effects of varying rotor speed on CO₂ capture level for 56 wt% and 75 wt% lean MEA concentrations at 20.9 °C and 39.5 °C lean MEA temperatures. The results show that CO₂ capture level increases with increase in rotor speed for both 20.9 °C and 39.5 °C lean MEA temperatures due to enhanced mass transfer. Rotation of the absorber enhances mass transfer by stimulating combined droplet and film flow [212]. This behaviour increases with rotor speed. Also, at higher rotor speed the problem of liquid maldistribution is overcome leading to higher wetted area which subsequently contributes to improving mass transfer.

Figure 4-2 and Figure 4-3 also show that CO₂ capture levels at different rotor speed are affected by the lean MEA temperatures. At 20.9°C lean MEA temperature, CO₂ capture level increases more significantly with increase in rotor speed than at 39.5 °C lean MEA temperature even though actual capture level is higher at 39.5 °C lean MEA temperature. The capture level at 39.5 °C lean MEA temperature is close to 100% and as such increasing rotor speed has less effect on it. Again, comparing **Figure 4-2 and Figure 4-3** for 20.9°C lean MEA temperatures in **Figure 4-2** the capture level increases from 81.61 % to 84.93 % as rotor speed increases, but in **Figure 4-3**, capture level increase from 83.06 % to 90.40 % which is more significant than in **Figure 4-2**. The reason for this behaviour is that CO₂ capture level is higher at 75 wt% MEA concentration than at 56 wt% MEA concentration since reaction rate is a function of concentration.

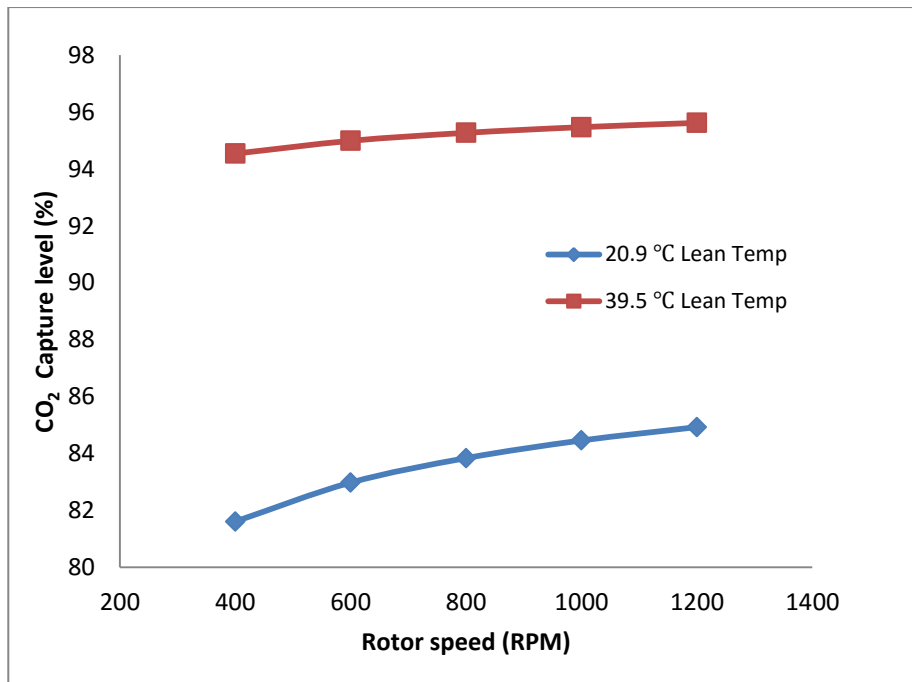


Figure 4-2 Effect of rotor speed on CO₂ capture level at 56wt% MEA

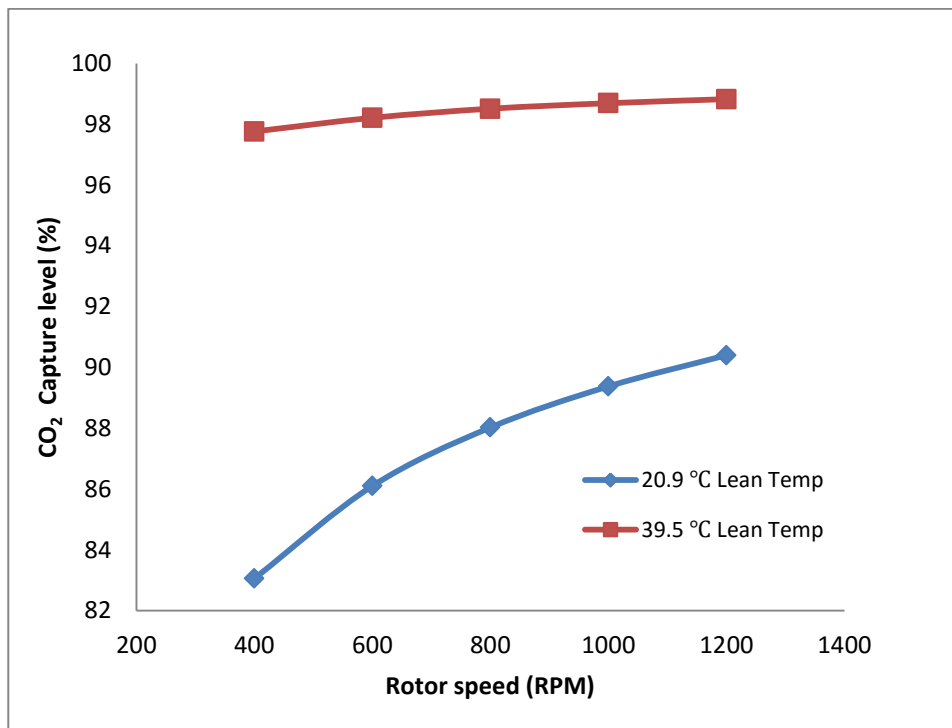


Figure 4-3 Effect of rotor speed on CO₂ capture level at 75wt% MEA

4.4.2 Effect of MEA concentration on CO₂ capture level

4.4.2.1 Justification for case study

Increasing lean MEA concentration leads to higher capture level and greater tendency for equipment corrosion. Good understanding of this relationship is needed to determine the needed concentration that gives best capture level with the least consequence for corrosion.

4.4.2.2 Setup of the case study

To implement this case study, 1000 rpm rotor speed and 0.66 kg/s Lean-MEA flow rate were used. The operating conditions are as shown in **Table 4-9**. MEA concentration was varied 55 wt%, 65 wt% and 75 wt% at two lean MEA temperature conditions, 39.5 °C and 20.9 °C. Set 1 correlations was used for this study.

Table 4-9 Process conditions for MEA concentration studies

Variable	20.9°C lean Temperature			39.5°C lean Temperature		
	Run 1	Run2	Run3	Run 1	Run2	Run3
Rotor speed (RPM)	1000	1000	1000	1000	1000	1000
Lean pressure (atm.)	1	1	1	1	1	1
Flue gas flow rate (kmol/hr)	2.87	2.87	2.87	2.87	2.87	2.87
CO ₂ composition in flue gas (vol %)	4.35	4.35	4.35	4.35	4.35	4.35
Lean-MEA flow rate (kg/s)	0.66	0.66	0.66	0.66	0.66	0.66
Lean-MEA composition (wt %)						
H ₂ O	41.39	33.22	22.96	41.39	33.22	22.96
CO ₂	3.61	0.178	2.04	3.61	0.178	2.04
MEA	55.00	65.00	75.00	55.00	65.00	75.00

4.4.2.3 Results and discussions

Figure 4-4 shows the effect of MEA concentration on CO₂ capture level at the input conditions shown in **Table 4-9**. Capture level increases with increase in MEA concentration at 39.5°C and also at 20.9°C lean-MEA temperature. The behaviour reflects increase in hydroxide ions per unit volume resulting in higher degree of CO₂ absorption in the lean solvent. This agrees with the findings of Freguia and Rochelle [213] which showed that the rate coefficient of pseudo-first-order reaction is a function of MEA concentration, meaning that higher concentration of MEA contributes to higher reaction rate. At different temperatures, CO₂ capture level shows similar behaviour with MEA concentration though

actual capture level is higher at 39.5 °C lean-MEA temperature than at 20.9°C lean-MEA temperature.

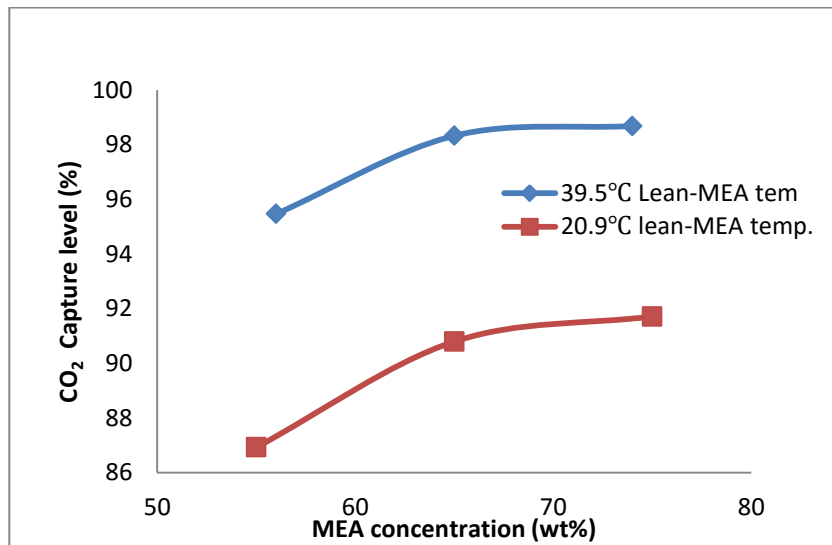


Figure 4-4 Effect of MEA concentrations on CO₂ capture level

4.4.3 Effect of flue gas flow rate on CO₂ capture level

4.4.3.1 Justification for case study

In designing RPB absorbers, flue gas flow rate is an important parameter in determining the size of the absorption column, while this process analysis is also necessary in order that the CO₂ emission target can be met.

4.4.3.2 Setup of the case study

For this study, Set 2 of the correlations in **Table 4-6** was used and the input conditions in **Table 4-2 Case 1 Run 3** and **Table 4-3 Case 3 Run 3** having constant rotor speed of 1000rpm were selected for the analysis. The RPB absorber size is fixed, as well as the lean MEA flow rate. The flue gas flow rate was varied from 0.02 kg/s to 1 kg/s.

4.4.3.3 Results and discussions

Figure 4-5 shows that for both Runs CO₂ capture level decreases as the flue gas flow rate increases. This is associated with decrease in contact time (i.e. residence time) between the flue gas and liquid MEA solvent resulting in more CO₂ escaping the RPB without being captured. Also from **Figure 4-5**, it can be seen that whatever the MEA concentration of the solvent the trend is the same.

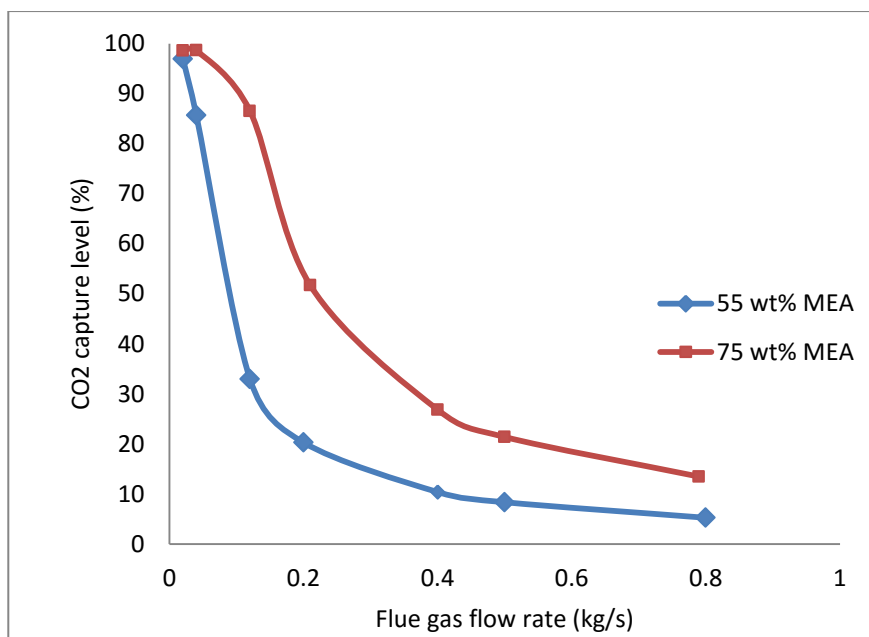


Figure 4-5 Effect of flue gas flow rate of CO₂ capture level

4.4.4 Effect of lean-MEA temperature on CO₂ capture level

4.4.4.1 Justification for case study

The study is performed to investigate the effect of lean MEA temperature on the performance of RPB absorber. The key driving forces for absorption, mass transfer and chemical reaction, are known to respectively decrease and increase with temperature [69]. Conventional absorber performance is already known to be hindered by increase in lean MEA temperature due to the possibility of temperature bulge within the absorber column [213]. Based on this, capture performance with lean MEA temperature should be studied for RPB absorbers.

4.4.4.2 Setup of the case study

To implement the case study Set 2 correlations, 1000 rpm rotor speed, 0.66 kg/s lean MEA flow rate were used. Process conditions are shown in **Table 4-10**. The lean MEA temperature is varied from 25 °C, 30 °C, 35 °C, 40 °C to 80 °C at 55 wt% and 75 wt% lean MEA concentrations.

Table 4-10 Process conditions for lean MEA temperature studies

Variable	55 wt% MEA Con.	75 wt% MEA Con.
Rotor speed (RPM)	1000	1000
Lean pressure (atm.)	1	1
Flue gas flow rate (kmol/hr)	2.87	2.87
Flue gas composition (vol %)		
H ₂ O	17.1	17.1
CO ₂	4.4	4.4
N ₂	78.5	78.5
Lean-MEA flow rate (kg/s)	0.66	0.66
Lean-MEA composition (wt %)		
H ₂ O	41.03	22.32
CO ₂	3.97	2.68
MEA	55.00	75.00

4.4.4.3 Results and discussions

Figure 4-6 shows the effect of varying lean MEA temperature on CO₂ capture level at different lean MEA concentrations (55 wt% MEA and 75 wt% MEA). The results show that CO₂ capture level increases significantly when lean-MEA temperature increases from 25 °C to 50 °C. Lean MEA temperature above 50 °C has no significant impact on the CO₂ capture level. Improvement of RPB performance as temperature increases can be associated to decrease in viscosity of the lean MEA solvent as explained by Lewis and Whitman [214] that the ratio of viscosity to density (kinematic viscosity) of the film fluid is probably the controlling factor in determining film thickness. Haslam *et al.* [215] said that if film resistance is directly proportional to film thickness, then film conductivity is the inverse of kinematic viscosity. The effect of temperature on density of gas is great, but temperature affects the density of lean MEA only slightly [216]. Again an increase in temperature causes an increase in viscosity of a gas but the same increase in temperature might greatly lower the viscosity of lean MEA. This improves mass transfer due to thinner liquid film since absorption of CO₂ into alkanolamines solutions is a liquid film controlled process [114]. Also Increasing lean solvent temperature leads to increase in chemical reaction rate.

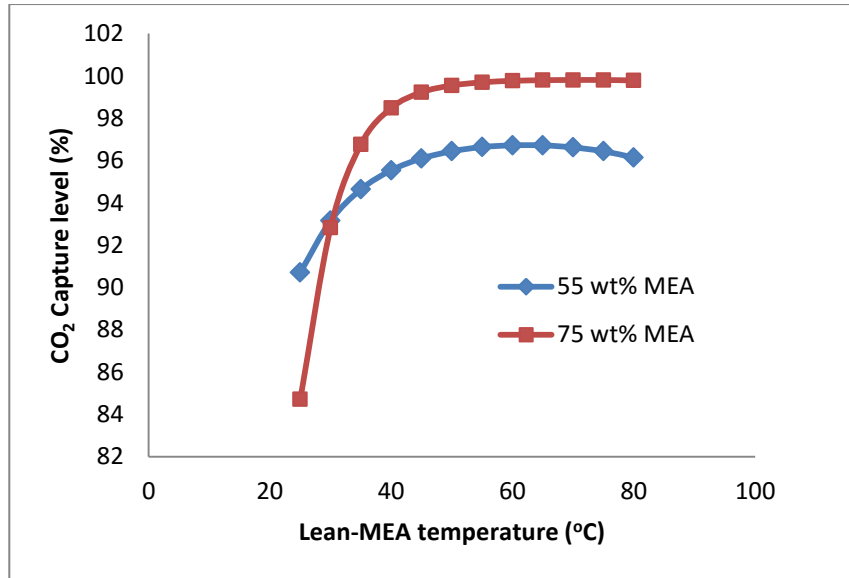


Figure 4-6 Effect of lean-MEA temperature on CO₂ capture level

4.4.5 Effect of flue gas temperature on CO₂ capture level

4.4.5.1 Justification for case study

Moisture content of a flue gas is dependent on temperature, pressure and the type of fuel used. Study of flue gas temperature is necessary since additional cost will be incurred in cooling flue gas prior to entering conventional absorber [68,69].

4.4.5.2 Setup of the case study

Set 2 correlations in **Table 4-6** were used for the formulation of this case study. **Table 4-2 Case 1 Run 3** and **Table 4-3 Case 3 Run 3** were selected which are at 56 wt% and 74 wt% MEA concentration respectively. The simulations were run at rotor speed of 1000 rpm, the lean-MEA temperature was kept constant 40.1 °C for Run 2 and 40.2 °C for Run 2, in both cases flue gas temperature was varied from 30 °C to 80 °C.

4.4.5.3 Results and discussions

Figure 4-7 shows the effect of flue gas temperature on CO₂ capture level, where the results show that the CO₂ capture level is maintained despite increase in the flue gas temperature. 55 wt% MEA and 75 wt% MEA gives the same trend, this shows that even if the solvent is having higher MEA concentration, CO₂ capture level behaves the same way. The reason for this behaviour is because of no temperature bulge as reported in Joel *et al.* [115] since the evaporated vapour condensate does not have enough residence time for energy build-up in the column. Again because of high liquid to gas (L/G) ratio in an RPB, makes the CO₂

capture level not sensitive to the flue gas temperature change. Maintained CO₂ capture level shown in **Figure 4-7** indicates that flue gas cooling energy cost can be saved.

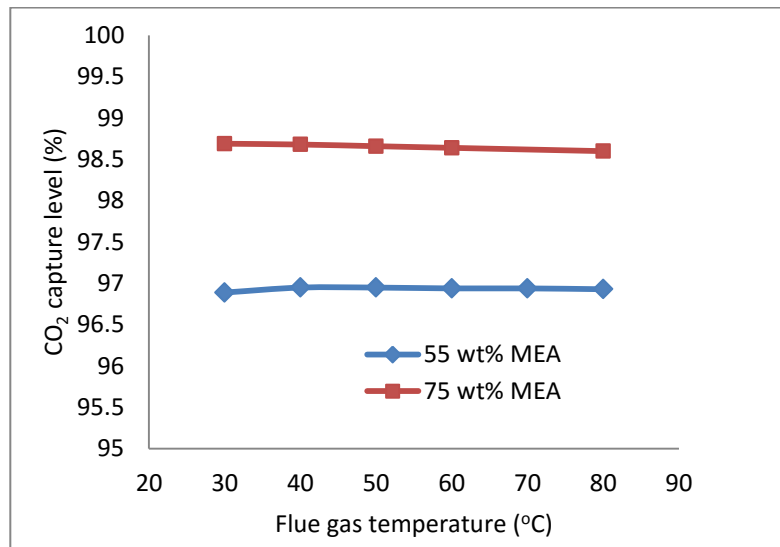


Figure 4-7 Effect of flue gas temperature on CO₂ capture level

4.4.6 Temperature profile in RPB absorber

4.4.6.1 Justification for case study

Temperature bulge in conventional absorber was reported by Freguia and Rochelle [213], Kvamsdal and Rochelle [67], Kvamsdal *et al.* [68], this limits the overall performance of the absorber. It is necessary to investigate temperature profile in RPB absorbers to determine whether similar phenomenon exists.

4.4.6.2 Setup of the case study

To implement this case study, lean MEA flow rate of 0.66 kg/s, rotor speed of 1000 rpm were selected. For 56 wt% lean-MEA concentration input conditions refer to **Case 1 Run 1 of Table 4-2** while for 75 wt% lean-MEA concentration input conditions refer to **Case 3 Run 1 of Table 4-3**. The flue gas temperature was maintained at 47 °C during the study. The temperature profile studies were performed over two lean MEA temperatures of 25 °C and 50 °C.

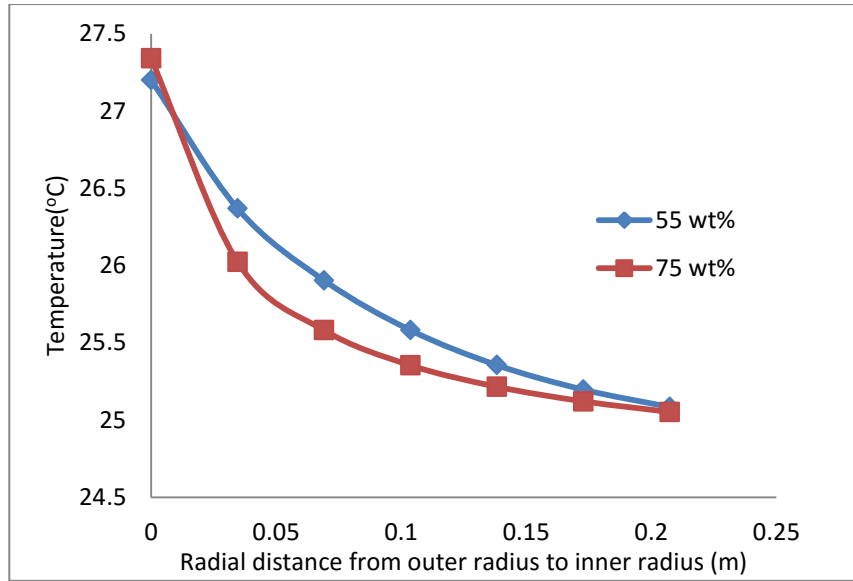


Figure 4-8 Liquid temperature profile in RPB absorber at 25 °C lean MEA temperature

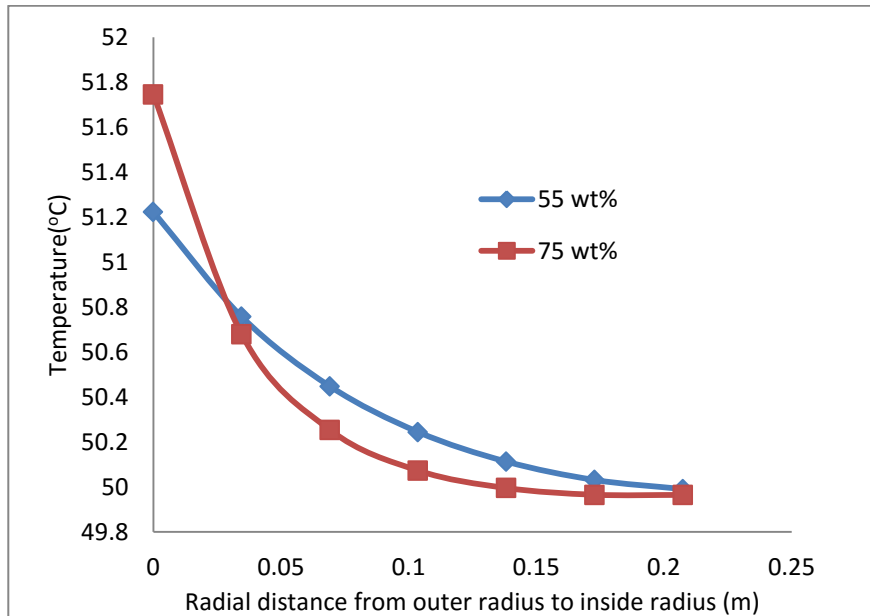


Figure 4-9 Liquid temperature profile in RPB absorber at 50 °C lean MEA temperature

4.4.6.3 Results and discussions

As stated in Kvamsdal and Rochelle [67] that the magnitude and location of temperature bulge are represented by liquid temperature profile, this is because gas and liquid temperature profile are similar in shape but the gas temperature profile will be lagged due to the difference in heat capacities of the two phases and the L/G ratio.

Figure 4-8 and Figure 4-9 showed that the liquid temperature profile in RPB, outer radius where flue gas enter RPB is taken as 0 m. At 55 wt% MEA concentration, temperature

profile has a steady gradient for the two temperatures under study. On the other hand, steeper gradient is noticed close to the outer radius. Both results show there is no temperature bulge observed in RPB. This is likely due to higher solvent to gas ratio (L/G) which is 30 (kg/kg). Kvamsdal and Rochelle [67] stated for conventional absorber in case where no temperature bulge, the enthalpy of reaction must leave with the gas or liquid. At high liquid rates, the enthalpy will leave with the liquid, while at high gas rates it will leave with the gas. In **Figure 4-8 and Figure 4-9** it can be observed that the temperature of lean MEA increases from the inner diameter to the outer diameter. This is because of the gain in the enthalpy of reaction since we have greater liquid rate than the gas rate. Also it can be observed from **Figure 4-8 and Figure 4-9** that exit temperature for the solvent at 0 m is higher for 75 wt% MEA concentration than for 55 wt%. This is because of greater enthalpy of reaction at higher concentration.

Another factor that contributes to having no temperature bulge in RPB absorber is high mixing capability, which enhances heat transfer and significantly reduces residence time. This is also because there are no liquid build-up since high gravity in RPB stimulates mainly droplet flow rather than film flow [212].

From the above findings, it can be concluded that RPB absorber does not need inter-cooling provided it is operated at the conditions being studied. From this, we can see that the cost of energy for inter-cooling is saved if we are using RPB absorber. The temperature profile shows that a better column performance could be achieved in intensified absorber using RPB.

4.5 Comparison between intensified absorber and conventional absorber

4.5.1 Justification for case study

For comparison between the conventional absorber using packed column and the intensified absorber using RPB, detailed study of their process parameters is necessary. This section is aimed to provide a comparison between the intensified absorber using RPB and the conventional absorber using packed column under some fixed conditions such as CO₂ capture level, flue gas flow rate, pressure, temperature and compositions.

4.5.2 Setup of the case study

For this study, **Table 4-11** presents the input conditions for the conventional absorber and intensified absorber using RPB. In both simulation runs, the capture level was fixed at 90%.

The flue gas conditions for the intensified absorber using RPB were also maintained the same for the conventional absorber simulation. L/G ratio used for the conventional absorber was adapted from Canepa *et al.* [217]. MEA concentration of the conventional absorber was kept at 30 wt% to minimize the problem of corrosion. It is believed that the size of conventional absorber with packed column as reported by Lawal *et al.* [17] is huge and using stainless steel as material of construction is too expensive. But for RPB absorber, the size of the intensified absorber can drastically reduce compared to conventional absorber [218]. The use of stainless steel as material of construction is feasible. In the RPB absorber simulation, MEA concentration of 74 wt% is used.

Table 4-11 Process input conditions for conventional and RPB absorbers

Description	Conventional absorber		RPB absorber	
	Flue gas	Lean-MEA	Flue gas	Lean-MEA
Temperature (K)	323.15	313.25	323.15	313.25
Pressure (10^5 Pa)	1.186	1.013	1.186	1.013
Total flow (kg/s)	0.0228	0.0454	0.0228	0.0440
L/G (kg/kg)	1.99		1.93	
Mass-Fraction				
H ₂ O	0.0030	0.6334	0.0030	0.23426
CO ₂	0.0666	0.0618	0.0666	0.02574
N ₂	0.9304	0	0.9304	0
MEA	0	0.3048	0	0.74000

4.5.3 Results and discussions

Keeping the CO₂ capture level at 90%, the simulation results of the conventional absorber using packed column and intensified absorber using RPB are shown in **Table 4-12**. Calculating the volume of the conventional absorber and RPB absorber without the sump, it was found that conventional absorber is 12 times the volume of RPB absorber using the assumption in Agarwal *et al.* [141] that the casing volume of RPB is taken as 4.5 times the RPB volume. In RPB absorber, MEA concentration is higher than what was used in the conventional absorber. That is why the lean loading in RPB is lower than what was found in conventional absorber. But looking at the rich loading in both cases, it can be seen that there is significant increase in rich-MEA loading in RPB absorber than the convention absorber which means more CO₂ in flue gas stream has been absorbed. The observed

height of transfer unit (HTU) for conventional packed column absorber from this simulation studies is 48.9 cm while for the RPB absorber is 2.7 cm. The small HTU in RPB absorber is responsible for smaller RPB absorber size compared to conventional packed column.

Table 4-12 Comparison between conventional and RPB absorber

Description	Conventional absorber	RPB absorber
Height of packing (m)	3.85	0.2885 (r_o) 0.078 (r_i)
diameter (m)	0.395	0.0377 axial depth
Packing Volume (m^3)	0.4718	0.0091
Packing volume reduction		52 times
Volume of unit (m^3)	0.4718 ^a	0.04095 ^b
Volume reduction factor		12 times
Specific area (m^2/m^3)	145	2132
Void fraction	0.79	0.76
Lean-MEA loading (mol CO ₂ /mol MEA)	0.2814	0.0483
Rich-MEA loading (mol CO ₂ /mol MEA)	0.4189	0.1069

^a excluding sump

^b using the assumption given by Agarwal *et al.* [141]

4.6 Summary

Modelling, validation and analysis of a PCC with MEA using intensified absorber was carried out. The RPB absorber was modelled in Aspen Plus® which is dynamically linked with visual FORTRAN.

Two sets of correlations were implemented for the validation of the intensified absorber model and the model predictions showed good agreement with the experimental results. The second set of correlations gives better prediction compared to the first set of correlation.

Process analysis was performed to explore the effect of rotational speed, lean-MEA concentration, lean-MEA temperature, flue gas flow rate and flue gas temperature on CO₂ capture level was studied.

Temperature profile study was done for 55 wt% and 75 wt% MEA concentration at lean MEA temperature of 25 °C and 50 °C

Comparison between the conventional absorber using packed column and intensified absorber using RPB indicates that the latter gives 12 times reduction in volume without sumps.

Chapter 5 Modelling, model validation and process analysis of standalone intensified stripper

Section 5.1 gives process description of intensified stripper. Steady state modelling of a standalone intensified stripper is described in Section 5.2. Section 5.3 presents steady state model validation of the RPB stripper based on experimental data from Newcastle University UK and Tsing Hua University Taiwan. Process analysis of the intensified stripper is presented in Section 5.4. Comparison between conventional stripper and intensified stripper is presented in Section 5.5. The research findings are summarised in Section 5.6.

5.1 Process description

A process diagram of the intensified stripper based on RPB technology is shown in **Figure 5-1**. The operating temperature and pressure is higher than that of absorber, the reaction between the solvent and CO_2 is reversed which liberates CO_2 into a concentrated stream obtained at the top of the intensified stripper. Rich-MEA solvent enters through the liquid distributor (at the centre) and sprays the solvent into the inner diameter of the RPB. Rich-MEA solvent moves from the inner to the outer diameter driven by centrifugal force. Vapour from the reboiler contacts the rich-MEA solvent counter-currently in the packing, stripping off CO_2 from the rich-MEA solvent. The solvent lower in CO_2 loading known as lean-MEA solvent is collected at the bottom of the RPB for further use. The stripper in this design uses a conventional reboiler which is not intensified and is located at the outside of the RPB stripper as shown in **Figure 5-1**. The disadvantage of using the conventional reboiler is that the size is too big. In Chapter 7, recommendation was made on how to improve.

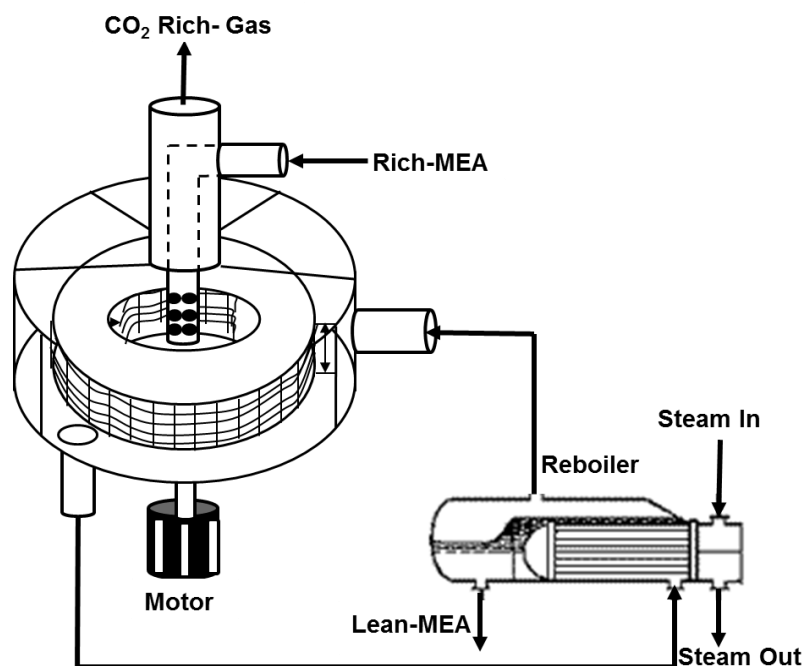


Figure 5-1 Schematic diagram of a RPB regenerator [120]

5.2 Steady state modelling of intensified stripper

The steady state modelling procedure for the intensified stripper main body is the same as that of intensified absorber. Therefore refer to Section 4.2 in Chapter 4 for the steady state modelling of the intensified stripper main body, but the reboiler and partial condenser models in Aspen Plus[®] were adopted. Set 2 correlations in **Table 4-6** are used for this model development.

5.3 Model validation of intensified stripper

5.3.1 Model validation based on experimental data from Jassim et al. [114]

The experimental data used for the model validation was obtained from Jassim *et al.* [114]. From their experiments, MEA concentrations of 32.9 wt%, 35.7 wt%, 30.8 wt%, 57.4 wt% and 52 wt% were selected for the validation study. The equipment specification and process input conditions for the model validation study are shown in **Table 5-1** and **Table 5-2**. In this study, two different rotor speed conditions 800 rpm and 1000 rpm were used.

Table 5-1 RPB stripper packing specifications used by Jassim et al. [114]

Description	value
RPB outer diameter	0.398 m
RPB inner diameter	0.156 m
RPB axial depth	0.025 m
Packing specific surface area	2132 m ² /m ³
Packing void fraction (i.e. porosity)	0.76

Table 5-2 Input process conditions for Run 1 to Run 5 [114]

	Runs				
	Run 1	Run 2	Run 3	Run 4	Run 5
Rotor speed (RPM)	800	800	800	1000	1000
Rich-MEA temperature (°C)	67.1	69	70	57.2	58.4
Rich-MEA pressure (atm.)	1	1	1	1	1
Rich-MEA flow rate (kg/s)	0.2	0.2	0.4	0.4	0.2
Rich-MEA composition (wt. %)					
H ₂ O	58.116	54.013	61.536	25.142	32.895
CO ₂	8.984	10.287	7.664	17.458	15.105
MEA	32.900	35.700	30.800	57.400	52.000
Rich-MEA CO ₂ loading (mol CO ₂ /mol MEA)	0.3790	0.3999	0.3454	0.4221	0.4030
Steam rate (kg/s)	0.072	0.069	0.072	0.069	0.072

Table 5-3 Simulation results compared to experimental data [114] for Run 1 to Run 5

	Runs				
	Run 1	Run 2	Run 3	Run 4	Run 5
Rotor speed (RPM)	800	800	800	1000	1000
Experimental measurement					
Lean-MEA CO ₂ loading (mol CO ₂ /mol MEA)	0.321	0.329	0.329	0.403	0.334
Model prediction					
Lean-MEA CO ₂ loading (mol CO ₂ /mol MEA)	0.316	0.295	0.298	0.355	0.320
Relative error (%)	1.558	10.334	9.422	11.911	4.192

Model validation results are shown in **Table 5-3** which gives percentage error prediction of not more than 12 % on the lean-MEA CO₂ loading. The lean-MEA CO₂ loading was evaluated on mole basis as shown in **Equation 4.13**.

Jassim *et al.* [114] did not include reboiler duty data in their experimental studies. Therefore, the authors cannot compare model predictions with experimental tests based on reboiler duty.

5.3.2 Model validation based on experimental data from Cheng et al. [120]

Cheng et al. [120] carried out an experimental study on the thermal regeneration of alkanolamines solutions in an RPB for two different aqueous solvents (a) 30 wt% MEA aqueous solution (b) mixed solvent (i.e. 20 wt% diethylenetriamine (DETA) and 10 wt% piperazine (PZ)). For the purpose of this study, experimental data with 30 wt% MEA aqueous solution was used for the model validation. RPB stripper specification and process input conditions for the model are shown in Table 5-4 and Table 5-5

Table 5-4 RPB stripper packing specifications used by Cheng et al [120]

Description	value
RPB outer diameter	0.16 m
RPB inner diameter	0.076 m
RPB axial depth	0.02 m
Packing specific surface area	803 m ² /m ³
Packing porosity	0.96

Table 5-5 Input process conditions for different reboiler temperatures [120]

Variable	Reboiler Temperature		
	105 °C	115 °C	120 °C
Rotor speed (RPM)	900	900	900
Rich-MEA temperature (°C)	96.6	97	97
Rich-MEA pressure (atm.)	2	2	2
Rich-MEA flow rate (mL/min)	400	400	400
Rich-MEA CO ₂ loading (mol CO ₂ /mol MEA)	0.484	0.484	0.484

Table 5-6 Simulation results compared to experimental data [120]

Variable		Reboiler Temperature (°C)		
		105	115	120
Lean Loading (mol/mol)	Experimental	0.418	0.340	0.271
	Modelling	0.423	0.367	0.289
	Relative error (%)	1.132	8.054	6.848
Reboiler duty (kW)	Experimental	0.620	0.900	1.240
	Modelling	0.629	0.989	1.383
	Relative error (%)	1.487	9.951	11.498

Model validation results with experimental data from Cheng et al. [120] shown in **Table 5-6** gives a good agreement with the experimental data with relative error on lean loading of less than 9% and reboiler duty percentage error of less than 12% for different reboiler temperature conditions.

In summary, the model has predicted all experimental data reasonably well with not more than 12% error prediction, the model developed can then be use to carry out process analysis in order to study the process behaviour when there is a change in some variables.

5.4 Process analysis for intensified regenerator

With the validated models, process analysis was carried out to explore the effect of rich-MEA flow rate, rotor speed and reboiler temperature on the (a) regeneration efficiency calculated based on loading (Equation 5.1) and calculated based on amount of CO₂ in rich-MEA and lean-MEA solvent (Equation 5.2), (b) regeneration energy (with and without motor power) expressed in Equations 5.3 and 5.4 respectively. RPB solvent residence time estimation Equations 5.5 and 5.6 were adopted from Basic and Dudukovic [219] which assumed that the packing surface was completely wetted and the solvent flows through the RPB in the form of films. The RPB stripper used for the process analysis has the following packing geometry: Outer radius = 0.371; Inner radius = 0.152; axial depth of packing = 0.167; Packing void fraction = 0.76; packing specific surface area = 2132 m²/m³.

$$\text{Regeneration efficiency 1} = \left(\frac{\text{Rich CO}_2 \text{ loading} - \text{Lean CO}_2 \text{ loading}}{\text{Rich CO}_2 \text{ loading}} \right) \times 100 \quad (5.1)$$

Regeneration efficiency 2

$$= \left(\frac{\text{Amount of CO}_2 \text{ in Rich (kg/s)} - \text{Amount of CO}_2 \text{ in Lean(kg/s)}}{\text{Amount of CO}_2 \text{ in Rich (kg/s)}} \right) \times 100 \quad (5.2)$$

$$\text{Regeneration energy (without motor power)} = \frac{\text{Reboiler duty}}{\text{Mass of CO}_2 \text{ desorbed}} \quad (5.3)$$

$$\text{Regeneration energy (with motor power)} = \frac{(\text{Reboiler duty} + P_{\text{motor}})}{\text{Mass of CO}_2 \text{ desorbed}} \quad (5.4)$$

$$\text{Residence time (t}_{\text{res}}) = \frac{V}{Q_L} \quad (5.5)$$

where V is the volume of the liquid films in the bed calculated using Equation 5.6

$$V = \left(\frac{3v_L Q_L}{2\pi Z a \omega^2} \right)^{1/3} (a2\pi Z) \left[r_o^{4/3} - r_i^{4/3} \right] \quad (5.6)$$

Q_L is the liquid volumetric flowrate (m³/s)

5.4.1 Effect of rich-MEA flow rate on regeneration efficiency

5.4.1.1 Justification for case study

Rich-MEA solvent flow rate not only has influence on the amount of CO₂ that will be stripped in the regenerator, but also has relationship with the reboiler duty. Therefore, study on the right quantity of rich-MEA solvent coming into the regenerator is necessary.

5.4.1.2 Setup of the case study

For this study, the process input conditions are shown in **Table 5-7** with the rich-MEA flow rate varying from 0.2 kg/s to 0.6 kg/s. Here the rich-MEA loading is kept constant (i.e. 0.482 mol CO₂/mol MEA) for all the three cases. MEA concentration of 32.9 wt%, 50.443 wt% and 60.431 wt% were selected to cover the MEA concentration for conventional packed which is around 30 wt% and high to 60.431 wt% which is beneficial for intensified PCC process because of short residence time.

Table 5-7 Process inputs

Variable	Case 1	Case 2	Case 3
Rich-MEA temperature (°C)	104	104	104
Rich-MEA pressure (kPa)	202.65	202.65	202.65
Rich-MEA flow rate (kg/s)	0.2 – 0.6	0.2 – 0.6	0.2 – 0.6
Rich-MEA composition (wt. %)			
H ₂ O	58.116	32.027	18.559
CO ₂	8.984	17.53	21.01
MEA	32.9	50.443	60.431
Rich loading (mol CO ₂ /mol MEA)	0.482	0.482	0.482
Reboiler temperature (°C)	120	120	120
Rotor speed (RPM)	1000	1000	1000

5.4.1.3 Results and discussion

Figure 5-2a (using Equation 5.1) and **Figure 5-2b** (using Equation 5.2) shows a decrease in regeneration efficiency as the rich-MEA solvent flow rate increases. This is because of decrease in residence time of the solvent in the regenerator as shown in **Figure 5-3a**, and relatively same amount of CO₂ stripped off from the rich-MEA stream (**Figure 5-3b**). The percentage reduction in regeneration efficiency as the rich-MEA solvent flow rate increases from 0.2 kg/s to 0.6 kg/s is 67.3 %, 66.59 % and 66.60% for Case 1, Case 2 and Case 3

respectively. **Figure 5-2a,b** indicates that the higher the MEA concentration in the rich-MEA solvent the lower the regeneration efficiency, this is because the simulation was performed under the same rich-MEA loading which means more CO₂ will be loaded in the higher MEA concentration rich-MEA stream in order to have same loading. **Figure 5-4** shows that the lowest lean loading is at rich-MEA flow rate of 0.2 kg/s which corresponds to the highest regeneration efficiency of 55.72 %, 35.95% and 29.93% for Case 1, 2 and 3 respectively in **Figure 5-2a,b**.

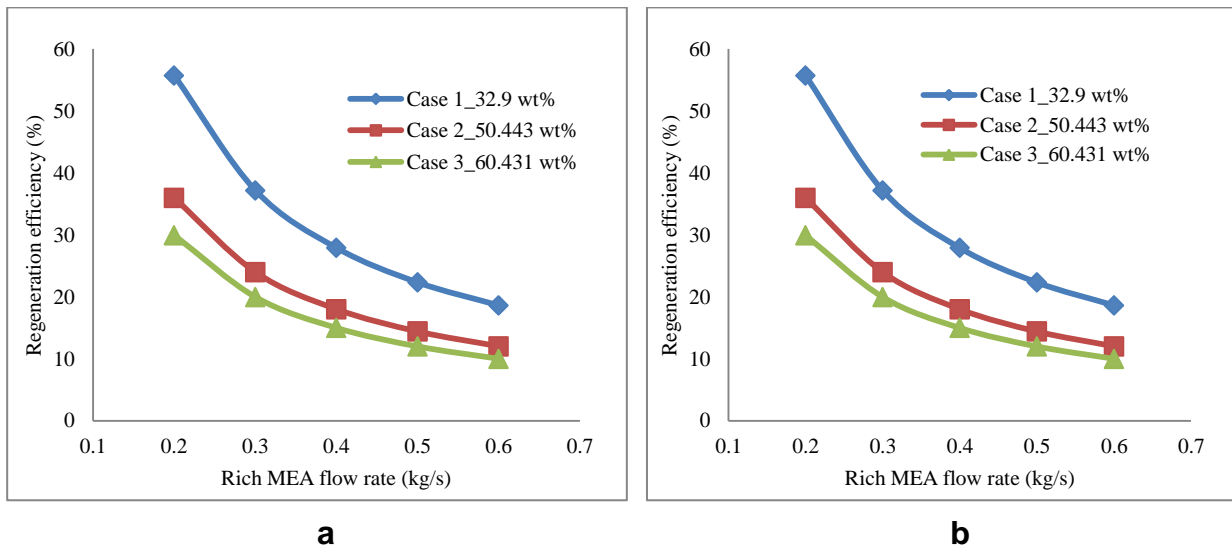


Figure 5-2 Effect of rich-MEA flow rate on regeneration efficiency (a) using Equation 5.1 (b) using Equation 5.2

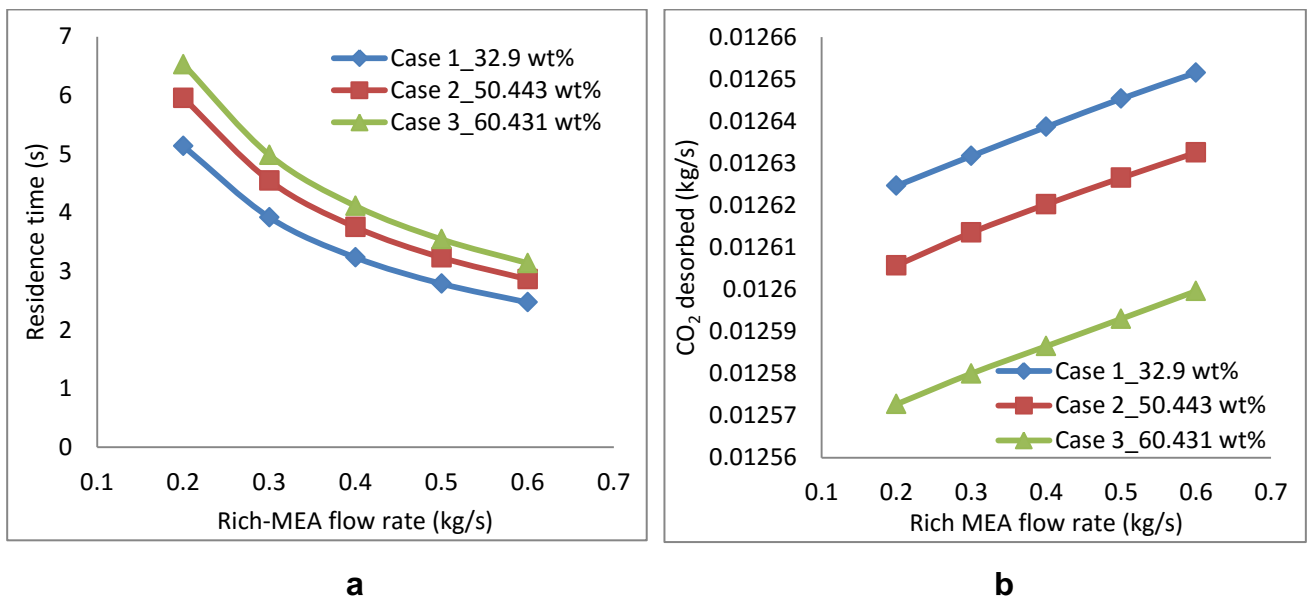


Figure 5-3 Effect of rich-MEA flow rate on (a) Residence time (b) CO₂ desorbed

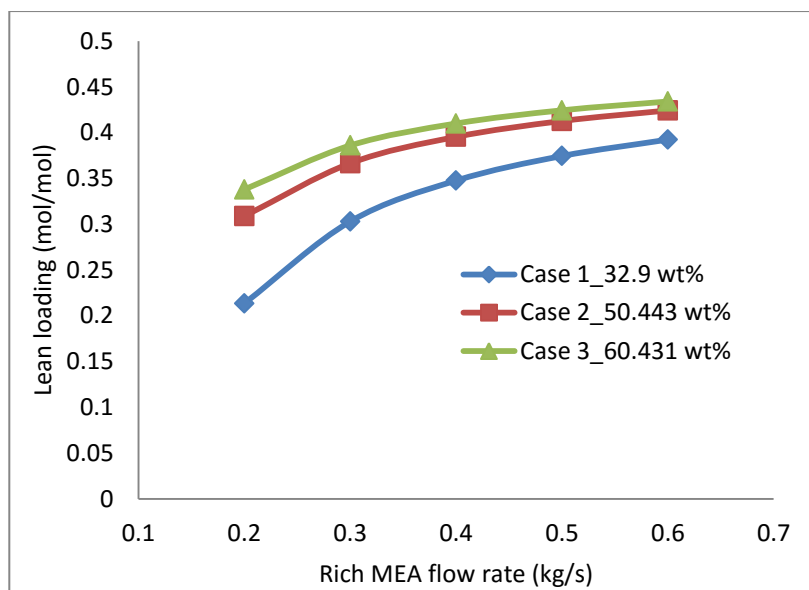


Figure 5-4 Effect of rich-MEA flow rate on lean loading

5.4.2 Effect of rich-MEA flow rate on regeneration energy

5.4.2.1 Justification for case study

The cost implication of running any capture plant is heavily dependent on the energy to regenerate per kilogram of CO₂ from the rich solvent. Therefore study on the right quantity of rich-MEA solvent coming into the regenerator is necessary so that regeneration energy consumption can be minimised.

5.4.2.2 Setup of the case study

For this study, the process input conditions are same as **Table 5-7** with the rich-MEA flow rate varying from 0.2 kg/s to 0.6 kg/s. The reboiler temperature and rotor speed were kept constant at 120 °C and 1000 rpm respectively.

5.4.2.3 Results and discussion

It can be observed from **Figure 5-5a,b** that the regeneration energy decreases with increase in rich-MEA flow rate from 0.2 kg/s to 0.3 kg/s. This is because mass and heat transfer coefficients increase with an increase in the solution flow rate since it is beneficial in the formation of thinner liquid boundary layer on packing surfaces and more smaller liquid droplets, resulting in decrease of mass and heat transfer resistance. But as the flow rate exceeds 0.3 kg/s the benefit is outweighed by the need to heat more solvent in the reboiler leading to increase in reboiler duty. The lowest regeneration energy obtained from the study is at flow rate of 0.3 kg/s rich-MEA for all cases. For Case 1 the regeneration energy is 4.30

GJ/ton CO₂ (without motor energy) and 4.43 GJ/ton CO₂ (with motor energy) while Case 2 is 4.03 GJ/ton CO₂ (without motor energy) and 4.17 GJ/ton CO₂ (with motor energy) and Case 3 has 3.97 GJ/ton CO₂ (without motor energy) and 4.10 GJ/ton CO₂ (with motor energy). Therefore to operate intensified regenerator under these specifications, 0.3 kg/s rich-MEA flow rate is the best operating point because of lowest regeneration energy and relatively good regeneration efficiency of 36.67 %, 23.99 % and 19.97 % for Case 1, 2 and 3 respectively as shown in **Figure 5-2a,b**.

The percentage increase in energy for regeneration when rich-MEA flowrate increases from 0.3 kg/s to 0.6 kg/s is 18.58 %, 16.87% and 14.88% for Case 1, 2 and 3 respectively. Also **Figure 5-5a,b** shows the effect of rich-MEA concentration on regeneration energy. It was found that the higher the rich-MEA concentration the lower the regeneration energy this is because of the lower amount of H₂O vaporising in higher rich-MEA concentration than in lower rich-MEA concentration. The trend of increase in regeneration energy as the rich-MEA flow rate increases can be further explained by **Figure 5-6** showing how the reboiler duty increases as the rich-MEA flow rate increases.

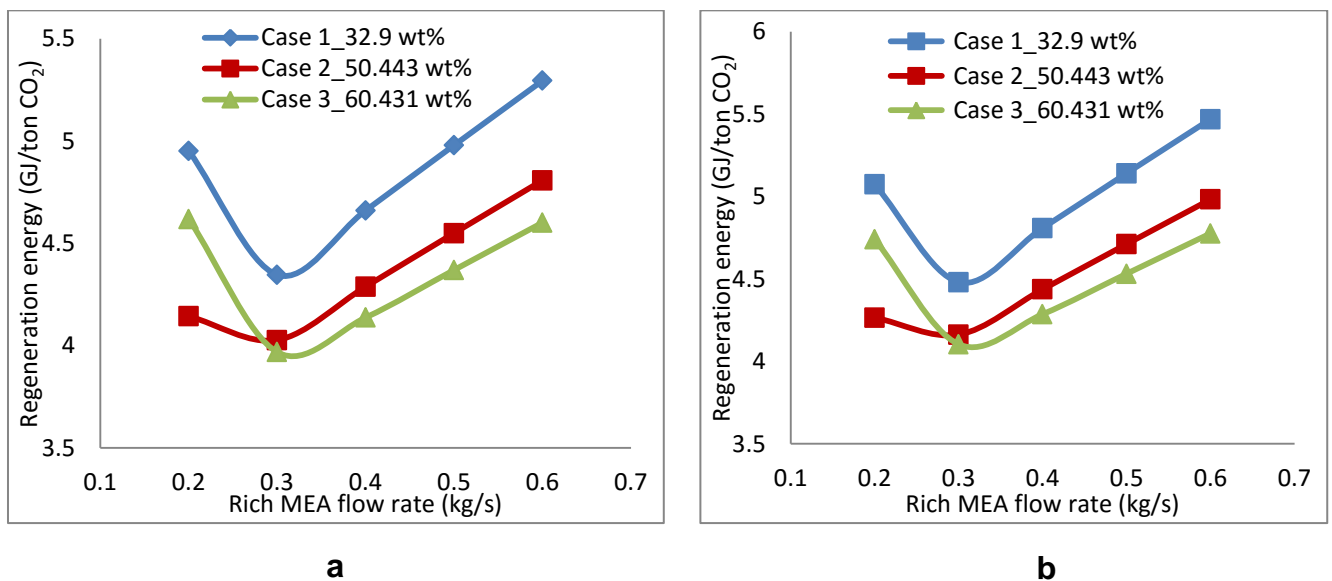


Figure 5-5 Effect of rich-MEA flow rate on regeneration energy (a) without motor energy (b) with motor energy

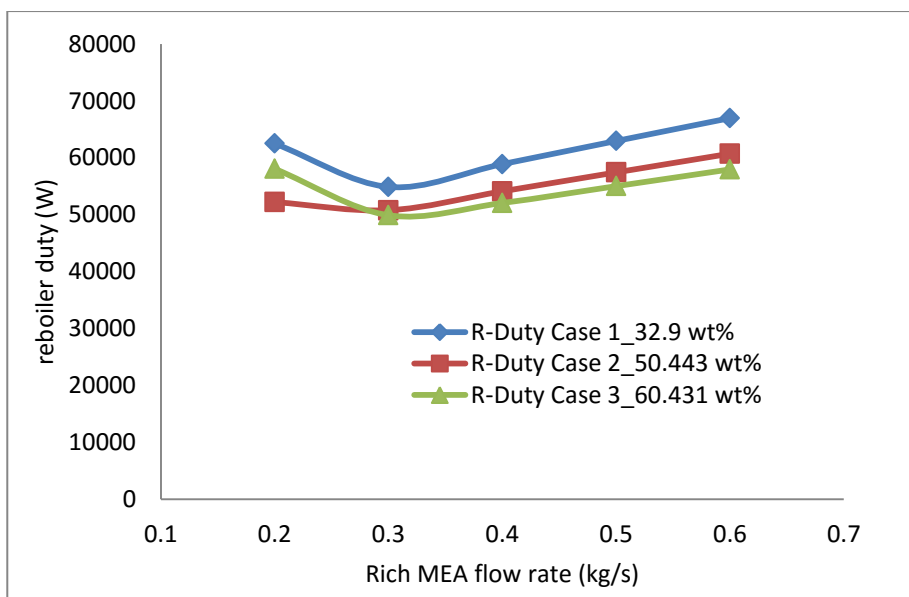
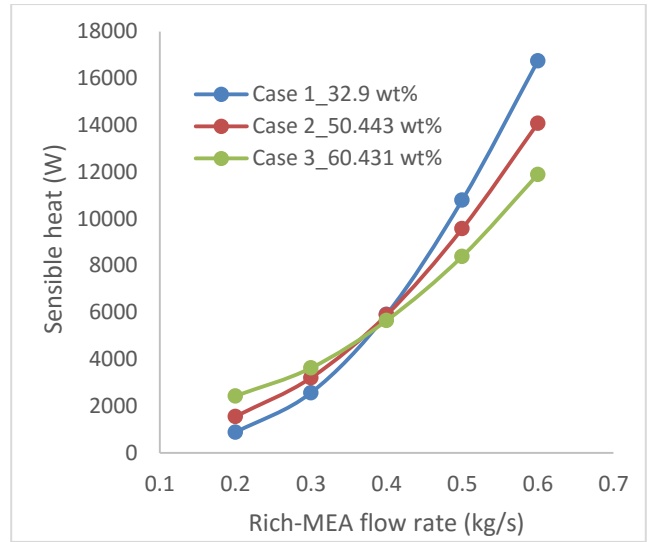
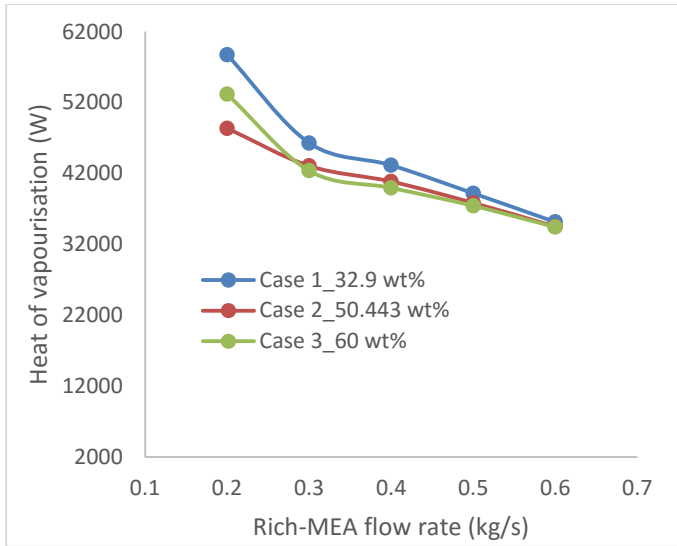


Figure 5-6 Effect of rich-MEA flow rate on reboiler duty

To further account for why there is a decrease and increase (i.e. the minimum point) in the regeneration energy as shown in **Figure 5-5a,b** the author divided the heat duty requirement in the reboiler into three different part (i.e. (i) Sensible heat to raise the temperature of the rich-MEA stream in the reboiler (ii) Heat of reaction to reverse the absorption reaction and release CO₂ (iii) Heat of vaporisation to maintain the driving force for transfer of CO₂ from liquid phase to gas phase). **Figure 5-7a,b** and **Figure 5-8** shows how the heat of vaporisation decreases with increase in rich-MEA flowrate, sensible heat increases with increase in rich-MEA flow rate and heat of reversible reaction increases with increase in rich-MEA flow rate respectively. The combined effect of these heat duty requirements is responsible to having 0.3 kg/s rich-MEA flow rate as the minimum regeneration energy under the process input conditions shown in **Table 5-7**.



a

b

Figure 5-7 Effect of Rich-MEA flow rate on (a) Heat of vaporisation (b) Sensible heat

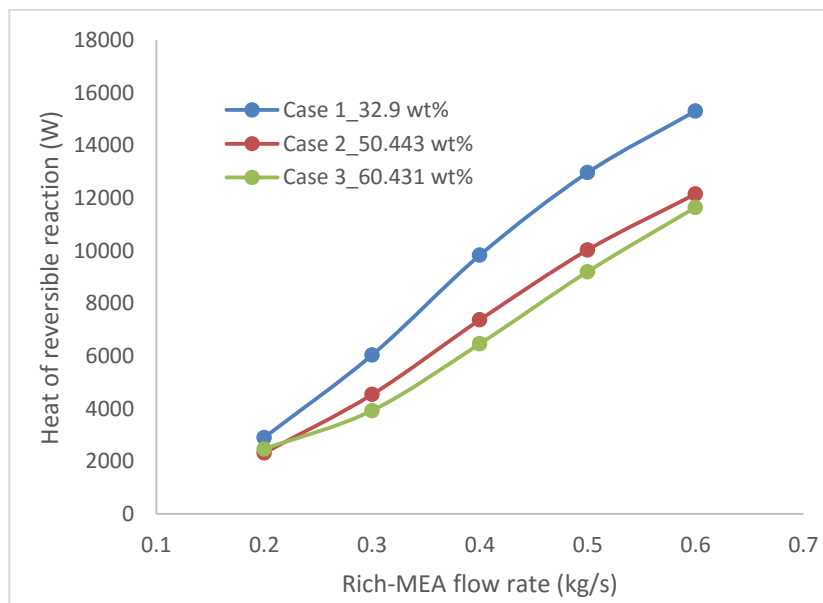


Figure 5-8 Effect of Rich-MEA flow rate on heat of reversible reaction

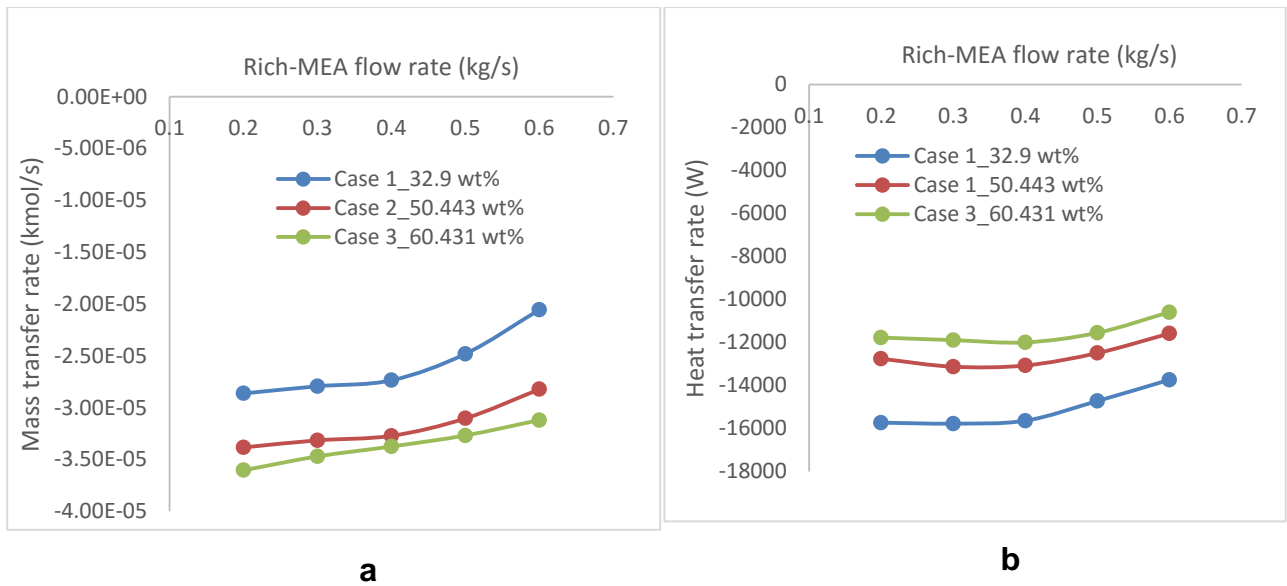


Figure 5-9 Effect of Rich-MEA flow rate on (a) mass transfer rate (b) heat transfer rate

Figure 5-9a shows how the CO₂ mass transfer rate increases as the rich-MEA flow rate increases. The negative sign indicates transfer from liquid to vapour. In **Figure 5-9b** heat transfer rate increases with increase in rich-MEA flow rate, the negative sign indicate transfer from liquid to vapour. The CO₂ mass transfer rate and the heat transfer rate study look at mass and heat transfer from the inner to outer radius of the RPB excluding the mass and heat transfer in the condenser and reboiler.

5.4.3 Effect of rotor speed on regeneration efficiency

5.4.3.1 Justification for case study

Regeneration efficiency defines the amount of CO₂ that is strip-off in the regenerator to the total amount of CO₂ in the rich solvent stream. Study of this parameter is very important because when recycling the lean solvent to the absorber, the CO₂ lean loading determines the rate at which CO₂ absorbed in the absorber.

5.4.3.2 Setup of the case study

For this study, the rotor speed was varied from 200 rpm and 1200 rpm in order to cover the experimental range of rotor speed reported in Jassim *et al* [114] and Cheng *et al* [120]. Input process conditions for this study are shown in **Table 5-7**. The reboiler temperature and rich-MEA flow rate were kept constant at 120 °C and 0.3 kg/s respectively for all the cases.

5.4.3.3 Results and discussion

Figure 5-10a shows that the regeneration efficiency increases with increase in the rotor speed. The impact of rotor speed on lean-MEA loading is shown in **Figure 5-10b**. Though higher rotor speed can produce opposite effect on mass and heat transfer by decreasing the residence time (as shown in Figure 5-11a) but this effect was counter balanced by the increase in the interfacial area which enhances mass and heat transfer. Burns *et al.* [212] stated that at higher rotor speed there are more of smaller liquid droplets and thinner liquid films in the packing regions of the bed, which means increase in interfacial area. The amount of CO₂ desorbed from the stripper increases as the rotor speed increases as shown in **Figure 5-11b**.

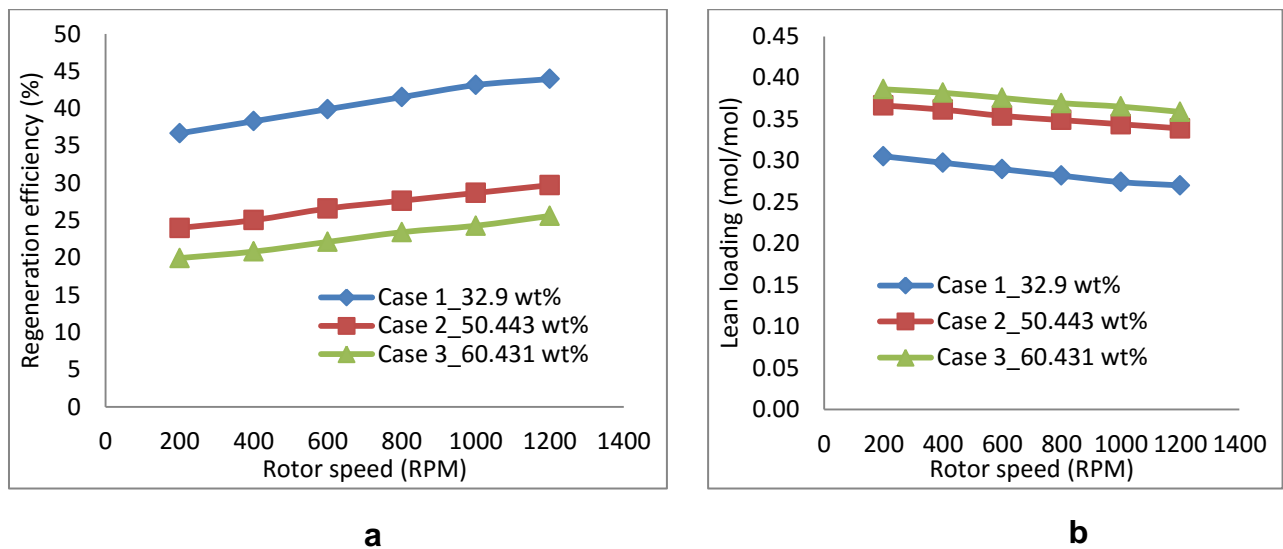


Figure 5-10 Effect of rotor speed on (a) regeneration efficiency (b) lean loading

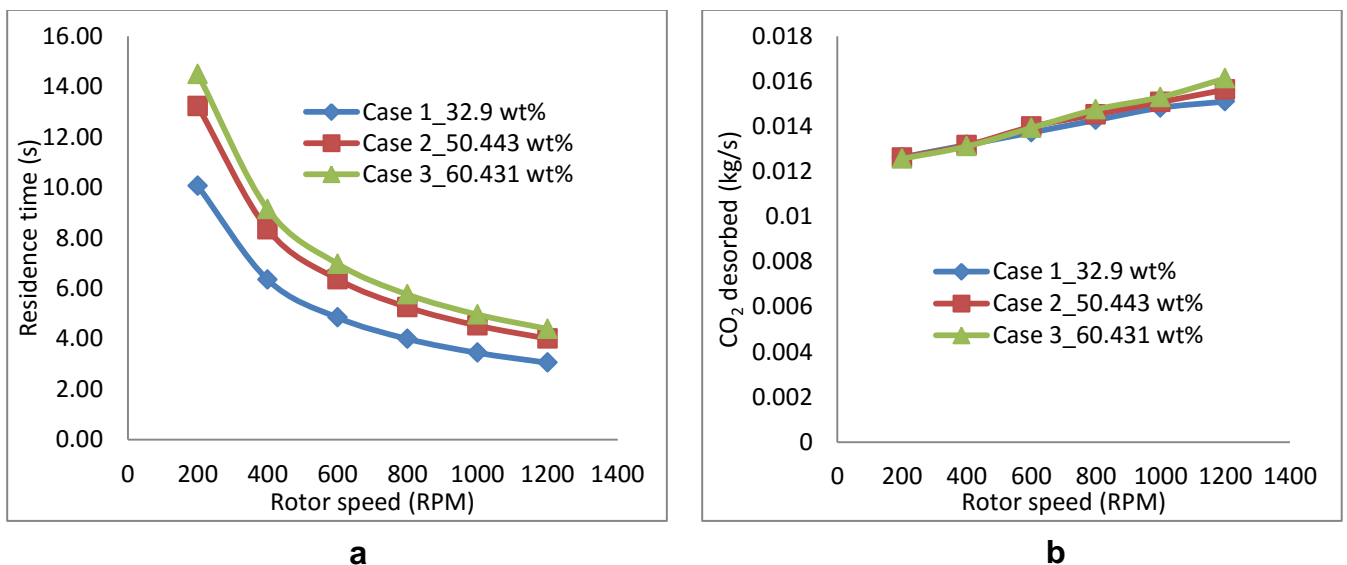


Figure 5-11 Effect of rotor speed on (a) Residence time (b) CO₂ desorbed

5.4.4 Effect of rotor speed on regeneration energy

5.4.4.1 *Justification for case study*

The higher the rotating speed of the intensified regenerator the higher the energy consumed. Therefore, it is important to understand the relationship that rotor speed has with rich-MEA solvent regeneration so that the energy requirement for maintaining the speed can be minimized with respect to amount of rich-MEA solvent regenerated.

5.4.4.2 *Setup of the case study*

For this study the input process condition is same as **Table 5-7**. The reboiler temperature, rich-MEA flow rate and CO₂ recovery rate were kept constant at 120 °C, 0.3 kg/s and 46 kg/hr respectively for all the cases. Rotor speed was varied from 200 rpm to 1200 rpm

5.4.4.3 *Results and discussion*

Increase in rotor speed decreases the regeneration energy as shown in **Figure 5-12a**. This is because of the increase in mass and heat transfer as the rotors speed increases, since liquid droplet and thin liquid films dominate the packed bed. Also at higher rotational speed the problem of liquid mal-distribution is overcome leading to higher wetted area which subsequently contributes to improving mass transfer. For all cases, the trend in **Figure 5-12a** (without motor energy) shows a drop in the regeneration energy as the rotor speed increases from 200 rpm to 1200 rpm this is because of increase in the rate of CO₂ stripped-off (Figure 5-11b). But when energy consumed by the motor is included shown in **Figure 5-12b** (with motor energy) there is an increase in regeneration energy at rotor speed above 1000 rpm for Case 3, at rotor speed above 600 rpm for Case 2 and at rotor speed above 400 rpm for Case 1. This is because the motor energy is the function of square of rotor speed. Case 3 shows a continuous decrease in regenerator energy as the rotor speed increases from 200 rpm to 1200 rpm this is because viscosity is high in higher MEA concentration and when the rotor speed becomes higher this problem will reduced leading to more CO₂ stripped. The average percentage increase in regeneration energy when motor power is included is 3.41%, 3.64% and 3.72% for Case 1, Case 2 and Case 3 respectively at 1200 rpm. At 1000 rpm the percentage increase is 3.03 %, 3.23 % and 3.29% for Case 1, 2 and 3 respectively. **Figure 5-13** shows how the reboiler duty changes with the rotor speed. This shows that there is operating condition limit to which you can increase the rotor speed to avoid energy waste.

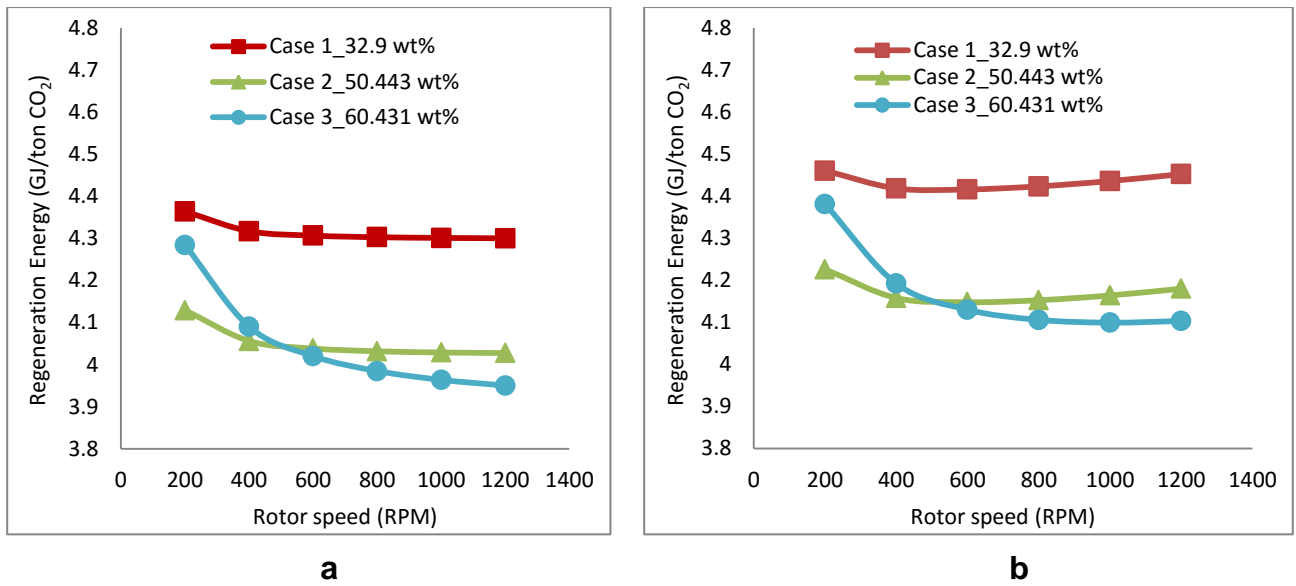


Figure 5-12 Effect of rotor speed on regeneration energy (a) without motor energy (b) with motor energy

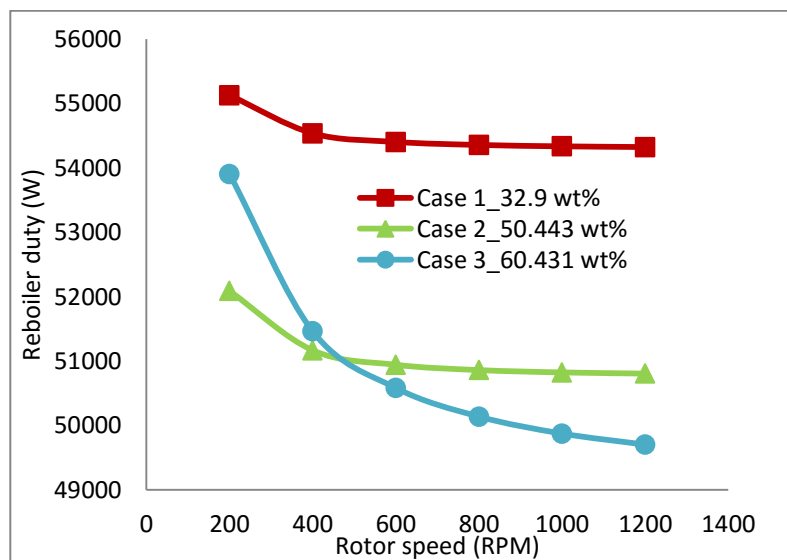


Figure 5-13 Effect of rotor speed on reboiler duty

5.4.5 Effect of reboiler temperature on regeneration efficiency

5.4.5.1 Justification for case study

Reboiler duty has a direct relationship with the temperature of the reboiler, therefore it is important to look at the best operating reboiler temperature that will give the needed reboiler duty that can strip off the CO₂ from the rich-MEA solvent.

5.4.5.2 Setup of the case study

For this study, the reboiler temperature was varied from 105 to 125 °C. Process input conditions are the same as **Table 5-7** with rich-MEA flow rate at 0.3 kg/s and rotor speed of 1000 rpm.

5.4.5.3 Results and discussion

Figure 5-14a shows that the regeneration efficiency increases with increase in reboiler temperature. In **Figure 5-14b** there is decrease in lean-MEA loading as the reboiler temperature increases, this is because of the increase in the amount of CO₂ desorbed as shown in **Figure 5-15**.

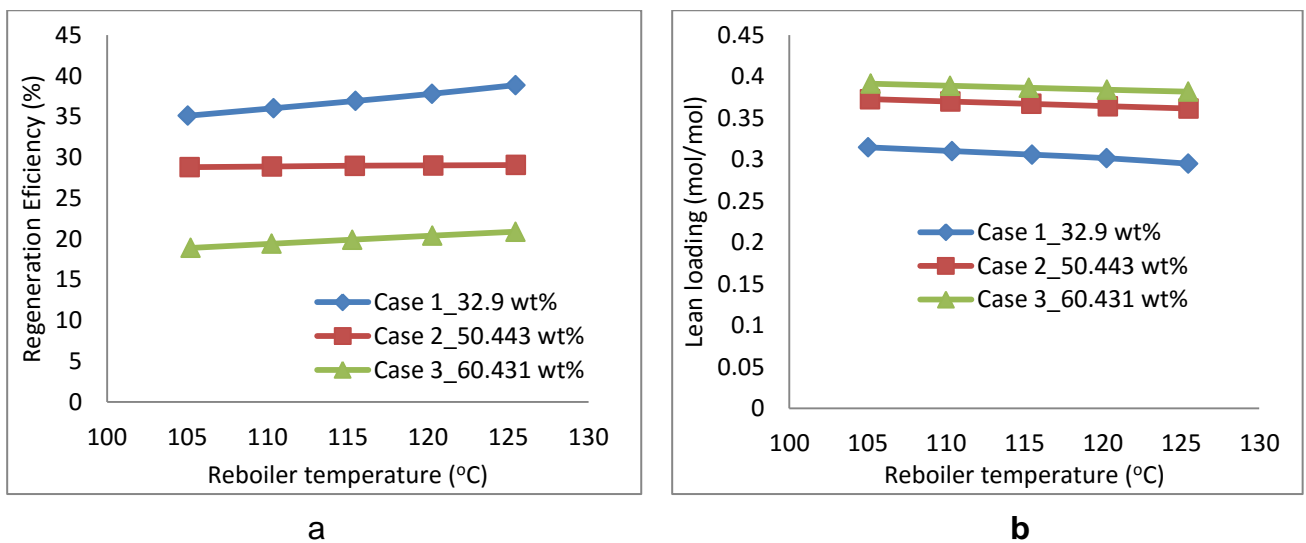


Figure 5-14 Effect of reboiler temperature on (a) regeneration efficiency (b) lean loading

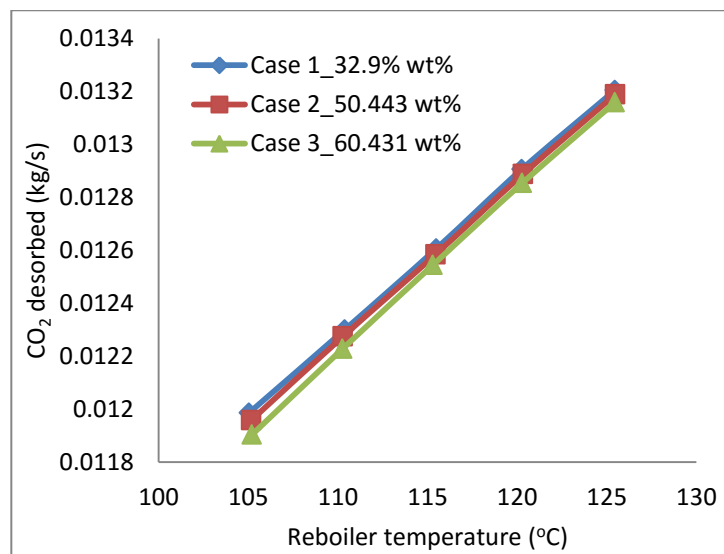


Figure 5-15 Effect of reboiler temperature on amount of CO₂ desorbed

5.4.5 Effect of reboiler temperature on regeneration energy

5.4.5.1 *Justification for case study*

Operating intensified regenerator at the right reboiler temperature will lead to good system performance by minimising regeneration energy waste and also having high regeneration efficiency.

5.4.5.2 *Setup of the case study*

Process input condition is same as **Table 5-7**. The CO₂ recovery rate of 46 kg/hr was kept constant in all the cases. Reboiler temperature was varied from 105 to 125 °C

5.4.5.3 *Results and discussion*

There is a decrease and an increase in regeneration energy as the reboiler temperature increases from 105 °C to 125 °C. From **Figure 5-16a,b** (with and without motor energy) the regeneration energy decreases as the reboiler temperature increases from 105 °C to 115 °C for Case 1 and 3, but this behaviour changes when the reboiler temperature exceed 115 °C. For Case 3, the regeneration energy decreases as the reboiler temperature increases from 105 to 120 °C, but when the reboiler temperature is more than 120 °C the regeneration energy increases. This is because at higher temperature we expect an increase in water vapour flow rate which results in an increase in regeneration energy because of the heat of vaporisation of water. Case 2 gives lower regeneration energy than Case 3 at temperature lower than 115 °C even though it has higher amount of water content than Case 3 this could be associated to the high viscosity of Case 3 which affect the rate of mass transfer at lower temperature but once the reboiler temperature reaches around 120 °C, Case 3 has the lowest regeneration energy. Therefore at reboiler temperature of 120 °C, Case 3 which has the highest MEA concentration and lower water content gives the lowest regeneration energy. **Figure 5-17** shows how the reboiler duty increases with increase in reboiler temperature.

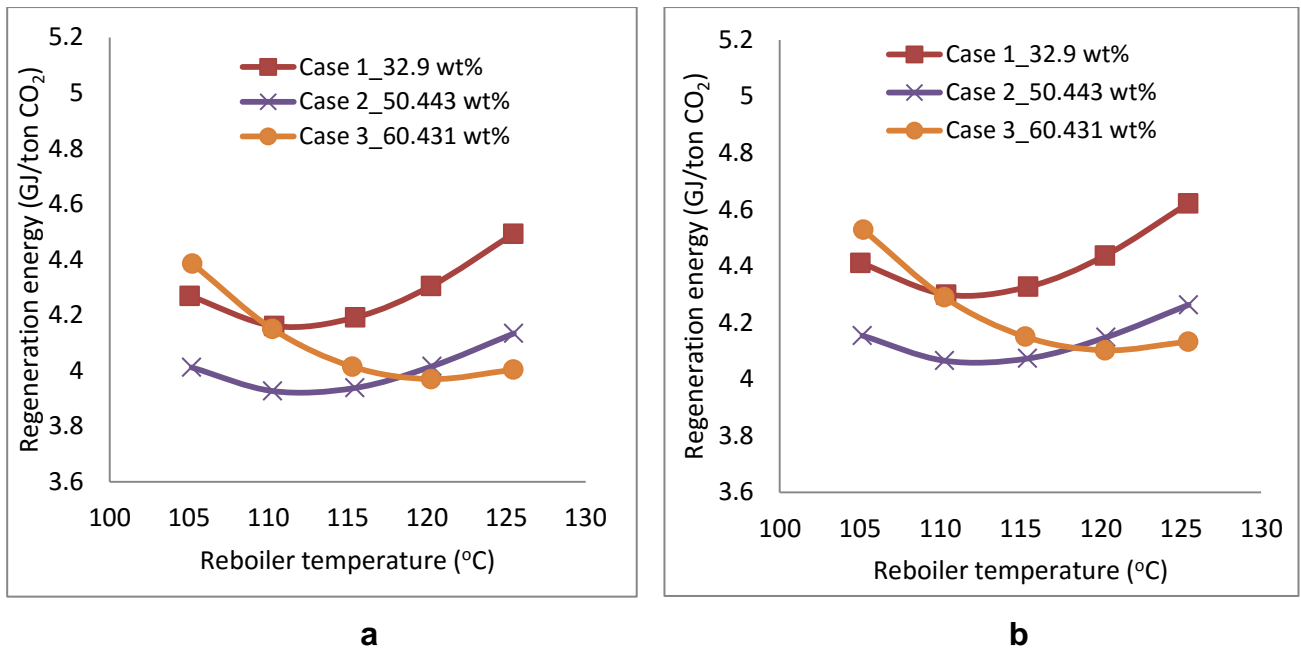


Figure 5-16 Effect of reboiler temperature on regeneration energy (a) without motor energy (b) with motor energy

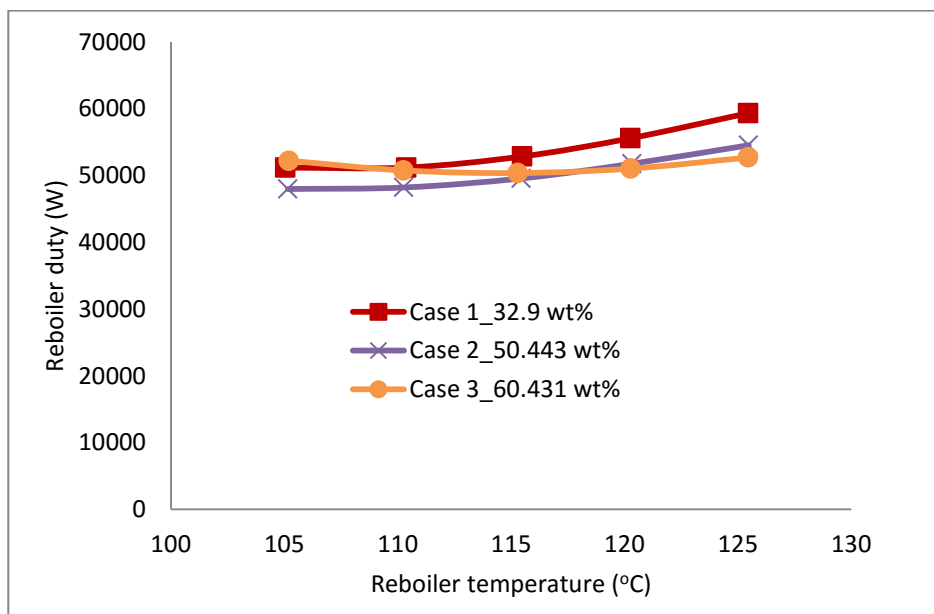


Figure 5-17 Effect of reboiler temperature on reboiler duty

5.5 Comparison between intensified and conventional stripper

5.5.1 Justification for the case study

This study was carried out to provide a comparison under some fixed conditions such as Rich-MEA flowrate, pressure, temperature, rich-MEA loading and lean-MEA loading between intensified regenerator and conventional regenerator.

5.5.2 Setup of the case study

For this study, **Table 5-8** is used as the input conditions for the conventional and intensified regenerator. The rotor speed for the intensified regenerator is kept constant at 1000 rpm. Regeneration efficiency was kept constant at 37.16 % for both the conventional and the intensified regenerators.

Table 5-8 Process conditions for Conventional and RPB regenerator

Description	Conventional regenerator	RPB regenerator
	Rich-MEA	Rich-MEA
Rich-MEA temperature (°C)	97	97
Rich-MEA pressure (atm.)	2	2
Rich-MEA flowrate (kg/s)	0.300	0.300
Rich-MEA loading (mol CO ₂ /mol MEA)	0.482	0.482
Mass-Fraction (%)		
H ₂ O	58.116	58.116
CO ₂	8.984	8.984
MEA	32.900	32.900

5.5.3 Results and discussion

The study in **Table 5-9** showed 44 times packing volume reduction in an intensified regenerator compared to conventional packed column regenerator without sumps. By using the assumption given by Agarwal *et al.* [141] that the casing volume of RPB is 4.5 times the rotating packing volume then volume reduction compared to conventional packed column regenerator is found to be 10 times smaller. The height of transfer unit (HTU) for conventional packed column regenerator is calculated as 20.8 cm while for the intensified regenerator is 1.7 cm. The smaller HTU in RPB regenerator is responsible for smaller RPB regenerator size compared to conventional packed column.

Table 5-9 Comparison between conventional and RPB stripper

Description	Conventional regenerator	RPB regenerator
Height of packing (m)	3.700	0.371 (r_o) 0.152 (r_i)
diameter (m)	0.476	0.167 axial depth
Packing Volume (m^3)	0.659	0.015
Packing volume reduction		44 times
Volume of unit (m^3)	0.659 ^a	0.068 ^b
Volume reduction factor		10 times
Specific area (m^2/m^3)	151	2132
Void fraction	0.980	0.760
Lean-MEA loading (mol CO ₂ /mol MEA)	0.303	0.303

^a Excluding sump

^b Using the assumption given by Agarwal et al [141]

5.6 Summary

Intensified regenerator using RPB technology was modelled in this study. The model developed was validated by the experimental data reported in Jassim et al. [114] and Cheng et al. [120]. The model validation shows good agreement with the experimental data.

Process analyses on the effect of rich-MEA flow rate, rotational speed and reboiler temperature on CO₂ regeneration efficiency and regeneration energy were done. The study shows that an increase in the rich-MEA flow rate leads to a decrease in the regeneration efficiency. Also the regeneration energy increases as the rich-MEA flow rate increases. There is an increase in the regeneration efficiency as the rotor speed increases but the regeneration energy decreases as the rotor speed increases since mass and heat transfer is enhanced at higher rotor speed. Reboiler temperature was varied from 105 °C to 125 °C, the result shows a decrease in regeneration energy at reboiler temperature between 105 °C to 120 °C, but when the reboiler temperature exceeds 120 °C the regeneration energy begins to increase. Under the same process conditions, intensified regeneration has volume reduction of 10 times compared to conventional packed column.

Chapter 6 Process analysis, technical and economic assessment of intensified PCC process based on RPB technology

In this chapter, process description of closed loop intensified PCC process using conventional cross heat exchanger and reboiler is presented in Section 6.1. Process analysis on the intensified PCC model is discussed in Section 6.2. Section 6.3 presents the technical comparison between intensified PCC process and conventional PCC process. Economic assessment of intensified PCC process is discussed in Section 6.4. Finally summary of the findings is presented in Section 6.5.

6.1 Process description

A closed loop intensified PCC process using conventional cross heat exchanger and reboiler is shown in **Figure 6-1**. The absorber has packing materials, which provides sufficient surface area for the absorption of CO₂. Flue gas enters the RPB through the side from the outer diameter contacting counter-currently with the lean-MEA solvent entering through liquid distributor in the inner diameter. The solvent is collected as rich-MEA solvent at the bottom of the RPB absorber. Lean gas is released at the top of the RPB. Lean-MEA refers to the amine stream that is strip-off of CO₂ (i.e. the amine stream that enters the RPB from inner diameter). When the lean-MEA stream is loaded with CO₂, as is the case with the stream that leaves the bottom of the RPB absorber, it is referred to as a rich-MEA stream. The rich-MEA leaves from the bottom of the RPB absorber from where it is sent to the cross-heat exchanger. In the cross heat-exchanger, the rich-MEA from the RPB absorber exchanges heat with the lean-MEA stream from the RPB stripper resulting in heating up the rich-MEA stream and cooling down the lean-MEA stream. The rich-MEA stream flows from the cross-heat exchanger to the RPB stripper. The RPB stripper has a kettle reboiler. The stripper typically operates at slightly elevated pressures (~1.5 – 2 bars) than the absorber. The rich-MEA enters the intensified stripper through the liquid distributor at the centre of the RPB and flows from the inner diameter to the outer diameter of the packing, contacting counter-currently with the vapours from the reboiler. The stream from the top of the RPB stripper is taken to a condenser in order to condense the water and lower the temperature and then to flash to separate the CO₂ and H₂O. In the reboiler of the stripper, steam from the power plant is used to produce the heat duty. The heat duty in the reboiler arises from three different requirements [220]:

1. Sensible heat to raise the temperature of the rich stream to that in the stripper
2. Heat of reaction to reverse the absorption reaction and release CO₂
3. Heat to produce steam to maintain driving force for transfer of CO₂ from liquid phase to gas phase

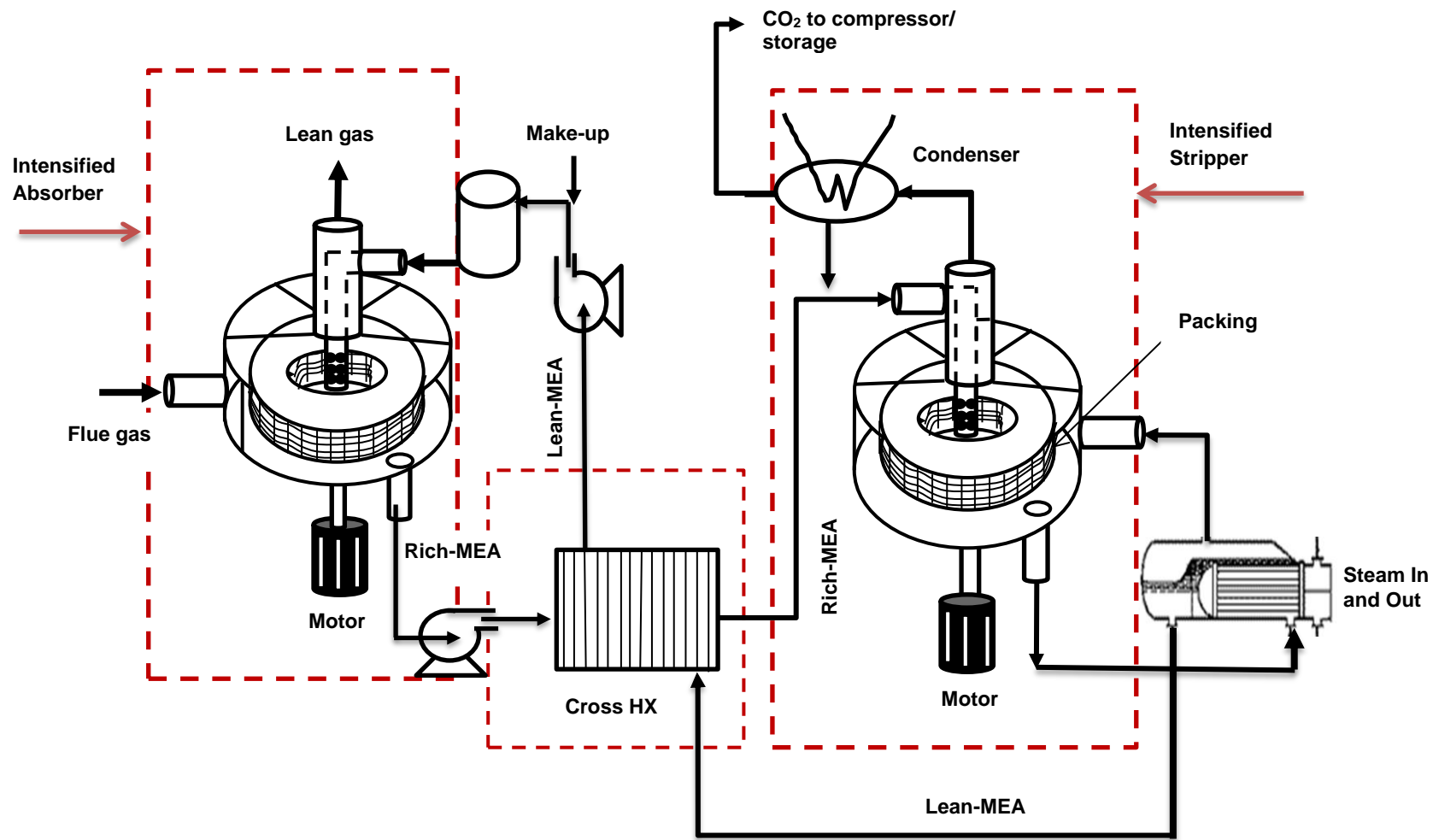


Figure 6-1 Simplified PFD of intensified chemical absorption process for PCC using conventional reboiler and cross heat exchanger

6.2 Process analysis on intensified PCC process

To have full insight into the system behaviour, process analysis of the intensified PCC process is necessary. Experimental data for validation of closed loop intensified absorber is not available anywhere in an open literature. To carry out model validation, the author decided to validate standalone intensified absorber and intensified stripper as described in Chapters 4 and 5. The RPB absorber and stripper used for the process analysis has the following packing geometry: Outer radius = 0.371; Inner radius = 0.152; axial depth of packing = 0.167; Packing void fraction = 0.76; packing specific surface area = 2132 m²/m³.

6.2.1 Impact of liquid to gas (L/G) ratio

6.2.1.1 *Justification for case study*

Solvent recirculation rate is an important parameter in decision making in terms of operating cost of any PCC process plant. High L/G ratio mean high amount of solvent that will be regenerated in the reboiler resulting in high reboiler duty. Also if the L/G ratio is too low we expect lower CO₂ recovery rate in the absorber. Therefore, it is necessary to know the impact L/G ratio has on system performance of intensified PCC process.

6.2.1.2 *Setup of the case study*

Table 6-1 presents the process input condition for study on the impact of L/G ratio on regeneration energy and CO₂ capture rate. The lean-MEA concentration used is 50 wt% and the L/G ratio was varied from 5.63 to 14.06 kg/kg. This L/G ratio range was chosen because of convergence problem that was observed below and above the range.

Table 6-1 Design assumptions used for the design cases in this thesis

Process conditions	Value
lean MEA inlet temp (°C)	40
Lean-MEA flow rate (kg/s)	0.300
Lean-MEA composition (wt%)	
H ₂ O	39.027
CO ₂	10.530
MEA	50.443
Flue gas flow rate (kg/s)	0.050
Flue gas composition (vol%)	
CO ₂	4.710
H ₂ O	2.590
N ₂	92.930
stripper condenser temp (°C)	30
Stripper condenser press. (bar)	1.991
CO ₂ capture rate (%)	90
Rich-MEA pump discharge press. (bar)	2

6.2.1.3 Results and discussion

L/G ratio was varied from 5.63 to 14.06 kg/kg to understand the impact of L/G ratio changes on regeneration energy and the resulting impact on the CO₂ capture level. It can be observed from **Figure 6-2** that as the L/G ratio increases the regeneration energy increases too, this is associated to the increase in the amount of solvent circulating. The regeneration energy calculation in **Figure 6-2** is done in three separate parts. (a) Reg_Energy_1 represents regeneration energy calculation based on **Equation 5.3** (not including the motor energy for rotating the RPBs) (b) Reg_Energy_2 represents regeneration energy calculation based on **Equation 5.4** (including the motor energy for rotating the RPB stripper only) and (c) Reg_Energy_3 represents the regeneration energy calculation including the reboiler duty and motor energy for both absorber and stripper. From **Figure 6-2** the trend in the regeneration energy is the same for all the calculations (i.e. based on reboiler duty only, based on reboiler duty and motor power for stripper and lastly based on reboiler duty with motor power for both absorber and stripper). **Figure 6-3** shows how the CO₂ capture level

increases as the L/G ratio increases this is due increase in CO₂ absorption rate in the absorber since high superficial velocity enhances mass transfer.

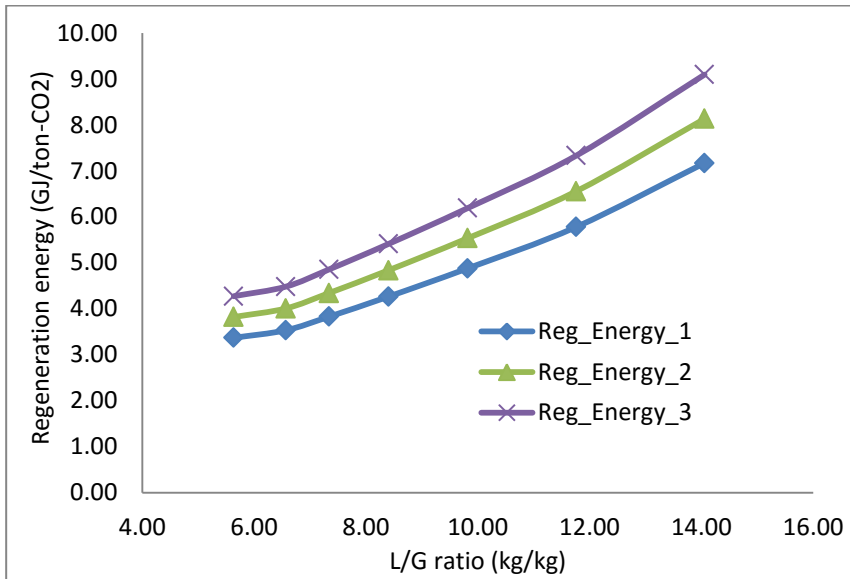


Figure 6-2 Effect of L/G ratio on regeneration energy

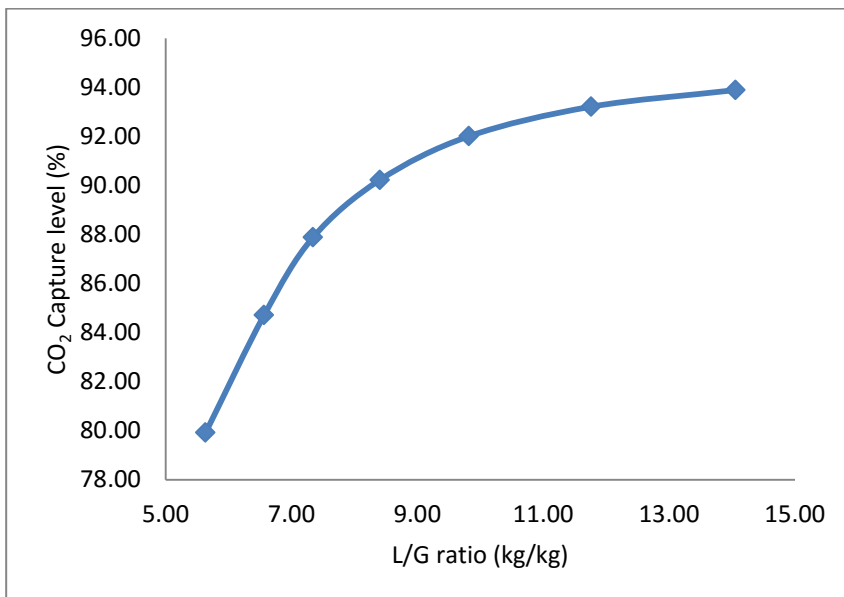


Figure 6-3 Effect of L/G ratio on CO₂ capture level

6.2.2 Impact of lean-MEA loading

6.2.2.1 Justification for case study

Reboiler duty of PCC process will be affected by increase or decrease in lean-MEA loading. Also CO₂ recovery rate can be impacted by the level of the lean-MEA loading. Therefore study on the impact of lean MEA loading on the performance of intensified PCC process is necessary.

6.2.2.2 Setup of the case study

Table 6-1 presents the process input conditions for this study. The lean-MEA loading was varied from 0.2845 to 0.3110 mol/mol. This range of lean-MEA loading was chosen because it is within the range considered best for conventional PCC process and going below this range will result in good absorption efficiency but specific energy duty becomes very big and going above this range will result in low absorption efficiency which is not good for CO₂ capture and lower regeneration energy which is quite good [17,20]. Also above or below this range convergence is not reached for the specified input conditions, therefore this lean-MEA loading range was used.

6.2.2.3 Results and discussion

The effect of lean-MEA loading on regeneration energy is shown in **Figure 6-4**. Regeneration energy (i.e. calculated based on Equation 5.3) decreases as the lean-MEA loading increases this is because of the decrease in the CO₂ capture level as shown in the **Figure 6-5** which mean less CO₂ will be absorbed in the absorber because of lower absorption capacity. Also at lower lean-MEA loading there is higher amount of H₂O which mean increase in the heat of vaporisation in the reboiler.

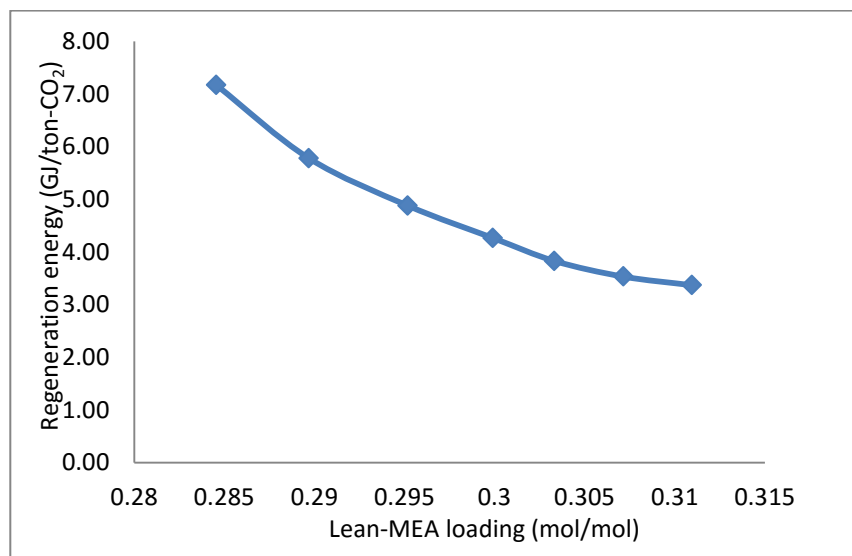


Figure 6-4 Effect of lean-MEA loading on regeneration energy

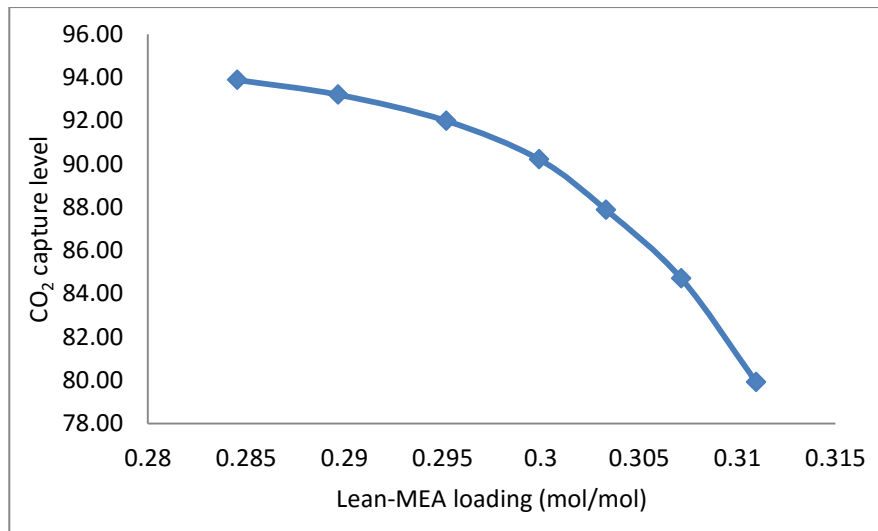


Figure 6-5 Effect of lean-MEA loading on CO₂ capture level

6.3 Technical performance comparison between intensified process and conventional process

6.3.1 Size reduction

Joel *et al.* [115] carried out comparative study between conventional absorber and intensified absorber, and found size reduction factor of about 12 times. Study in this thesis also shows that for a standalone intensified stripper compared to conventional stripper a size reduction factor of 10 times is observed. Another unit operation in intensified PCC process that needs to be intensified is the heat exchanger. Li *et al.* [221] reported a reduction factor of 4-6 times for PCHE compared to shell-and-Tube heat exchanger operating at the same duty. Therefore the major units in intensified PCC process have been reduced resulting in lower footprint.

6.3.2 Energy consumptions

Energy consumption in intensified PCC process includes the electricity (motor) energy consumed to drive the RPB absorber and stripper and also heat energy required to generate steam for solvent regeneration. Therefore, in intensified PCC process there is additional parasitic energy (i.e. motor electricity consumption) for carbon capture but some of this is offset by the reduction in the pumping energy required to get the solvent to the top of a packed tower. Study in Chapter 5 shows that the regeneration energy requirement for intensified stripper is comparable to that of conventional packed column even though the reduction in pumping power requirement compared to conventional packed column is not included in the regeneration energy calculation. Generally the higher the rotating speed, the higher the electricity consumption by the motor. Study in thesis and Agarwal *et al.* [141]

shows that electricity consumption is quite low at rotor speed less than 1000 rpm but the number increased significantly at 1500 rpm, the reason being that power consumption increases as the square of the rotational speed since most of it can be attributed to the kinetic energy gain of the liquid flowing through the RPB.

6.4 Economic assessment

Total cost for operating an industrial process plant includes the capital expenditure (CAPEX) and operating expenditure (OPEX). The CAPEX includes the cost of equipment material and installation, the labour cost, engineering and management cost and others cost comes from contracture and commissioning. OPEX is divided into two components, fixed OPEX and variable OPEX. Fixed OPEX is the cost for operating and maintenance (O&M) while variable cost is basically the energy and utilities cost [222].

6.4.1 Capital cost estimations

Cost calculation for the intensified PCC process adapted in this thesis is the factorial method of cost estimation. In this thesis the costs are calculated based on data from Wood [223], Turton et al. [224] and Towler and Sinnott [222]. To perform an economic analysis, it is necessary to estimate the capital cost of major equipment [222-225]. Preliminary cost estimates for some of the equipment's is done using correlations and graphs available for various types of common equipment [224]. Here, the base condition equipment price calculated by Equation 6.4.1 [224].

$$\text{Log}_{10}C_p^o = K_1 + K_2 \log_{10}(A) + K_3 [\log_{10}(A)]^2 \quad (6.4.1)$$

where A is the size parameter of the equipment. K_1 , K_2 and K_3 are given by Turton et al. [224] for different equipment. The correlation (6.4.1) is valid on a specific range of size parameter above the correlation is not valid. Table B-2 gives the valid range for pressure factor for process equipment. If the size parameter is outside the valid range, the best alternative is to use cost data based on previously purchased equipment of the same type

Equation 6.4.2 [224]

$$\frac{C_a}{C_b} = \left(\frac{A_a}{A_b}\right)^n \quad (6.4.2)$$

where A is the equipment capacity, C is the purchased cost and n is a cost exponent. The estimated cost is for base equipment made from carbon steel and at atmospheric pressure.

To calculate the purchased equipment cost with different materials and different operating pressure we can use material factor (F_M) and pressure factor (F_P), respectively [224].

$$C_{p,Eq} = \sum_i F_{M,i} F_{P,i} C_{p,i}^o \quad (6.4.3)$$

Capital cost estimation for chemical plant can be done using Lang factor method. The total cost is determined by multiplying the total purchased cost for all the major equipment by a constant [222,224,225]. The Lang factor is set equal to 4.74 (i.e. for fluids processing plant) in this thesis.

Turton et al. [224] introduced another technique for calculating module cost of the main equipment. For some equipment such as heat exchangers, vessels and pumps, bare module cost is calculated using Equation 6.4.4 and Equation 6.4.5 is for calculating bare module cost for packing [222,224,225].

$$C_{BM} = C_p^o (B_1 + B_2 F_M F_P) \quad (6.4.4)$$

$$C_{BM} = C_p^o F_{BM} \quad (6.4.5)$$

$$C_{TM} = 1.18 \sum_i^n C_{BM,i} \quad (6.4.6)$$

$$C_{GR} = C_{TM} + 0.5 \sum_i^n C_{BM,i}^o \quad (6.4.7)$$

where C_{BM} is the bare module price, B_1 and B_2 are the constants, F_M is the material factor, F_P is the pressure factor, F_{BM} is the bare module factor, C_{TM} is the cost of making small-to moderate expansion, and C_{GR} is the cost of completely new facilities for construction in a gross field.

6.4.1.1 Investment cost estimation for RPB absorber and Stripper

Capital and operating cost calculations for RPB is new, there is no to little industrial data and experience in investment and operating costs of RPB absorber and RPB stripper, Sudhoff et al. [226] divided the investment cost for RPB distillation column into three groups (i) the costs for the motor $C_{IC,mot}$ (2) costs for the bearings, drives and rotating parts $C_{IC,drive}$ and (3) costs for the rotors including casing, packing, shafts and distributors $C_{IC,rotors}$. They all contribute to the total investment costs given in Equation (6.4.8) in Euros (€). For the total investment costs, the separate costs are increased by taxes using the factor C_{tax}

$$C_{IC,RPB} = (C_{IC,mot} + C_{IC,drive} + C_{IC,rotors}) C_{tax} \quad (6.4.8)$$

Where the costs for each of the parts division ($C_{IC,mot}$, $C_{IC,drive}$, $C_{IC,rotors}$) are calculated using Equations (6.4.9), (6.4.10), (6.4.11), C_{tax} is the adds taxes on the material costs

$$C_{IC,mot} = C_{IC,FOB,mot} (1 + C_{L+M,mot} C_{L/M,mot}) \frac{C_{CEPCI}}{1000} C_{ER} \quad (6.4.9)$$

$$C_{IC,drive} = C_{IC,FOB,drive} (1 + C_{L+M,drive} C_{L/M,drive}) \frac{C_{CEPCI}}{1000} C_{ER} \quad (6.4.10)$$

$$C_{IC,rotors} = C_{IC,FOB,rotors} (1 + C_{L+M,rotors} C_{L/M,rotors}) \frac{C_{CEPCI}}{1000} C_{ER} \quad (6.4.11)$$

where $C_{IC,FOB,mot}$, $C_{IC,FOB,drive}$ and $C_{IC,FOB,rotors}$ are the free-on-board costs for motor, drive and rotor respectively, $C_{L+M,mot}$, $C_{L+M,drive}$, and $C_{L+M,rotors}$ are the adds labour and material costs for motor, drive and rotor respectively, $C_{L/M,mot}$, $C_{L/M,drive}$ and $C_{L/M,rotors}$ reduces the addition of labour costs if a special alloy is considered in C_{al} for motor, drive and rotor respectively, C_{CEPCI} is the cost digression based on the Chemical Engineering Plant Cost Index, C_{ER} is the conversion to Euro based on exchange rate

The “free-on-board” (FOB) costs in Equations (6.4.9), (6.4.10), (6.4.11) are calculated using Equations (6.4.12), (6.4.13), (6.4.14) representing the three divided parts of the investment costs for the RPBs.

$$C_{IC,FOB,mot} = C_{IC,mot,ref} \left(\frac{P_{mot}}{P_{mot,ref}} \right)^{n_{mot}} C_{RS} C_{en} C_{al} \quad (6.4.12)$$

$$C_{IC,FOB,drive} = C_{IC,drive,ref} \left(\frac{P_{mot} C_{trans}^{0.5}}{P_{drive,ref}} \right)^{n_{drive}} C_{al} \quad (6.4.13)$$

$$C_{IC,FOB,rotors} = C_{IC,rotors,ref} \left(\frac{\dot{V}_{RPB}}{\dot{V}_{RPB,ref}} \right)^{n_{rotors}} \quad (6.4.14)$$

where \dot{V}_{RPB} is the liquid capacity of the RPB calculated as:

$$\dot{V}_{RPB} = \sum \dot{V}_{feed,j} + \dot{V}_{reflux} \quad (6.4.15)$$

$C_{IC,mot,ref}$, $C_{IC,drive,ref}$ and $C_{IC,rotors,ref}$ are the reference value for investment costs for the motor, drives and rotors respectively, P_{mot} is the electrical power for motor, $P_{mot,ref}$ and $P_{drive,ref}$ are the reference value for electrical power of the motor and drives respectively, $\dot{V}_{RPB,ref}$ is the reference value for the liquid capacity of the RPB, C_{trans} is the adds cost for engine transmission ratio to the drives, n_{mot} , n_{drive} and n_{rotors} is the scaling factor of the actual to the reference condition for motor, drives and rotors respectively, C_{RS} is the adds costs for higher rotational speed, C_{en} is the adds costs for fan and enclosure of motor, C_{al} is the adds costs for more expensive alloys.

The cost indexes for calculating the investment costs for the RPBs (i.e. absorber and stripper) adopted from Sudhoff et al. [226] are shown in **Table 6-2**. Continuous extraction

centrifuge proposed by Wood [223] was used as the reference value for the rotor (i.e. casing, packing, shafts and distributors) calculations this is due to its complex nature and lack of reference or scaling experience [226].

6.4.1.2 Investment cost estimation for Pump

The investment cost for the rich-MEA pump was calculated using the FOB cost relation shown in equation 6.4.16. The cost factors for the investment cost calculation is presented in Table 6-3

The “free-on-board” (FOB) costs ($C_{IC,FOB,pump}$) calculation for pump

$$C_{IC,FOB,pump} = C_{IC,pump,ref} \left(\frac{P_{pump}}{P_{pump,ref}} \right)^{n_{pump}} C_{pf} C_{tf} C_{al} C_{sf} \quad (6.4.16)$$

Investment costs for pump ($C_{IC,pump}$)

$$C_{IC,pump} = C_{IC,FOB,pump} \left(1 + C_{L+M,pump} C_{L/M,pump} \right) \frac{C_{CEPCI}}{1000} C_{ER} C_{tax} \quad (6.4.17)$$

where $C_{IC,pump,ref}$ is the reference value for investment costs for the pump, $P_{pump,ref}$ is the reference value for drive power of the pump, P_{pump} is the drive power of the pump, C_{pf} is the adds costs for pressure factor, C_{tf} is the adds costs for type factor, C_{sf} is the adds costs for stage factor, $C_{L+M,pump}$ is the adds labour and material costs, $C_{L/M,pump}$ is the reduces the addition of labour costs, if a special alloy is considered in C_{al} .

6.4.1.3 Investment cost estimation for heat exchangers (CRHE, HX1, HX2, HX3)

The cost factors for calculating the FOB and investment costs for the four heat exchangers used in the simulation of the intensified PCC process is shown in Table 6-4

‘Free on board’ (FOB) cost for the heat exchangers

$$C_{IC,FOB,HX} = C_{IC,HX,ref} \left(\frac{A_{HX}}{A_{HX,ref}} \right)^{n_{HX}} C_{tf} C_{al} C_{sf} \quad (6.4.18)$$

Investment costs for heat exchanger

$$C_{IC,HX} = C_{IC,FOB,HX} \left(1 + C_{L+M,HX} C_{L/M,HX} \right) \frac{C_{CEPCI}}{1000} C_{ER} C_{tax} \quad (6.4.19)$$

where $C_{IC,HX,ref}$ is the reference value for investment costs for heat exchanger, $A_{HX,ref}$ is the reference value for heat exchanger area, n_{HX} is the scaling factor of the actual to the reference condition, C_{tf} is the adds costs for type factor C_{sf} is the Adds costs for stage factor, $C_{IC,FOB,HX}$ is the free-on-cost of heat exchanger, $C_{L+M,HX}$ is the Adds labour and material costs $C_{L/M,HX}$ reduces the addition of labour costs, if a special alloy is considered in C_{al} ,

6.4.1.4 Investment cost estimation for reboiler and condenser

The reboiler and condenser investment cost calculation was done using Equation 6.4.4 and purchased cost are estimated using Appendix B Figure B.1 and the constant B_1 and B_2 found from Turton et al. [224]. Table B.1 in Appendix B for shell and tube heat exchanger made of stainless steel identification number = 5 and using Figure B.2 material factor (F_m) = 2.73. Pressure factor (F_p) is calculated from equation 6.4.1. From Table B.2, for pressure < 5 barg, $K_1 = K_2 = K_3 = 0$, therefore $F_p = 1$.

Reboiler:

$$C_p^o(2001) = 1100 \times 12 = \$13,200$$

Condenser:

$$C_p^o(2001) = 600 \times 10 = \$6,000$$

The evaluation path for purchase cost both the reboiler and condenser is shown on Figure B.1

The Bare module cost for both the reboiler and the condenser is calculated using Equation 6.4.4

Reboiler:

$$C_{BM}(2001) = C_p^o [B_1 + B_2 F_p F_m] = \$13200 \times [1.63 + 1.66 \times 1 \times 2.73] = \$81,335$$

Condenser:

$$C_{BM}(2001) = C_p^o [B_1 + B_2 F_p F_m] = \$6000 \times [1.63 + 1.66 \times 1 \times 2.73] = \$36,970$$

The bare module costs are calculated with reference to 2001. Therefore Chemical Engineering Plant Cost Index in Table 6-4 was used to update the costs to recent time.

Reboiler:

$$C_{BM} = \$81335 \times \frac{585.70}{397} = \$119,994$$

Condenser:

$$C_{BM} = \$36,970 \times \frac{585.70}{397} = \$54,543$$

Converting the bare module cost from Dollar to Euro using conversion factor of 0.9

Reboiler:

$$C_{BM} = \$119,994 \times 0.9 = \text{€}107,994.60$$

Condenser:

$$C_{BM} = \$54,543 \times 0.9 = \text{€}49,088.70$$

Table 6-2 Cost factors for the cost calculation for RPBs [226]

Factor	Description or purpose	value	Refs.
$C_{tax}(-)$	Adds taxes on the material costs	1.19	Woods [223]
$C_{L+M,mot}(-)$	Adds labour and material costs	1.36	Woods [223]
$C_{L+M,drive}(-)$	Adds labour and material costs	1.50	Woods [223]
$C_{L+M,rotors}(-)$	Adds labour and material costs	1.70	Woods [223]
$C_{L/M,mot}(-)$	Reduces the addition of labour costs, if a special alloy is considered in C_{al}	0.58	Woods [223]
$C_{L/M,drive}(-)$	Reduces the addition of labour costs, if a special alloy is considered in C_{al}	0.20	Woods [223]
$C_{L/M,rotors}(-)$	Reduces the addition of labour costs, if a special alloy is considered in C_{al}	1.00	Woods [223]
$C_{CEPCI}(-)$	Considers the cost digression based on the Chemical Engineering Plant Cost Index	585.70	Lozowski and Nessen [227]
$C_{ER}(\text{€}\$^{-1})$	Converts to Euro based on exchange rate (if necessary)	0.90	
$C_{IC,mot,ref}(\$)$	Reference value for investment costs for the motor	19,000	Woods [223]
$C_{IC,drive,ref}(\$)$	Reference value for investment costs for the drives	5300	Woods [223]
$C_{IC,rotors,ref}(\$)$	Reference value for investment costs for the rotors	220,000	Woods [223]
$P_{mot,ref}(kW)$	Reference value for electrical power of the motor	75	Woods [223]
$P_{drive,ref}(kW)$	Reference value for electrical power for the drives	180	Woods [223]
$\dot{V}_{RPB,ref}(Ls^{-1})$	Reference value for the liquid capacity of the RPB	2.20	Woods [223]
$n_{mot}(-)$	Scaling factor of the actual to the reference condition	0.90	Woods [223]
$n_{drive}(-)$	Scaling factor of the actual to the reference condition. (a) $P_{mot}C_{trans}^{0.5} < 180$ (b) $P_{mot}C_{trans}^{0.5} > 180$	0.54 (a) 1.90 (b)	Woods [223]
$n_{rotors}(-)$	Scaling factor of the actual to the reference condition (a) $\dot{V}_{RPB} < 2.2 Ls^{-1}$ (b) $\dot{V}_{RPB} > 2.2 Ls^{-1}$	0.25 (a) 0.38 (b)	Woods [223]
$C_{RS}(-)$	Adds costs for higher rotational speed	1.30	Woods [223]
$C_{en}(-)$	Adds costs for fan and enclosure of motor (here: TEFC-type)	1.00	Woods [223]
$C_{al}(-)$	Adds costs for more expensive alloys (here: stainless steel) (a) motor (b) drive	(a) 2.80 (b) 3.00	Woods [223]
$C_{trans}(-)$	Adds cost for engine transmission ratio to the drives (here: 1 to 20)	20.00	Woods [223]
$\tau_{h/a}(ha^{-1})$	Number of operating hours per year	8000	Baerns

Table 6-3 Cost factors for the cost calculation for pump

Factor	Description or purpose	value	Refs.
$C_{tax}(-)$	Adds taxes on the material costs	1.19	Woods [223]
$C_{L+M^*,pump}(-)$	Adds labour and material costs	1.47	Woods [223]
$C_{L/M,pump}(-)$	Reduces the addition of labour costs, if a special alloy is considered in C_{al}	0.28	Woods [223]
$C_{CEPCI}(-)$	Considers the cost digression based on the Chemical Engineering Plant Cost Index	585.70	Lozowski and Nessen [227]
$C_{ER}(\text{€}\$^{-1})$	Converts to Euro based on exchange rate (if necessary)	0.90	
$C_{IC,pump,ref}(\$)$	Reference value for investment costs for the pump	7,000	Woods [223]
$P_{pump,ref}(kW)$	Reference value for drive power of the pump	16	Woods [223]
$n_{pump}(-)$	Scaling factor of the actual to the reference condition. (a) $0.2 < p < 16$ (b) $16 < p < 400$	(a)0.26 (b)0.43	Woods [223]
$C_{pf}(-)$	Adds costs for pressure factor	1	Woods [223]
$C_{tf}(-)$	Adds costs for type factor (here: self-priming-type)	1.5	Woods [223]
$C_{al}(-)$	Adds costs for more expensive alloys (here: stainless steel)	1	Woods [223]
$C_{sf}(-)$	Adds costs for stage factor (here: single stage)	1	Woods [223]

Table 6-4 Cost factors for the cost calculation for heat exchangers (CRHE, HX1, HX2, HX3)

Factor	Description or purpose	value	Refs.
$C_{tax}(-)$	Adds taxes on the material costs	1.19	Woods [223]
$C_{L+M^*,HX}(-)$	Adds labour and material costs	2.2 – 2.8	Woods [223]
$C_{L/M,HX}(-)$	Reduces the addition of labour costs, if a special alloy is considered in C_{al}	0.35 - 0.37	Woods [223]
$C_{CEPCI}(-)$	Considers the cost digression based on the Chemical Engineering Plant Cost Index	585.70	Lozowski and Nessen [227]
$C_{ER}(\text{€}\$^{-1})$	Converts to Euro based on exchange rate (if necessary)	0.90	
$C_{IC,HX,ref}(\$)$	Reference value for investment costs for heat exchanger	70,000	Woods [223]
$A_{HX,ref}(m^2)$	Reference value for heat exchanger area	100	Woods [223]
$n_{HX}(-)$	Scaling factor of the actual to the reference condition	0.71	Woods [223]
$C_{tf}(-)$	Adds costs for type factor (here: U-tube)	0.87	Woods [223]
$C_{al}(-)$	Adds costs for more expensive alloys (here: stainless steel)	3	Woods [223]
$C_{sf}(-)$	Adds costs for stage factor (here: single stage)	1	Woods [223]

6.4.1.5 Summary of Investment cost for major units

Table 6-5 presents the total capital cost for intensified PCC process by calculating “free-on-board cost” of the equipment which represents the cost for material and construction. The investment cost is calculated from FOB by applying cost factors for labour and labour related material cost, cost digression and exchange rate [226].

Table 6-5 Investment costs for major units

Item	Cost (€)
RPB absorber	282836.21
RPB stripper	287006.64
Reboiler	107995.00
Condenser	49088.00
Pump	3027.22
Cross heat exchanger	62103.56
Heat exchanger (HX1)	51784.49
Heat exchanger (HX2)	56685.64
Heat exchanger (HX3)	50552.91
Total Investment cost	€951,079.68

6.4.2 Operating cost (OPEX) estimations

6.4.2.1 RPB motors electrical energy consumption cost

The operating cost for the motors used for rotating the RPBs can be determined by simply multiplying the electrical power of the motor P_{mot} with the operating time per year $\tau_{h/a}$ and the costs for electricity C_{el} [226].

$$C_{OC,RPB} = P_{mot} \times \tau_{h/a} \times C_{el} \quad (6.4.20)$$

6.4.2.2 Operating labour cost estimation

Estimation of labour cost is difficult because it depends on whether the process is batch or continuous, the level of automation, number of process steps and the level of production [228]. Therefore in this process it was assumed that we have one person per shift

Using the analysis given in Turton *et al.* [224] the number of operators needed to provide this number of shifts is [(1095 shifts/year)/(245 shifts/operator/year)] or approximately 4 operators.

To estimate the cost of labour, average hourly wage of an operator is needed. Bureau of Labour and Statistics [229] gives the hourly rate of \$33.58 in May 2014 for operator working in Electric Power Generation, Transmission and Distribution industry. Total pay for 2080 hour a year is \$69,840. Converting this value to Euro base on exchange rate of 0.9 is €62,856

Therefore the operating labour cost = 4 x €62,856 = **€251,424**

Operating cost estimation of closed loop intensified PCC process is presented in Table 6-6. Column 2 in the table give unit price for utilities and raw materials and also the factors needed to determine some of the cost parameters.

Table 6-6 Operating cost estimation for intensified PCC process

Variable Operating Costs (VOC)	Factor/Unit price	Cost
MEA solvent price (\$/ton)	1500	82.41
Steam cost (\$/kWh)	0.064	579.07
Electrical energy cost (\$/kWh)	0.011	534.44
Miscellaneous operating materials	2% of M	1426.62
Converts to Euro based on exchange rate (if necessary)	0.900	
Total VC		€2,360.28
Fixed Operating Costs (FOC)		
Maintenance (M)	3% of FCI	28532.39
Operating labour (OL)		251424.00
Laboratory costs	20% of OL	50284.80
Supervision	20% of OL	50284.80
Plant overheads	50% of OL	125712.00
Capital Charges	10% of FCI	95107.97
Insurance	1% of FCI	9510.80
Local taxes	1% of FCI	5028.48
Royalties	1% of FCI	9510.80
Total FOC		625396.03
Total Operating Cost (OPEX)	VOC + FOC	€627,756.31

6.4.3 Annualized total cost (TOTEX)

The annualized total cost (TOTEX) is given by the following equation [20]:

$$\text{TOTEX} = C_1(\text{OPEX}) + C_2(\text{CAPEX}) \left[\frac{i(1+i)^n}{(1+i)^n - 1} \right] \quad (6.4.3.1)$$

Where C_1 and C_2 are scaling factors

The annualized total cost (TOTEX) for the intensified PCC process plant is calculate by assuming 20 year ($n = 20$) of the service life of the plant. Assuming 10% interest rate ($i = 0.1$ and also assuming no scaling ($C_1 = 1.0$ and $C_2 = 1.0$)

Therefore

$$\text{TOTEX} = 1 \times 627756.31 + 1 \times 951079.68 \times \left[\frac{0.1(1 + 0.1)^{20}}{(1 + 0.1)^{20} - 1} \right]$$

$$\text{TOTEX} = \mathbf{\text{€}739,469.78}$$

Total amount of CO₂ strip-off from the rich-MEA stream per annum assuming number of operating hours per year 8000 hr/a

$$\text{CO}_2 \text{ strip – off per annum} = 607 \text{ ton/a}$$

6.5 Summary

Process analysis on the effect of L/G ratio on regeneration energy and CO₂ capture level was performed and it was observed that capture level increase with increases in L/G ratio which is quite good, but the negative aspect is that the regeneration energy also increase which will result in increase in operating cost, therefore compromise has be made to get balance between CO₂ capture level and regeneration energy requirement. The impact of lean-MEA CO₂ loading was also explored. It was found that as the lean-MEA loading increases regeneration energy decreases, but the CO₂ capture level decreases which is not good for intensified PCC performance. Appropriate lean-MEA loading operating point is needed so as get a balance between regeneration energy and CO₂ capture level.

In this thesis, cost estimation calculations (i.e. CAPEX, OPEX and TOTEX) for closed intensified PCC process was performed. The estimated CAPEX is €951,079.68, while OPEX is estimated as €627,756.31 and finally TOTEX is calculated as €739,469.78 assuming the plant has 20 year service life and at interest rate of 10%. Agbonghae *et al.* [20] reported total costs of the plants per ton of CO₂ captured as 51.35 £/ton of CO₂ (i.e. 64.78 €/ton of CO₂) and 51.44 £/ton of CO₂ (i.e. 64.90 €/ton of CO₂) for the 400MWe NGCC plant and the 450MWe NGCC plant, respectively. In this thesis, the intensified PCC plant cost per ton of CO₂ capture is found to be 60.83 €/ton of CO₂ captured which is less than that of conventional PCC process. Taking into account the error margin for lower and upper band of the capital investment estimation, the Author is of the opinion that the cost of the

intensified PCC process per ton of CO₂ can improve by at least 10%. This value will be improved if systematic scale-up and cost optimization is done during the cost calculation.

Chapter 7 Conclusions and recommendations for future study

7.1 Conclusions

This work studies modelling, model validation, and process analysis of intensified standalone absorber, intensified standalone stripper and then intensified closed loop PCC process for flue gas from CCGT power plant. The study uses MEA as a solvent for the chemical absorption process. The models were developed using Aspen Plus[®] process modelling software and then dynamically linked with Intel[®] Visual FORTRAN.

7.1.1 Modelling of RPB column

Implementation procedure used in modelling and simulation of intensified PCC process is presented in Chapter 3. This method was adopted because no commercial software has RPB model in their model library. Thermodynamic and physical properties were discussed in Chapter 3. In this research eNRTL property model was used because it is very good in handling electrolytes. Modelling equations suitable for PCC process were discussed in Chapter 3 and selection of the most preferred correlations sets were made based on the validation results in Chapter 4.

7.1.2 Modelling, validation and process analysis of RPB absorber

Modelling, validation and process analysis of standalone intensified absorber using MEA solvent were done in Chapter 4. The RPB absorber was modelled in Aspen Plus[®]. However, some built-in correlations in Aspen Plus[®] rate-based model were replaced with new correlations suitable for RPB. Rate-based model approach was used and chemical reactions are assumed to be at equilibrium. Therefore, with these modifications, the model is equivalent to developing a new model for RPB even though it is still in Aspen Plus[®]. To test the validity of the model developed, experimental data reported in Jassim *et al.* [114] was used for the validation. Two sets of correlations (shown in **Table 4-6**) were implemented for the validation and the model predictions showed good agreement with the experimental results. The second set of correlations gives better prediction compared to the first set of correlation. This was due to some assumption made while developing some of the correlations in the first set.

To understand the response of the intensified absorber to changes in the process conditions, process analysis were performed in Chapter 4 to explore the effect of rotational speed, lean-MEA concentration, Flue gas flow rate, lean-MEA temperature and Flue gas temperature on

CO₂ capture level. It was found that as the rotational speed increases, the CO₂ capture level increases due to enhanced mass transfer. Again as the lean-MEA concentration increases, the CO₂ capture level also increases. Increase in flue gas flow rate leads to decrease in CO₂ capture level. Also as the lean-MEA temperature increases, the CO₂ capture level increases. CO₂ capture level can be maintained as flue gas temperature increases which mean that cooling duty cost in RPB absorber can be greatly reduced. Temperature profile study was done for 55 wt% and 75 wt% MEA concentration at lean MEA temperature of 25 °C and 50 °C. The results indicate that temperature bulge is not noticed for the process condition used. Comparison between the conventional absorber using packed column and intensified absorber using RPB indicates that the latter gives 12 times reduction in volume without sumps.

7.1.3 Modelling, validation and process analysis of RPB stripper

In Chapter 5, modelling, validation and process analysis of intensified stripper was done. The modelling implementation procedure is the same with that of intensified absorber presented in Chapter 4. The model was validated with experimental data from Jassim et al. [114] and Cheng et al. [120]. The validated model shows good agreement with the experimental results. From the analyses it shows that increase in the rich-MEA flow rate leads to a decrease in the regeneration efficiency, this is due to increase in the lean-MEA loading. Regeneration energy decreases at first and then increases as the rich-MEA flow rate increases, this is due to increase in superficial velocity which enhances rate of CO₂ desorbed with lower energy but this advantage was counter balance when more amount of solvent needs to be heated in the reboiler thereby increasing the reboiler duty. Regeneration efficiency increases with increase in rotor speed, while regeneration energy decreases as the rotor speed increases. Reboiler temperature was varied from 105°C to 125°C the result shows a decrease in regeneration energy at reboiler temperature between 105 °C to 115°C for Case 1 and Case 2 while for Case 3 is from 105 °C to 120 °C but when the reboiler temperature exceeds 120 °C the regeneration energy begins to increase. Under same process condition there is 10 times reduction in volume for intensified stripper compared to conventional packed column. Finally it can be concluded that the RPB stripper has potential for application in intensified PCC process.

7.1.4 Process analysis and costs estimation of intensified PCC process

Process analysis, technical and economic performance assessment of closed loop intensified PCC process compared with conventional packed column are presented in

Chapter 6. The model was validated based on standalone RPB models as discussed in Chapter 4 and 5. Process analysis was done to study system performance due to changes in process input conditions, the results shows that as the L/G ratio increases the regeneration energy increases, also CO₂ capture level increases with increase in L/G ratio. The impact of lean-MEA loading on regeneration energy was also discussed. CAPEX and OPEX estimation were done for the whole intensified PCC process based on major equipment investment costs.

7.2 Recommendations for future study

7.2.1 Scale-up study

Harzog [230] reported that the challenge for CCS commercial deployment is the integration and scale up of the components (absorber, heat exchanger the regenerator). Shi *et al.* [231] and Yang *et al.* [232] used computational fluid dynamic (CFD) to study fluid flow in RPB to understand the hydrodynamics and liquid distribution inside the RPB system but, more studies are required for scale-up of RPB. To be able to carry out the scale-up study of an intensified PCC process, it is recommended to couple process modelling software with CFD software so as to accurately predict the hydraulic behaviour and the mass transfer behaviour of the RPB. Three-dimensional (3D) CFD simulations can be used to unveil details about the pressure field and velocity distribution, the gross flow patterns, maldistribution [208] and process modelling software can study the mass transfer behaviour.

7.2.2 Detailed technical and economic assessment for intensified PCC process

The accuracy of cost estimation will be more viable if the model of the intensified PCC process is scale-up. This is because for large scale intensified PCC process the rotational speed will not be high since high rotor speed will affect the system stability which will in turn be a safety risk. Therefore more detailed cost estimation will be needed for large scale intensified PCC process.

7.2.3 Detail analysis of energy consumed by RPB motor

Lee et al, [132] reported the research efforts Newcastle University is making in quantifying the power requirement for an RPB motor for PCC process but more experimental studies are required to quantify the contribution of electricity used by motors to overall energy consumption in intensified PCC process.

7.2.4 Proposed Simplified PFD of intensified chemical absorption process for PCC

For the application of RPB technology to PCC to be successful, the whole closed loop PCC process units needs to be intensified. The proposed PFD shown in **Figure 7-1** suggest the use of intensified heat exchanger (i.e. PCHE) which benefit from multi-fluidic capability thereby making it to function as cross heat exchanger and also as condenser. These arrangements eliminate the condenser unit in conventional packed tower. But it is recommended that detailed thermodynamic analysis be performed on this arrangement to know if this is thermodynamically realistic. Again, stripper unit is design to incorporate the reboiler underneath its packing and both of them rotating on the same motor to enhance heat and mass transfer. The way the reboiler is placed under the stripper packing is to benefit in directing the vapour stream counter-currently with the in-coming rich solvent. It is recommended that if the PFD is thermodynamically realistic steady state modelling or experimental studies be done based on this proposed PFD to assess its cost benefit in terms of energy saving and size reduction. Also, it is vital to develop dynamic models for future work in process control.

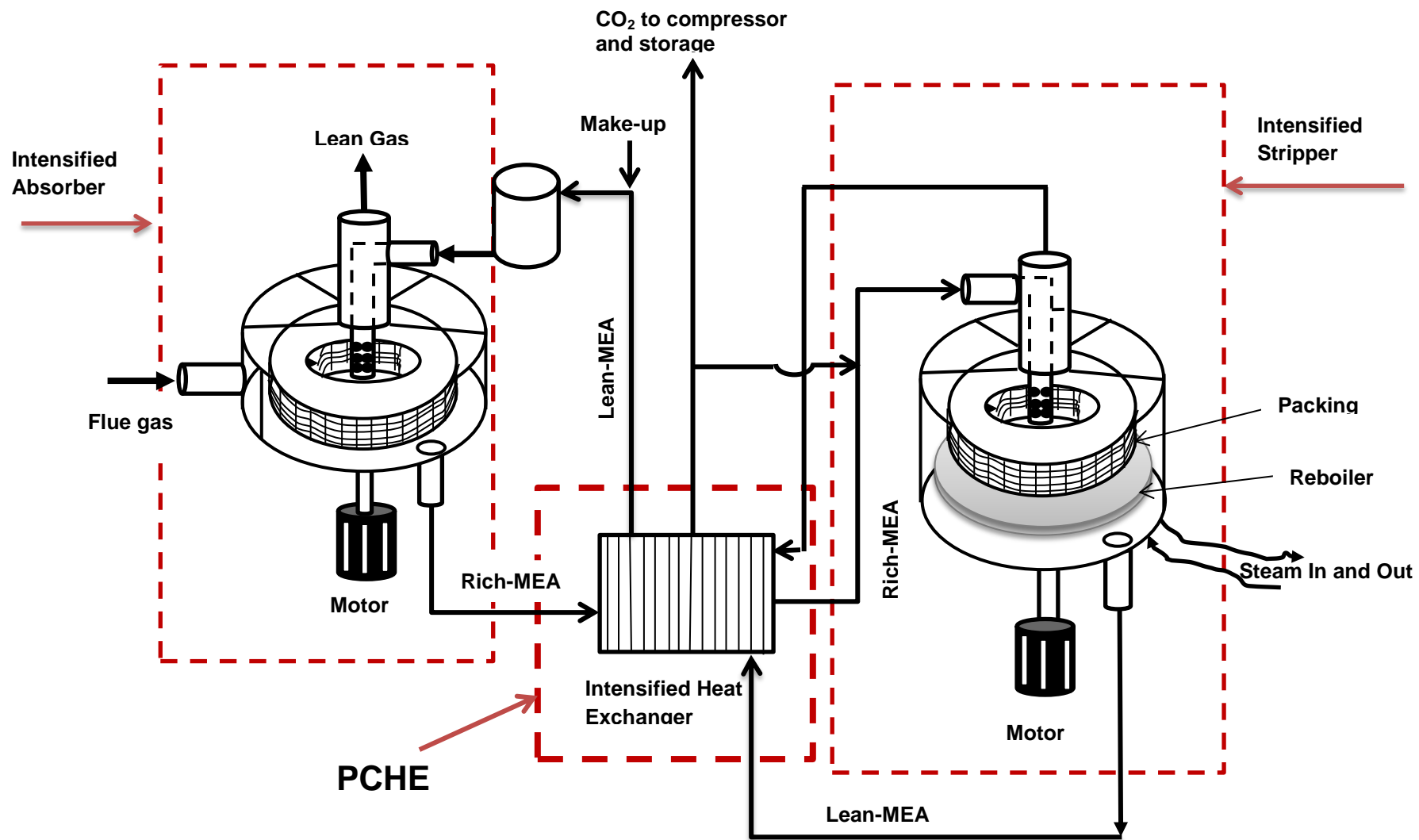


Figure 7-1 Proposed simplified PFD of intensified chemical absorption process for PCC

References

- [1] Biliyok C, Lawal A, Wang M, Seibert F. Dynamic modelling, validation and analysis of post-combustion chemical absorption CO₂ capture plant. *International Journal of Greenhouse Gas Control* 2012;9:428-45.
- [2] World Nuclear Association. Renewable energy and electricity. Available at: <http://www.world-nuclear.org/information-library/energy-and-the-environment/renewable-energy-and-electricity.aspx> (accessed March, 2016).
- [3] IEA. CO₂ Emissions from Fuel Combustion IEA Statistics Highlights. Available at: <https://www.iea.org/publications/freepublications/publication/CO2EmissionsFromFuelCombustionHighlights2015.pdf> (accessed January, 2016) 2015.
- [4] Taylor Peter, Lavagne d'orTigue Olivier, Trudeau N, Francoeur M. Energy efficiency indicators for public electricity production from fossil fuels. 2008.
- [5] Department of Energy and Climate Change (DECC). Solid Fuels and Derived Gases Statistics: Data Sources and Methodologies. 2012; Available at: http://webarchive.nationalarchives.gov.uk/20121217150421/http://decc.gov.uk/en/content/cms/statistics/energy_stats/source/electricity/electricity.aspx; (accessed May, 2013).
- [6] CO₂-Earth. Daily CO₂: Mauna Loa Observatory/ Atmospheric CO₂ Concentration. Available at: <https://www.co2earth.com/daily-co2> (accessed March, 2016).
- [7] World Meteorological Organization (WMO). Press Release No. 991. 26 May 2014; http://www.wmo.int/pages/mediacentre/press_releases/pr_991_en.html (accessed June, 2014).
- [8] Simons S. The Chemical Engineer: Our hard work starts now. *ICHEME News letter*, February, 2016;896:36-7.
- [9] Intergovernmental Panel on Climate Change (IPCC). Contribution of Working Group III to the Fourth Assessment Report of the Intergovernmental Panel on Climate Change. Cambridge, United Kingdom/New York, United States: Cambridge University Press, 2007.
- [10] International Energy Agency. Carbon Capture and Storage Model Regulatory Framework. IEA 2010; Available at: http://www.iea.org/publications/freepublications/publication/model_framework.pdf, (accessed May 2013).
- [11] Metz B, Davidson O, De Coninck H, Loos M, Meyer L. IPCC, 2005: IPCC special report on carbon dioxide capture and storage. Prepared by Working Group III of the Intergovernmental Panel on Climate Change. Cambridge, United Kingdom and New York, NY, USA, 442 pp 2005.

- [12] GLOBAL CCS INSTITUTE. Global Status of CCS. Canberra, Australia, Available at: <http://decarbonise/sites/default/files/publications/22562/global-status-ccs-2011.pdf> (accessed October, 2015) 2011.
- [13] Rao AB, Rubin ES. A technical, economic, and environmental assessment of amine-based CO₂ capture technology for power plant greenhouse gas control. *Environ Sci Technol* 2002;36:4467-75.
- [14] Abanades JC, Arias B, Lyngfelt A, Mattisson T, Wiley DE, Li H et al. Emerging CO₂ capture systems. *International Journal of Greenhouse Gas Control* <http://dx.doi.org/10.1016/j.ijggc.2015.04.018> 2015:1750-5836.
- [15] Goto K, Yogo K, Higashii T. A review of efficiency penalty in a coal-fired power plant with post-combustion CO₂ capture. *Appl Energy* 2013;111:710-20.
- [16] Folger P. Carbon capture: a technology assessment. 2013. <http://oai.dtic.mil/oai/oai?verb=getRecord&metadataPrefix=html&identifier=ADA590346> (accessed January, 2015).
- [17] Lawal A, Wang M, Stephenson P, Obi O. Demonstrating full-scale post-combustion CO₂ capture for coal-fired power plants through dynamic modelling and simulation. *Fuel* 2012;101:115-28.
- [18] Resnik KP, Yeh JT, Pennline HW. Aqua ammonia process for simultaneous removal of CO₂, SO₂ and NO_x. *Int J Environ Technol Manage* 2004;4:89-104.
- [19] Haszeldine RS. Carbon capture and storage: how green can black be? *Science* 2009;325:1647-52.
- [20] Agbonghae EO, Hughes KJ, Ingham DB, Ma L, Pourkashanian M. Optimal Process Design of Commercial-Scale Amine-Based CO₂ Capture Plants. *Ind Eng Chem Res* 2014;53:14815-29.
- [21] Abu-Zahra MRM, Niederer JPM, Feron PHM, Versteeg GF. CO₂ capture from power plants: Part II. A parametric study of the economical performance based on mono-ethanolamine. *International Journal of Greenhouse Gas Control* 2007;1:135-42.
- [22] GLOBAL CCS INSTITUTE. CO₂ Capture Technologies: Post Combustion Capture (PCC). January, 2012 Available at: <http://hub.globalccsinstitute.com/sites/default/files/publications/29721/co2-capture-technologies-pcc.pdf>; (accessed June, 2015).
- [23] Bounaceur R, Lape N, Roizard D, Vallieres C, Favre E. Membrane processes for post-combustion carbon dioxide capture: a parametric study. *Energy* 2006;31:2556-70.
- [24] Favre E. Carbon dioxide recovery from post-combustion processes: Can gas permeation membranes compete with absorption? *J Membr Sci* 2007;294:50-9.

- [25] International Energy Agency (IEA). Prospects for CO₂ Capture and Storage. OECD/IEA, Paris, France. 2004; Available at: http://ccs-info.org/onewebmedia/iea_oecd_ccs_prospects.pdf (accessed June, 2014).
- [26] Zhao L, Menzer R, Riensche E, Blum L, Stolten D. Concepts and investment cost analyses of multi-stage membrane systems used in post-combustion processes. *Energy Procedia* 2009;1:269-78.
- [27] Zhao L, Riensche E, Blum L, Stolten D. Multi-stage gas separation membrane processes used in post-combustion capture: Energetic and economic analyses. *J Membr Sci* 2010;359:160-72.
- [28] Zhao M, Minett AI, Harris AT. A review of techno-economic models for the retrofitting of conventional pulverised-coal power plants for post-combustion capture (PCC) of CO₂. *Energy & Environmental Science* 2013;6:25-40.
- [29] Yu C, Huang C, Tan C. A review of CO₂ capture by absorption and adsorption. *Aerosol and Air Quality Research* 2012;12:745-69.
- [30] Zhao W, Sprachmann G, Li Z, Cai N, Zhang X. Effect of K₂CO₃·1.5H₂O on the regeneration energy consumption of potassium-based sorbents for CO₂ capture. *Appl Energy* 2013;112:381-7.
- [31] Clausse M, Merel J, Meunier F. Numerical parametric study on CO₂ capture by indirect thermal swing adsorption. *International Journal of Greenhouse Gas Control* 2011;5:1206-13.
- [32] Kapica-Kozar J, Kusiak-Nejman E, Wanag A, Kowalczyk Ł, Wrobel RJ, Mozia S et al. Alkali-treated titanium dioxide as adsorbent for CO₂ capture from air. *Microporous and Mesoporous Materials* 2015;202:241-9.
- [33] Li K, Jiang J, Yan F, Tian S, Chen X. The influence of polyethyleneimine type and molecular weight on the CO₂ capture performance of PEI-nano silica adsorbents. *Appl Energy* 2014;136:750-5.
- [34] Maring BJ, Webley PA. A new simplified pressure/vacuum swing adsorption model for rapid adsorbent screening for CO₂ capture applications. *International Journal of Greenhouse Gas Control* 2013;15:16-31.
- [35] Parshetti GK, Chowdhury S, Balasubramanian R. Biomass derived low-cost microporous adsorbents for efficient CO₂ capture. *Fuel* 2015;148:246-54.
- [36] Plaza MG, Pevida C, Arias B, Feroso J, Rubiera F, Pis JJ. A comparison of two methods for producing CO₂ capture adsorbents. *Energy Procedia* 2009;1:1107-13.
- [37] Wei L, Jing Y, Gao Z, Wang Y. Development of a pentaethylenehexamine-modified solid support adsorbent for CO₂ capture from model flue gas. *Chin J Chem Eng* 2015;23:366-71.

- [38] Xu C, Hedin N. Microporous adsorbents for CO₂ capture – a case for microporous polymers? *Materials Today* 2014;17:397-403.
- [39] Zhang W, Liu H, Sun C, Drage TC, Snape CE. Capturing CO₂ from ambient air using a polyethyleneimine–silica adsorbent in fluidized beds. *Chemical Engineering Science* 2014;116:306-16.
- [40] Zhang W, Liu H, Sun C, Drage TC, Snape CE. Performance of polyethyleneimine–silica adsorbent for post-combustion CO₂ capture in a bubbling fluidized bed. *Chem Eng J* 2014;251:293-303.
- [41] Dasgupta S, Nanoti A, Gupta P, Jena D, Goswami AN, Garg MO. Carbon Di-Oxide Removal with Mesoporous Adsorbents in a Single Column Pressure Swing Adsorber. *Sep Sci Technol* 2009;44:3973-83.
- [42] Dasgupta S, Biswas N, Gode NG, Divekar S, Nanoti A, Goswami AN. CO₂ recovery from mixtures with nitrogen in a vacuum swing adsorber using metal organic framework adsorbent: A comparative study. *International Journal of Greenhouse Gas Control* 2012;7:225-9.
- [43] Krishna R, van Baten JM. A comparison of the CO₂ capture characteristics of zeolites and metal–organic frameworks. *Separation and Purification Technology* 2012;87:120-6.
- [44] Gil MV, Martínez M, García S, Rubiera F, Pis JJ, Pevida C. Response surface methodology as an efficient tool for optimizing carbon adsorbents for CO₂ capture. *Fuel Process Technol* 2013;106:55-61.
- [45] González AS, Plaza MG, Pis JJ, Rubiera F, Pevida C. Post-combustion CO₂ capture adsorbents from spent coffee grounds. *Energy Procedia* 2013;37:134-41.
- [46] González AS, Plaza MG, Rubiera F, Pevida C. Sustainable biomass-based carbon adsorbents for post-combustion CO₂ capture. *Chem Eng J* 2013;230:456-65.
- [47] Han SJ, Bang Y, Lee H, Lee K, Song IK, Seo JG. Synthesis of a dual-templated MgO–Al₂O₃ adsorbent using block copolymer and ionic liquid for CO₂ capture. *Chem Eng J* 2015;270:411-7.
- [48] Hlaing NN, Sreekantan S, Othman R, Hinode H, Kurniawan W, Thant AA et al. A novel (Zr–Ce) incorporated Ca(OH)₂ nanostructure as a durable adsorbent for CO₂ capture. *Mater Lett* 2014;133:204-7.
- [49] Huang Y, Chiueh P, Shih C, Lo S, Sun L, Zhong Y et al. Microwave pyrolysis of rice straw to produce biochar as an adsorbent for CO₂ capture. *Energy* 2015;84:75-82.
- [50] Samanta A, Zhao A, Shimizu GK, Sarkar P, Gupta R. Post-combustion CO₂ capture using solid sorbents: a review. *Ind Eng Chem Res* 2011;51:1438-63.
- [51] Drage TC, Snape CE, Stevens LA, Wood J, Wang J, Cooper AI et al. Materials challenges for the development of solid sorbents for post-combustion carbon capture. *Journal of Materials Chemistry* 2012;22:2815-23.

- [52] Durán-Guevara MB, Ortiz-Landeros J, Pfeiffer H, Espitia-Cabrera MI, Contreras-García ME. Potassium-based sorbents using mesostructured γ -alumina supports for low temperature CO₂ capture. *Ceram Int* 2015;41:3036-44.
- [53] Cheung O, Bacsik Z, Liu Q, Mace A, Hedin N. Adsorption kinetics for CO₂ on highly selective zeolites NaKA and nano-NaKA. *Appl Energy* 2013;112:1326-36.
- [54] Hedin N, Andersson L, Bergström L, Yan J. Adsorbents for the post-combustion capture of CO₂ using rapid temperature swing or vacuum swing adsorption. *Appl Energy* 2013;104:418-33.
- [55] Shakerian F, Kim K, Szulejko JE, Park J. A comparative review between amines and ammonia as sorptive media for post-combustion CO₂ capture. *Appl Energy* 2015;148:10-22.
- [56] Bernardo P, Drioli E, Golemme G. Membrane gas separation: a review/state of the art. *Ind Eng Chem Res* 2009;48:4638-63.
- [57] Brunetti A, Scura F, Barbieri G, Drioli E. Membrane technologies for CO₂ separation. *J Membr Sci* 2010;359:115-25.
- [58] Car A, Stropnik C, Yave W, Peinemann K. PEG modified poly (amide-b-ethylene oxide) membranes for CO₂ separation. *J Membr Sci* 2008;307:88-95.
- [59] Dugas RE. Pilot plant study of carbon dioxide capture by aqueous monoethanolamine. MSE Thesis, University of Texas at Austin 2006.
- [60] Mangalapally HP, Hasse H. Pilot plant study of two new solvents for post combustion carbon dioxide capture by reactive absorption and comparison to monoethanolamine. *Chemical Engineering Science* 2011;66:5512-22.
- [61] Mangalapally HP, Hasse H. Pilot plant experiments for post combustion carbon dioxide capture by reactive absorption with novel solvents. *Energy Procedia* 2011;4:1-8.
- [62] Mangalapally HP, Notz R, Hoch S, Asprion N, Sieder G, Garcia H et al. Pilot plant experimental studies of post combustion CO₂ capture by reactive absorption with MEA and new solvents. *Energy Procedia* 2009;1:963-70.
- [63] Mangalapally HP, Notz R, Asprion N, Sieder G, Garcia H, Hasse H. Pilot plant study of four new solvents for post combustion carbon dioxide capture by reactive absorption and comparison to MEA. *International Journal of Greenhouse Gas Control* 2012;8:205-16.
- [64] Lawal A, Wang M, Stephenson P, Yeung H. Dynamic Modeling and Simulation of CO₂ Chemical Absorption Process for Coal-Fired Power Plants. *Computer Aided Chemical Engineering* 2009;27:1725-30.
- [65] Lawal A, Wang M, Stephenson P, Yeung H. Dynamic modelling of CO₂ absorption for post combustion capture in coal-fired power plants. *Fuel* 2009;88:2455-62.

- [66] Lawal A, Wang M, Stephenson P, Koumpouras G, Yeung H. Dynamic modelling and analysis of post-combustion CO₂ chemical absorption process for coal-fired power plants. *Fuel* 2010;89:2791-801.
- [67] Kvamsdal HM, Rochelle GT. Effects of the temperature bulge in CO₂ absorption from flue gas by aqueous monoethanolamine. *Ind Eng Chem Res* 2008;47:867-75.
- [68] Kvamsdal H, Jakobsen J, Hoff K. Dynamic modeling and simulation of a CO₂ absorber column for post-combustion CO₂ capture. *Chemical Engineering and Processing: Process Intensification* 2009;48:135-44.
- [69] Kvamsdal HM, Hetland J, Haugen G, Svendsen HF, Major F, Kårstad V et al. Maintaining a neutral water balance in a 450MWe NGCC-CCS power system with post-combustion carbon dioxide capture aimed at offshore operation. *International Journal of Greenhouse Gas Control* 2010;4:613-22.
- [70] Kvamsdal HM, Haugen G, Svendsen HF. Flue-gas cooling in post-combustion capture plants. *Chem Eng Res Design* 2011;89:1544-52.
- [71] MacDowell N, Shah N. Optimisation of Post-combustion CO₂ Capture for Flexible Operation. *Energy Procedia* 2014;63:1525-35.
- [72] Mac Dowell N, Shah N. Dynamic modelling and analysis of a coal-fired power plant integrated with a novel split-flow configuration post-combustion CO₂ capture process. *International Journal of Greenhouse Gas Control* 2014;27:103-19.
- [73] Mac Dowell N, Shah N. The multi-period operation of an amine-based CO₂ capture process integrated with a supercritical coal-fired power station. *Computers and Chemical Engineering* 2014.
- [74] Mac Dowell N, Samsatli N, Shah N. Dynamic modelling and analysis of an amine-based post-combustion CO₂ capture absorption column. *International Journal of Greenhouse Gas Control* 2013;12:247-58.
- [75] Lucquiaud M, Gibbins J. On the integration of CO₂ capture with coal-fired power plants: A methodology to assess and optimise solvent-based post-combustion capture systems. *Chem Eng Res Design* 2011;89:1553-71.
- [76] Lucquiaud M, Fernandez ES, Chalmers H, Dowell NM, Gibbins J. Enhanced Operating Flexibility and Optimised Off-design Operation of Coal Plants with Post-combustion Capture. *Energy Procedia* 2014;63:7494-507.
- [77] Errey O, Chalmers H, Lucquiaud M, Gibbins J. Valuing Responsive Operation of Post-combustion CCS Power Plants in Low Carbon Electricity Markets. *Energy Procedia* 2014;63:7471-84.
- [78] Agbonghae EO, Hughes KJ, Ingham DB, Ma L, Pourkashanian M. A Semi-Empirical Model for Estimating the Heat Capacity of Aqueous Solutions of Alkanolamines for CO₂ Capture. *Ind Eng Chem Res* 2014.

- [79] Asendrych D, Niegodajew P, Drobniak S. CFD modelling of CO₂ capture in a packed bed by chemical absorption. *Chemical and Process Engineering* 2013;34:269-82.
- [80] Sebastia-Saez D, Gu S, Ranganathan P, Papadikis K. 3D modeling of hydrodynamics and physical mass transfer characteristics of liquid film flows in structured packing elements. *International Journal of Greenhouse Gas Control* 2013;19:492-502.
- [81] Raynal L, Ben Rayana F, Royon-Lebeaud A. Use of CFD for CO₂ absorbers optimum design : from local scale to large industrial scale. *Energy Procedia* 2009;1:917-24.
- [82] Raynal L, Royon-Lebeaud A. A multi-scale approach for CFD calculations of gas–liquid flow within large size column equipped with structured packing. *Chemical Engineering Science* 2007;62:7196-204.
- [83] Siemens AG. Siemens PostCap™ Technology CO₂ Post Combustion Capture. Available at: http://www.energy.siemens.com/nl/pool/hq/power-generation/power-plants/carbon-capture-solutions/post-combustion-carbon-capture/214_131227_WS_Post_Combustion_CO2_Capture_US_Einzelseiten_HighRes.pdf (accessed Feb 2016) 2014.
- [84] Stéphenne K. Start-up of world's first commercial post-combustion coal fired ccs project: Contribution of shell cansolv to saskpower boundary dam iccs project. *Energy Procedia* 2014;63:6106-10.
- [85] ZERO CO₂.NO. Plant Barry CCS demo. ;Available at: <http://www.zeroco2.no/projects/southern-company-ccs-demonstration> (accessed November, 2014).
- [86] NRG Energy. WA Parish CO₂ capture project. 2014;Available at: <https://www.nrg.com/documents/business/pla-2014-petranova-waparish-factsheet.pdf> (accessed December, 2014).
- [87] Ramshaw C. The Incentive for Process Intensification. *Proceedings, 1st Intl Conf Proc Intensif for Chem Ind* , 18, BHR Group, London, p 1 1995.
- [88] Stankiewicz AI, Moulijn JA. Process Intensification: Transforming Chemical Engineering. *Chem Eng Prog* 2000;96:22-34.
- [89] Reay D, Ramshaw C, Harvey A. Process Intensification: Engineering for efficiency, sustainability and flexibility. : Butterworth-Heinemann, 2013.
- [90] Wang M, Joel AS, Ramshaw C, Eimer D, Musa NM. Process intensification for post-combustion CO₂ capture with chemical absorption: A critical review. *Appl Energy* 2015;158:275-91.
- [91] Charles Ross and Son Company. Charles Ross and Son Company. ;Available at: http://www.staticmixers.com/staticmixer_designs.pdf (accessed June, 2014).
- [92] Johns GA. Toxicity reduction for industrial effluent containing formaldehyde. MSc Thesis Cranfield University, UK 2006.

- [93] Meeuwse M, Van Der Schaaf J, Schouten JC. Mass Transfer in a rotor-stator spinning disk reactor with cofeeding of gas and liquid. *Industrial and Engineering Chemistry Research* 2010;49:1605-10.
- [94] Meeuwse M, Van der Schaaf J, Kuster B, Schouten J. Gas–liquid mass transfer in a rotor–stator spinning disc reactor. *Chemical Engineering Science* 2010;65:466-71.
- [95] Meeuwse M, Lempers S, van der Schaaf J, Schouten JC. Liquid– Solid Mass Transfer and Reaction in a Rotor– Stator Spinning Disc Reactor. *Ind Eng Chem Res* 2010;49:10751-7.
- [96] Dobie CG, MarijaVicevic, Boodhoo KVK. An evaluation of the effectiveness of continuous thin film processing in a spinning disc reactor for bulk free-radical photocopolymerisation. *Chemical Engineering and Processing: Process Intensification* 2013;71:97-106.
- [97] Boodhoo KVK, Jachuck RJ. Process intensification: Spinning disk reactor for styrene polymerization. *Appl Therm Eng* 2000;20:1127-46.
- [98] Brechtelsbauer C, Lewis N, Oxley P, Ricard F, Ramshaw C. Evaluation of a spinning disc reactor for continuous processing. *Organic Process Research and Development* 2001;5:65-8.
- [99] Riffat S, Zhao X. Preliminary study of the performance and operating characteristics of a mop-fan air cleaning system for buildings. *Build Environ* 2007;42:3241-52.
- [100] Shehata H, Riffat S, Shao L. Mop fan for removal of air-borne pollutants. 1995;2:45-59.
- [101] Riffat S, Shehata H, Srivastava N. The desiccant air-conditioning system. *Int J Ambient Energy* 2004;25:163-8.
- [102] BUSS ChemTech AG. Advanced BUSS Loop® Reactor Technology. 2009; Available at: http://www.buss-ct.com/up/files/PDFs_RT/Brochure_RT_Advanced_Loop_Reactor_operating_principle.pdf (accessed December, 2014).
- [103] Machado RM, Heier KR, Broekhuis RR. Developments in hydrogenation technology for fine-chemical and pharmaceutical applications. *Current Opinion in Drug Discovery and Development* 2001;4:745-55.
- [104] Cramers PHMR, Beenackers AACM. Influence of the ejector configuration, scale and the gas density on the mass transfer characteristics of gas-liquid ejectors. *Chem Eng J* 2001;82:131-41.
- [105] Roberge DM, Gottsponer M, Eyholzer M, Kockmann N. Industrial design, scale-up, and use of microreactors. *Chimica Oggi* 2009;27:8-11.
- [106] Roberge DM, Zimmermann B, Rainone F, Gottsponer M, Eyholzer M, Kockmann N. Microreactor technology and continuous processes in the fine chemical and pharmaceutical

industry: Is the revolution underway? *Organic Process Research and Development* 2008;12:905-10.

[107] Ehrfeld Mikrotechnik BTS. High Performance reactors for pharmaceutical and fine chemical production. 2011; Available at: <http://www.pharma-food.de/media/file/5474> (accessed December, 2014).

[108] Chambers H, Wall M. Some factors affecting the design of centrifugal gas absorbers. *Trans.Inst.Chem.Eng* 1954;32:S96-S107.

[109] Podbielniak WJ. Continuous Centrifugal Vapor-Liquid Contactor. 1966; US Patent 3,233,880.

[110] Wang G, Xu Z, Yu Y, Ji J. Performance of a rotating zigzag bed—A new HIGEE. *Chemical Engineering and Processing: Process Intensification* 2008;47:2131-9.

[111] Wang G, Xu Z, Ji J. Progress on Higee distillation—Introduction to a new device and its industrial applications. *Chem Eng Res Design* 2011;89:1434-42.

[112] Wang GQ, Xu OG, Xu ZC, Ji JB. New HIGEE-rotating zigzag bed and its mass transfer performance. *Industrial and Engineering Chemistry Research* 2008;47:8840-6.

[113] Li Y, Ji J. Study on Power Consumption of a Novel HIGEE—Rotating Zigzag Beds. 2009.

[114] Jassim MS, Rochelle G, Eimer D, Ramshaw C. Carbon dioxide absorption and desorption in aqueous monoethanolamine solutions in a rotating packed bed. *Ind Eng Chem Res* 2007;46:2823-33.

[115] Joel AS, Wang M, Ramshaw C, Oko E. Process analysis of intensified absorber for post-combustion CO₂ capture through modelling and simulation. *International Journal of Greenhouse Gas Control* 2014;21:91-100.

[116] Joel AS, Wang M, Ramshaw C. Modelling and simulation of intensified absorber for post-combustion CO₂ capture using different mass transfer correlations. *Appl Therm Eng* 2015;74:47-53.

[117] Cheng H, Tan C. Reduction of CO₂ concentration in a zinc/air battery by absorption in a rotating packed bed. *J Power Sources* 2006;162:1431-6.

[118] Cheng H, Shen J, Tan C. CO₂ capture from hot stove gas in steel making process. *International Journal of Greenhouse Gas Control* 2010;4:525-31.

[119] Cheng H, Tan C. Removal of CO₂ from indoor air by alkanolamine in a rotating packed bed. *Separation and Purification Technology* 2011;82:156-66.

[120] Cheng H, Lai C, Tan C. Thermal regeneration of alkanolamine solutions in a rotating packed bed. *International Journal of Greenhouse Gas Control* 2013;16:206-16.

- [121] Cheng H, Tan C. Carbon dioxide capture by blended alkanolamines in rotating packed bed. *Energy Procedia* 2009;1:925-32.
- [122] Chen Y, Hsu Y, Lin C, Tai CY, Liu H. Volatile organic compounds absorption in a cross-flow rotating packed bed. *Environ Sci Technol* 2008;42:2631-6.
- [123] Chen Y, Lin F, Lin C, Tai CY, Liu H. Packing characteristics for mass transfer in a rotating packed bed. *Ind Eng Chem Res* 2006;45:6846-53.
- [124] Chen Y, Lin C, Liu H. Mass transfer in a rotating packed bed with viscous Newtonian and non-Newtonian fluids. *Ind Eng Chem Res* 2005;44:1043-51.
- [125] BERR. Advanced power plant using high efficiency boiler/turbine. Report BPB010. BERR, Department for Business Enterprise and Regulatory Reform. 2006; Available at: <http://webarchive.nationalarchives.gov.uk/20090609003228/http://www.berr.gov.uk/files/file30703.pdf> (accessed August 2015).
- [126] Agbonghae EO, Best T, Finney KN, Palma CF, Hughes KJ, Pourkashanian M. Experimental and Process Modelling Study of Integration of a Micro-turbine with an Amine Plant. *Energy Procedia* 2014;63:1064-73.
- [127] Henderson C. Towards zero emission coal-fired power plant. IEA Clean Coal Centre Reports 2005, <http://www.iea-coal.org.uk/documents/81379/5947/Towards-zero-emission-coal-fired-power-plant%C2%A0> (accessed February, 2015).
- [128] Reay D. The role of process intensification in cutting greenhouse gas emissions. *Appl Therm Eng* 2008;28:2011-9.
- [129] Chen JF. The recent developments in the HiGee technology. Presentation at GPE-EPIC, 14-17 June 2009. 2009; Available at http://inpact.inp-toulouse.fr/GPE-EPIC2009/images/presentation_chen.pdf (accessed February, 2014).
- [130] Chen Y, Liu H, Lin C, Liu W. Micromixing in a rotating packed bed. *J Chem Eng Japan* 2004;37:1122-8.
- [131] Stankiewicz AI, Moulijn JA. Process intensification: transforming chemical engineering. *Chem Eng Prog* 2000;96:22-34.
- [132] Lee, J., Reay, D., Ramshaw C.,. Post-combustion carbon capture research at Newcastle University, Presentation to PIN, 2nd May, 2012. 2012; Available at: www.pinetwork.org (accessed June 2013).
- [133] Yi F, Zou H, Chu G, Shao L, Chen J. Modeling and experimental studies on absorption of CO₂ by Benfield solution in rotating packed bed. *Chem Eng J* 2009;145:377-84.
- [134] Luo Y, Chu G, Zou H, Zhao Z, Dudukovic MP, Chen J. Gas-liquid effective interfacial area in a rotating packed bed. *Ind Eng Chem Res* 2012;51:16320-5.

- [135] Luo Y, Chu G, Zou H, Xiang Y, Shao L, Chen J. Characteristics of a two-stage counter-current rotating packed bed for continuous distillation. *Chemical Engineering and Processing: Process Intensification* 2012;52:55-62.
- [136] Zhang L, Wang J, Xiang Y, Zeng X, Chen J. Absorption of carbon dioxide with ionic liquid in a rotating packed bed contactor: Mass transfer study. *Ind Eng Chem Res* 2011;50:6957-64.
- [137] Yu C, Cheng H, Tan C. CO₂ capture by alkanolamine solutions containing diethylenetriamine and piperazine in a rotating packed bed. *International Journal of Greenhouse Gas Control* 2012;9:136-47.
- [138] Tan C-, Chen J-. Absorption of carbon dioxide with piperazine and its mixtures in a rotating packed bed. *Separation and Purification Technology* 2006;49:174-80.
- [139] Lin C, Lin Y, Tan C. Evaluation of alkanolamine solutions for carbon dioxide removal in cross-flow rotating packed beds. *J Hazard Mater* 2010;175:344-51.
- [140] Lin C-, Chen Y-. Performance of a cross-flow rotating packed bed in removing carbon dioxide from gaseous streams by chemical absorption. *International Journal of Greenhouse Gas Control* 2011;5:668-75.
- [141] Agarwal L, Pavani V, Rao D, Kaistha N. Process intensification in HiGee absorption and distillation: design procedure and applications. *Ind Eng Chem Res* 2010;49:10046-58.
- [142] Rajan S, Kumar M, Ansari MJ, Rao D, Kaistha N. Limiting gas liquid flows and mass transfer in a novel rotating packed bed (HiGee). *Ind Eng Chem Res* 2010;50:986-97.
- [143] Rahimi MR, Mosleh S. CO₂ Removal from Air in a Countercurrent Rotating Packed Bed, Experimental Determination of Height of Transfer Unit. *Adv Environ Sci Technol* 2015;1:19-24.
- [144] Nikitin K, Kato Y, Ngo L. Printed circuit heat exchanger thermal–hydraulic performance in supercritical CO₂ experimental loop. *Int J Refrig* 2006;29:807-14.
- [145] Tsuzuki N, Kato Y, Ishiduka T. High performance printed circuit heat exchanger. *Appl Therm Eng* 2007;27:1702-7.
- [146] Kim DE, Kim MH, Cha JE, Kim SO. Numerical investigation on thermal–hydraulic performance of new printed circuit heat exchanger model. *Nucl Eng Des* 2008;238:3269-76.
- [147] Li X, Kininmont D, Le Pierres R, Dewson SJ. Alloy 617 for the high temperature diffusion-bonded compact heat exchangers. *Proceedings of ICAPP08, Anaheim, CA, Paper* 2008.
- [148] Li Q, Flamant G, Yuan X, Neveu P, Luo L. Compact heat exchangers: A review and future applications for a new generation of high temperature solar receivers. *Renewable and Sustainable Energy Reviews* 2011;15:4855-75.

- [149] Pierres R. L., Diffusion Bonded Compact Heat Exchangers - Compact Reactors Presentation to PIN, 23rd May, 2013. 2013; Available at: www.pinetwork.org (accessed November, 2013).
- [150] Heatric Ltd. Lower capital and operational costs by reducing coolant flows. available at: http://www.heatric.com/lower_capital_and_operational_costs_by_reducing_coolant_flows.html (accessed March 2016).
- [151] Hesselgreaves JE. Compact heat exchangers: selection, design and operation. : Gulf Professional Publishing, 2001.
- [152] Phillips, C. H., Symonds, K. T. Development of a novel integrated chemical reactor–heat exchanger. 2007; Available at: <http://lorien.ncl.ac.uk/ming/pdfs/bhrpaper1.pdf> (accessed August, 2013).
- [153] Reay D. Learning from experiences with compact heat exchangers. : CADDET Series 25, Centre for the Analysis and Dissemination of Demonstrated Energy Technologies. Sittard, The Netherlands, 1999.
- [154] Phillips CH. Development of a novel compact chemical reactor-heat exchanger. BHR Group Conf Ser Publ 1999;38:71-87.
- [155] Shah RK, Sekulic DP. Fundamentals of heat exchanger design. : John Wiley & Sons, 2003.
- [156] Thonon B, Breuil E. Compact heat exchanger technologies for the HTRs recuperator application. 2001; Available at: <http://www.iaea.org/inis/collection/NCLCollectionStore/Public/32/047/32047838.pdf> (accessed on May, 2014).
- [157] Picon-Nunez M, Canizalez-Davalos L, Martinez-Rodriguez G, Polley G. Shortcut design approach for spiral heat exchangers. Food Bioprod Process 2007;85:322-7.
- [158] Alfa Laval. Spiral heat exchangers. Available at: <http://www.thermaltransfersystems.com/pdf/alfa-laval-spiral-brochure.pdf> (accessed June 2014).
- [159] Yu C-, Wu T-, Tan C-. CO₂ capture by piperazine mixed with non-aqueous solvent diethylene glycol in a rotating packed bed. International Journal of Greenhouse Gas Control 2013;19:503-9.
- [160] Luo X, Hartono A, Hussain S, Svendsen FH. Mass transfer and kinetics of carbon dioxide absorption into loaded aqueous monoethanolamine solutions. Chemical Engineering Science 2015;123:57-69.
- [161] Lin C, Chen B. Carbon dioxide absorption into NaOH solution in a cross-flow rotating packed bed. Journal of Industrial and Engineering Chemistry-Seoul- 2007;13:1083.

- [162] Ji, L., Bonnin-Nartker, P., Klidas, M. G., Zang, R. Solvent Selection for Commercial Deployment of B&W PGG's RSAT™ CO₂ Scrubbing Process. The 35th International Technical Conference on Coal Utilization & Fuel Systems, US A, June 6-10 2010.
- [163] Munjal S, Duduković MP, Ramachandran P. Mass-transfer in rotating packed beds—II. Experimental results and comparison with theory and gravity flow. *Chemical Engineering Science* 1989;44:2257-68.
- [164] Lin C-, Liu W-, Tan C-. Removal of carbon dioxide by absorption in a rotating packed bed. *Industrial and Engineering Chemistry Research* 2003;42:2381-6.
- [165] Lin C, Chen B. Carbon dioxide absorption in a cross-flow rotating packed bed. *Chem Eng Res Design* 2011;89:1722-9.
- [166] Tontiwachwuthikul P, Meisen A, Lim CJ. CO₂ absorption by NaOH, monoethanolamine and 2-amino-2-methyl-1-propanol solutions in a packed column. *Chemical Engineering Science* 1992;47:381-90.
- [167] Wappel D, Gronald G, Kalb R, Draxler J. Ionic liquids for post-combustion CO₂ absorption. *International Journal of Greenhouse Gas Control* 2010;4:486-94.
- [168] Undewood, J., Dawson, G., Barney, C.,. Design of a CO₂ absorption system in an Ammonia plant. 1997; Available at: <http://www.owl.net.rice.edu/~ceng403/co2abs.html> (accessed April, 2014).
- [169] Kothandaraman A, Nord L, Bolland O, Herzog HJ, McRae GJ. Comparison of solvents for post-combustion capture of CO₂ by chemical absorption. *Energy Procedia* 2009;1:1373-80.
- [170] Benson H, Field J, Jameson R. CO₂ absorption: employing hot potassium carbonate solutions. *Chem.Eng.Prog.:(United States)* 1954;50.
- [171] Field JH, Benson H, Johnson G, Tosh J, Forney A. Pilot-plant studies of the hot-carbonate process for removing carbon dioxide and hydrogen sulfide.[Removal of CO₂ and H₂S from gas mixtures necessary in synthesizing liquid fuels from coal]. *US Bur.Mines, Bull.* 1962;597.
- [172] Bishnoi S, Rochelle GT. Absorption of carbon dioxide into aqueous piperazine: reaction kinetics, mass transfer and solubility. *Chemical Engineering Science* 2000;55:5531-43.
- [173] Freeman SA, Dugas R, Van Wagener DH, Nguyen T, Rochelle GT. Carbon dioxide capture with concentrated, aqueous piperazine. *International Journal of Greenhouse Gas Control* 2010;4:119-24.
- [174] Yu C-, Tan C-. Mixed alkanolamines with low regeneration energy for CO₂ capture in a rotating packed bed. *Energy Procedia* 2013;37:455-60.
- [175] Dugas R, Rochelle G. Absorption and desorption rates of carbon dioxide with monoethanolamine and piperazine. *Energy Procedia* 2009;1:1163-9.

- [176] Sander MT, Mariz CL. The Fluor Daniel® econamine FG process: Past experience and present day focus. *Energy Conversion and Management* 1992;33:341-8.
- [177] Reddy S. Econamine FG Plus SM Technology for Post-Combustion CO₂ Capture. 11th Meeting of the International Post-Combustion CO₂ Capture Network 2008.
- [178] Mimura T, Shimojo S, Suda T, Iijima M, Mitsuoka S. Research and development on energy saving technology for flue gas carbon dioxide recovery and steam system in power plant. *Energy Conversion and Management* 1995;36:397-400.
- [179] Mimura T, Simayoshi H, Suda T, Iijima M, Mitsuoka S. Development of energy saving technology for flue gas carbon dioxide recovery in power plant by chemical absorption method and steam system. *Energy Conversion and Management* 1997;38:S57-62.
- [180] Kishimoto S, Hirata T, Iijima M, Ohishi T, Higaki K, Mitchell R. Current status of MHI's CO₂ recovery technology and optimization of CO₂ recovery plant with a PC fired power plant. *Energy Procedia* 2009;1:1091-8.
- [181] Wu S, Bergins C, Kikkawa H, Kobayashi H, Kawasaki T. Technology options for clean coal power generation with CO₂ capture. 2010.
- [182] IEA-GHG. Improvements in power generation with post-combustion capture of CO₂. IEA Greenhouse Gas R&D Programme, Cheltenham, UK 2004.
- [183] Gibbins J, Crane R. Scope for reductions in the cost of CO₂ capture using flue gas scrubbing with amine solvents. *Proc Inst Mech Eng A: J Power Energy* 2004;218:231-9.
- [184] Just P, Mirfendereski Y, Geuzebroek F. Cansolv technologies: the value of integration. IEAGHG (International Energy Agency Greenhouse Gas) R&D Program (Eds), International Network for CO₂ Capture: Report on 12th Workshop, Report 2009.
- [185] Shaw D. Cansolv CO₂ capture: The value of integration. *Energy Procedia* 2009;1:237-46.
- [186] Stöver B, Bergins C, Klebes J. Optimized post combustion carbon capturing on coal fired power plants. *Energy Procedia* 2011;4:1637-43.
- [187] Oexmann J, Hasenbein C, Kather A. Semi-empirical model for the direct simulation of power plant with integrated post-combustion CO₂ capture processes by wet chemical absorption. *Energy Procedia* 2011;4:1276-85.
- [188] Danckwerts PV, Lannus A. Gas-liquid reactions. *J Electrochem Soc* 1970;117:369C-70C.
- [189] Danckwerts PV. The reaction of CO₂ with ethanolamines. *Chemical Engineering Science* 1979;34:443-6.
- [190] Krishna R, Wesselingh J. The Maxwell-Stefan approach to mass transfer. *Chemical Engineering Science* 1997;52:861-911.

- [191] Noeres C, Kenig E, Gorak A. Modelling of reactive separation processes: reactive absorption and reactive distillation. *Chemical Engineering and Processing: Process Intensification* 2003;42:157-78.
- [192] Austgen DM, Rochelle GT, Chen CC. Model of vapor-liquid equilibria for aqueous acid gas-alkanolamine systems. 2. Representation of hydrogen sulfide and carbon dioxide solubility in aqueous MDEA and carbon dioxide solubility in aqueous mixtures of MDEA with MEA or DEA. *Ind Eng Chem Res* 1991;30:543-55.
- [193] Austgen DM, Rochelle GT, Peng X, Chen CC. Model of vapor-liquid equilibria for aqueous acid gas-alkanolamine systems using the electrolyte-NRTL equation. *Ind Eng Chem Res* 1989;28:1060-73.
- [194] Li Y, Mather AE. Correlation and prediction of the solubility of carbon dioxide in a mixed alkanolamine solution. *Ind Eng Chem Res* 1994;33:2006-15.
- [195] Liu Y, Zhang L, Watanasiri S. Representing vapor-liquid equilibrium for an aqueous MEA-CO₂ system using the electrolyte nonrandom-two-liquid model. *Ind Eng Chem Res* 1999;38:2080-90.
- [196] Gibbs J. *The Scientific Papers of J. Willard Gibbs, Vol. 1: Thermodynamics*, 1962.
- [197] Edwards T, Maurer G, Newman J, Prausnitz J. Vapor-liquid equilibria in multicomponent aqueous solutions of volatile weak electrolytes. *AIChE J* 1978;24:966-76.
- [198] Aronu UE, Gondal S, Hessen ET, Haug-Warberg T, Hartono A, Hoff KA et al. Solubility of CO₂ in 15, 30, 45 and 60 mass% MEA from 40 to 120 C and model representation using the extended UNIQUAC framework. *Chemical Engineering Science* 2011;66:6393-406.
- [199] Mason JW, Dodge BF. Equilibrium absorption of carbon dioxide by solutions of the ethanolamines. *Trans.Am.Inst.Chem.Eng* 1936;32:27-48.
- [200] Zhang Y, Chen H, Chen C, Plaza JM, Dugas R, Rochelle GT. Rate-based process modeling study of CO₂ capture with aqueous monoethanolamine solution. *Ind Eng Chem Res* 2009;48:9233-46.
- [201] AspenTech. Aspen Physical Properties System – Physical Property Methods. 2010, Available at: <http://support.aspentech.com/> (accessed May 2014).
- [202] Hankinson RW, Thomson GH. A new correlation for saturated densities of liquids and their mixtures. *AIChE J* 1979;25:653-63.
- [203] Tung H, Mah RS. Modeling liquid mass transfer in hige separation process. *Chem Eng Commun* 1985;39:147-53.
- [204] Onda K, Sada E, Takeuchi H. Gas absorption with chemical reaction in packed columns. *J Chem Eng Japan* 1968;1:62-6.

- [205] Sandilya P, Rao D, Sharma A, Biswas G. Gas-phase mass transfer in a centrifugal contactor. *Ind Eng Chem Res* 2001;40:384-92.
- [206] Chen Y. Correlations of mass transfer coefficients in a rotating packed bed. *Ind Eng Chem Res* 2011;50:1778-85.
- [207] Burns J, Jamil J, Ramshaw C. Process intensification: operating characteristics of rotating packed beds—determination of liquid hold-up for a high-voidage structured packing. *Chemical Engineering Science* 2000;55:2401-15.
- [208] Llerena-Chavez H, Larachi F. Analysis of flow in rotating packed beds via CFD simulations—Dry pressure drop and gas flow maldistribution. *Chemical Engineering Science* 2009;64:2113-26.
- [209] Singh SP, Wilson JH, Counce RM, Lucero AJ, Reed GD, Ashworth RA et al. Removal of volatile organic compounds from groundwater using a rotary air stripper. *Ind Eng Chem Res* 1992;31:574-80.
- [210] AspenTech. Aspen Plus steady state simulation guide. available at: <https://chemengr.ucsb.edu/~ceweb/courses/che184b/aspenplus/UserGuideVol2.pdf> (accessed April, 2016) 1997.
- [211] Jassim MS. Process intensification: absorption and desorption of carbon dioxide from monoethanolamine solutions using Higee technology. Newcastle University, UK (PhD Thesis) 2002.
- [212] Burns J, Ramshaw C. Process intensification: visual study of liquid maldistribution in rotating packed beds. *Chemical Engineering Science* 1996;51:1347-52.
- [213] Freguia S, Rochelle GT. Modeling of CO₂ capture by aqueous monoethanolamine. *AIChE J* 2003;49:1676-86.
- [214] Lewis W, Whitman W. Principles of gas absorption. *Industrial & Engineering Chemistry* 1924;16:1215-20.
- [215] Haslam R, Hershey R, Kean R. Effect of Gas Velocity and Temperature on Rate of Absorption. *Industrial & Engineering Chemistry* 1924;16:1224-30.
- [216] Maceiras R, Álvarez E, Cancela MÁ. Effect of temperature on carbon dioxide absorption in monoethanolamine solutions. *Chem Eng J* 2008;138:295-300.
- [217] Canepa R, Wang M, Biliyok C, Satta A. Thermodynamic analysis of combined cycle gas turbine power plant with post-combustion CO₂ capture and exhaust gas recirculation. *Proc Inst Mech Eng Part E J Process Mech Eng* 2013;227:89-105.
- [218] Ramshaw C, Mallinson RH. Mass transfer process. 1981;US Patent 4,283,255.
- [219] Bašić A, Duduković MP. Liquid holdup in rotating packed beds: examination of the film flow assumption. *AIChE J* 1995;41:301-16.

- [220] Kothandaraman A. Carbon dioxide capture by chemical absorption: a solvent comparison study 2010.
- [221] Xiuqing L, Le Pierres R, Dewson SJ. Heat exchangers for the next generation of nuclear reactors. Proceedings of the 2006 international congress on advances in nuclear power plants-ICAPP'06 2006.
- [222] Towler G, Sinnott RK. Chemical engineering design: principles, practice and economics of plant and process design. : Elsevier, 2012.
- [223] Woods DR. Rules of thumb in engineering practice. : John Wiley & Sons, 2007.
- [224] Turton R, Bailie RC, Whiting WB, Shaeiwitz JA. Analysis, synthesis and design of chemical processes. : Pearson Education, 2008.
- [225] Karimi M, Hillestad M, Svendsen HF. Capital costs and energy considerations of different alternative stripper configurations for post combustion CO₂ capture. Chem Eng Res Design 2011;89:1229-36.
- [226] Sudhoff D, Leimbrink M, Schleinitz M, Górak A, Lutze P. Modelling, design and flexibility analysis of rotating packed beds for distillation. Chem Eng Res Design 2015;94:72-89.
- [227] Lozowski D, Nessen B. Chemical engineering plant costindex 2011. Chem Eng (August), 67-68 2011.
- [228] Smith R. Chemical process design. : Wiley Online Library, 2005.
- [229] Bureau of Labour and Statistics. Occupational employment wages, May 2014. Available at: <http://www.bls.gov/oes/current/oes518013.htm> (accessed March, 2016).
- [230] Herzog HJ. Scaling up carbon dioxide capture and storage: From megatons to gigatons. Energy Econ 2011;33:597-604.
- [231] Shi X, Xiang Y, Wen L, Chen J. CFD analysis of liquid phase flow in a rotating packed bed reactor. Chem Eng J 2013;228:1040-9.
- [232] Yang W, Wang Y, Chen J, Fei W. Computational fluid dynamic simulation of fluid flow in a rotating packed bed. Chem Eng J 2010;156:582-7.

Appendix A Procedure for writing user defined subroutines

Compiling and linking the subroutine adopted from Aspen Plus® [201]

The `aspcomp` command delivered in the Simulation Engine DOS prompt window will create the .OBJ file and ensure consistent compiler options. DLOPT (dynamic linking option) file control the linking process:

Compile the three Fortran Subroutines

1. Fortran file was written and save as *HOLUP.f*.
2. The compiler option was set by running *Start | Programs | Aspen Tech | Process Modelling <version> | Aspen Plus | Select Compiler for Aspen Plus*. The selection was done based on the option which represents the combination of Fortran compiler and linker.
3. Aspen Plus Simulation Engine Window was lunched. (From the *Start* menu click *Programs | Aspen Tech | Process Modelling <version> | Aspen Plus | Aspen Plus® Simulation Engine*.) The DOS window appears with the working directory as the default directory.
4. The command `cd` was entered on the DOS window to change the default directory to the location of *HOLUP.f* by typing `cd Case 1` so as to go the subfolder called *Case 1* in your working directory.
5. `aspcomp HOLUP` was typed so as compile to get an object file (*HOLUP.obj*) which is created in the same directory as *HOLUP.f*.
6. The same five steps were repeated so as to compiler *usrintfa.f* and *usrmtrfc.f*

The DOS window was left available for the linking step and a text editor was used to create a DLOPT file so as to control the creation of a shared library (also known as a dynamic linking library).

Creating shared library

1. Notepad was used to create a text file and save as called *ATUBIN_List_OBJs.opt* in your working folder.
2. *HOLUP.obj* was typed on the top line of the text file followed by *usrintfa.obj* and lastly *usrmtrfc.obj* as shown in Figure A-0-1

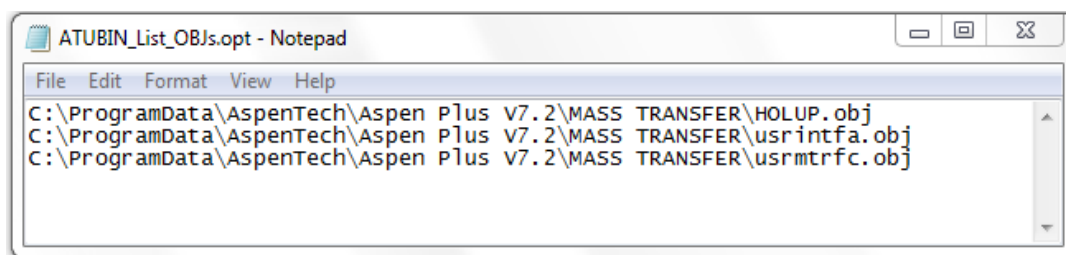


Figure A-0-1 Text file for creating DLOPT

3. The text file was saved and the file closed.
4. `asplink [dlopt Atubin_list_objs.opt] Ratesep` command was typed in the DOS window of the Aspen Plus® Simulation Engine, and the file *Ratesep.dll* was created. This file is the Fortran shared library file. The file created was used to avoid the linking steps when running the Aspen Plus® simulation. Once you have the shared library, it can be used with Aspen Plus® even if you don't have a Fortran compiler available.

Note: by typing `asplink Ratesep` on the DOS window, *Ratesep.dll* file will be created and the object files will be in default directory.

Running the simulation

Now that the compilation and creation of the DLL file was done, then the following steps will be followed run the simulation.

1. *Rate_Based MEA.apw.* was open
2. Selecting *Run | Reinitialize* (or press *Shift-F5*) and clicking *OK* twice was done to clear data from the previous run.

Note: If you have both the GUI and the Simulation Engine Window open at the same time, an *asplink* command will fail unless you reinitialize the open run.

3. Going to the *Blocks | ABSORBER | Packing rating | 1 | Rate based | Correlations* sheet.
4. On the *Correlations* sheet and on *mass transfer coefficient method: correlation* on drop down, selection of *user model* was done.
5. On the *Correlations* sheet and on *Interfacial area method: correlation* on drop down, selection of *user model* was done

Figure A-0-2 Correlation window for mass and heat transfer coefficient and interfacial area

6. Going to the *Blocks | ABSORBER | Packing rating | 1 | Rate based | Holdups* sheet.
7. On *Holdups* sheet and on *holdup method: Correlation* on drop down selection of *User model* was done

Figure A-0-3 Holdup correlation window

8. Go to *Blocks | ABSORBER | User Transport Subroutines* sheet.
9. On *Mass Transfer* sheet change on mass transfer subroutine to *USRMTRFC* was done
10. On *Interfacial Area* sheet change on interfacial area subroutine to *USRINTFA* was done
11. Also on *Holdup* sheet change on Holdup subroutine to *HOLUP* was done
12. From the Aspen Plus menu, *Run | Settings* was selected. On the *Run Settings* dialog box as shown in Figure A-0-4

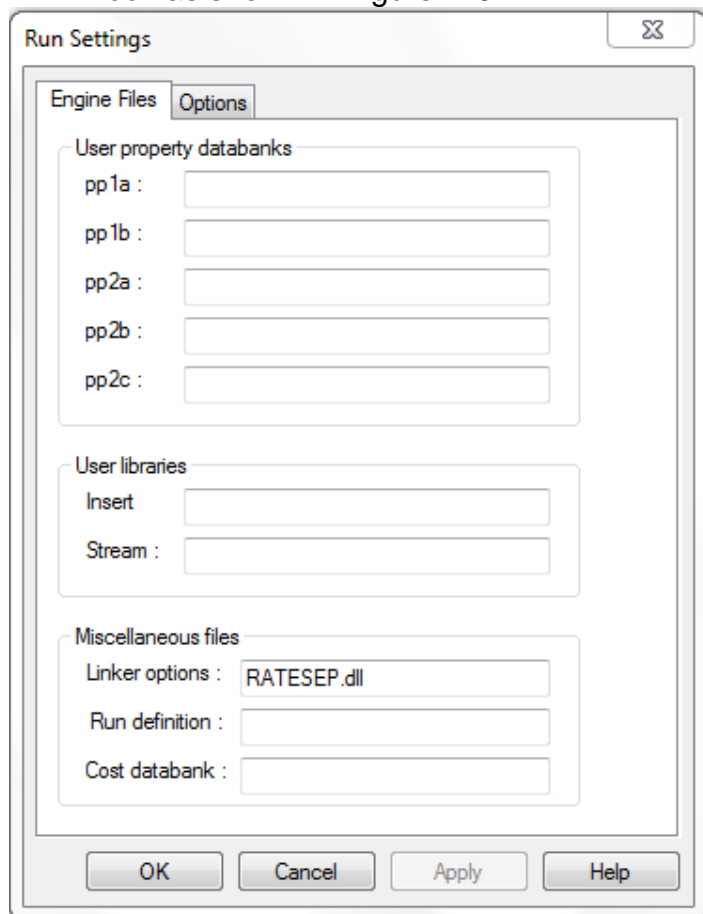


Figure A-0-4 Run setting window

13. In the *Linker options* field in the miscellaneous files area *RATESEP.dll* was typed.
14. Followed by clicking *OK*.
15. Then Run the simulation.

Appendix B Cost estimation graphs and tables

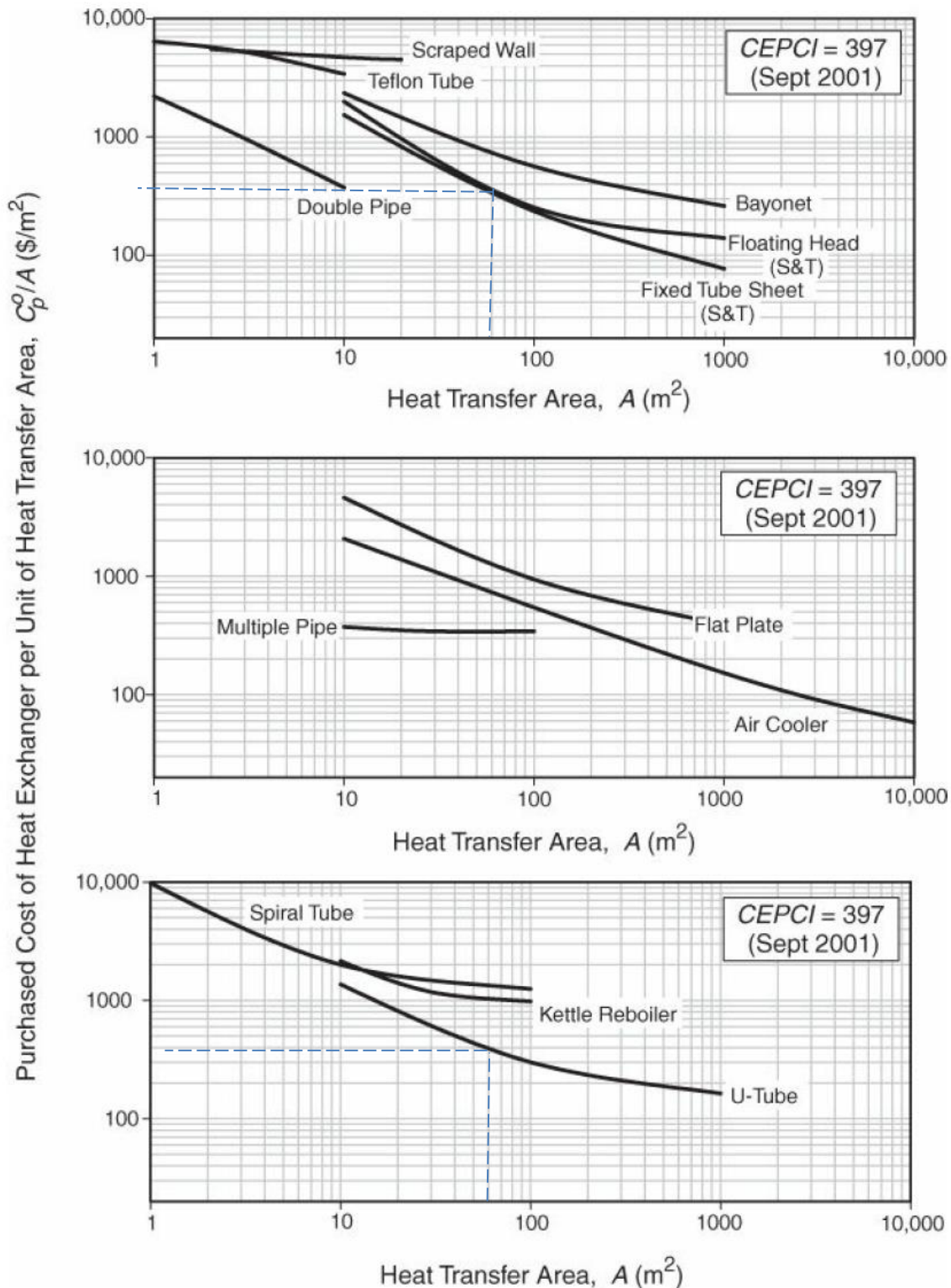


Figure B-0-1 Purchased costs for heat exchangers [224]

Table B-1 Identification numbers for material factors for heat exchangers, process vessels, and pumps to be used with Figure B-2 [224]

Identification Number	Equipment Type	Equipment Description	Material of Construction
1	Heat exchanger	Double pipe, multiple pipe,	CS-shell/CS-tube
2		fixed tube sheet, floating head,	CS-shell/Cu-tube
3		U-tube, bayonet, kettle reboiler, scraped	Cu-shell/Cu-tube
4		wall, and spiral tube	CS-shell/SS-tube
5			SS-shell/SS-tube
6			CS-shell/Ni alloy tube
7			Ni alloy, shell/Ni alloy-tube
8			CS-shell/Ti-tube
9			Ti-shell/Ti-tube
10		Air cooler	CS tube
11		Air cooler	Al tube
12		Air cooler	SS tube
13		Flat plate and spiral plate	CS (in contact with fluid)
14		Flat plate and spiral plate	Cu (in contact with fluid)
15		Flat plate and spiral plate	SS (in contact with fluid)
16		Flat plate and spiral plate	Ni alloy (in contact with fluid)
17		Flat plate and spiral plate	Ti (in contact with fluid)
18	Process vessels	Horizontal, vertical (including towers)	CS
19		Horizontal, vertical (including towers)	SS clad
20		Horizontal, vertical (including towers)	SS
21		Horizontal, vertical (including towers)	Ni alloy clad
22		Horizontal, vertical (including towers)	Ni alloy
23		Horizontal, vertical (including towers)	Ti clad
24		Horizontal, vertical (including towers)	Ti
25	Pumps	Reciprocating	Cast iron
26		Reciprocating	Carbon steel
27		Reciprocating	Cu alloy
28		Reciprocating	SS
29		Reciprocating	Ni alloy
30		Reciprocating	Ti
31		Positive displacement	Cast iron
32		Positive displacement	Carbon steel
33		Positive displacement	Cu alloy
34		Positive displacement	SS
35		Positive displacement	Ni alloy
36		Positive displacement	Ti
37		Centrifugal	Cast iron
38		Centrifugal	Carbon steel
39		Centrifugal	SS
40	Centrifugal	Ni alloy	

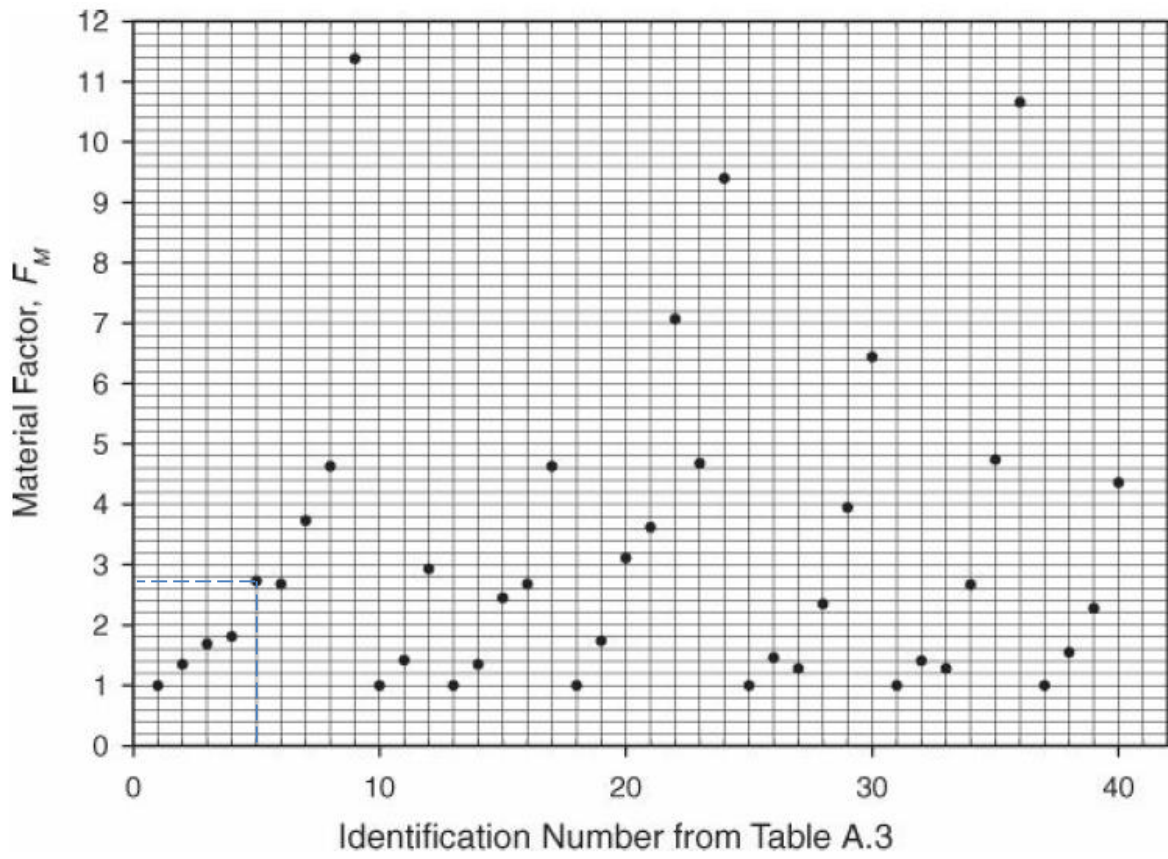


Figure B-0-2 Material factors for equipment in Table B-1 [224]

Table B-2 Pressure factors for process equipment [224]

Equipment Type	Equipment Description	C_1	C_2	C_3	Pressure Range (barg)
Compressors	Centrifugal, axial, rotary, and reciprocating	0	0	0	—
Drives	Gas turbine	0	0	0	—
	Intern. comb. engine	0	0	0	—
	Steam turbine	0	0	0	—
	Electric—explosion-proof	0	0	0	—
	Electric—totally enclosed	0	0	0	—
	Electric—open/drip-proof	0	0	0	—
	Evaporators	Forced circulation (pumped), falling film, agitated film (scraped wall), short tube, and long tube	0 0.1578	0 -0.2992	0 0.1413
Fans*	Centrifugal radial, and centrifugal backward curve	0	0	0	$\Delta P < 1 \text{ kPa}$
		0	0.20899	-0.0328	$1 < \Delta P < 16 \text{ kPa}$
	Axial vane and axial tube	0	0	0	$\Delta P < 1 \text{ kPa}$
		0	0.20899	-0.0328	$1 < \Delta P < 4 \text{ kPa}$
Furnaces	Reformer furnace	0	0	0	P<10
		0.1405	-0.2698	0.1293	10<P<200
	Pyrolysis furnace	0	0	0	P<10
		0.1017	-0.1957	0.09403	10<P<200
	Nonreactive fired heater	0	0	0	P<10
Heat exchangers	Scraped wall	0.1347	-0.2368	0.1021	10<P<200
		0	0	0	P<40
		0.6072	-0.9120	0.3327	40<P<100
	Teflon tube	13.1467	-12.6574	3.0705	100<P<300
		0	0	0	P<15
		0	0	0	P<5
	Bayonet, fixed tube sheet, floating head, kettle reboiler, and U-tube (both shell and tube)	0.03881	-0.11272	0.08183	5<P<140
		0	0	0	P<5
	Bayonet, fixed tube sheet, floating head, kettle reboiler, and U-tube (tube only)	-0.00164	-0.00627	0.0123	5<P<140
		0	0	0	P<40
	Double pipe and multiple pipe	0.6072	-0.9120	0.3327	40<P<100
		13.1467	-12.6574	3.0705	100<P<300
		0	0	0	P<19
	Flat plate and spiral plate	0	0	0	P<10
		-0.1250	0.15361	-0.02861	10<P<100
	Air cooler	0	0	0	P<10
		0	0	0	P<150
-0.4045		0.1859	0	150<P<400	
Spiral tube (both shell and tube)	0	0	0	P<150	
	0	0	0	P<150	
	-0.2115	0.09717	0	150<P<400	
Spiral tube (tube only)	0	0	0	P<2	
	-0.01633	0.056875	-0.00876	2<P<200	
	0	0	0	P<20	
Heaters	Diphenyl heater, molten salt heater, and hot water heater	2.594072	-4.23476	1.722404	20<P<40
	Steam boiler	0	0	0	—
Packing	Loose (for towers)	0	0	0	—
Process vessels	Horizontal and vertical			+	
Pumps	Reciprocating	0	0	0	P<10
		-0.245382	0.259016	-0.01363	10<P<100
	Positive displacement	0	0	0	P<10
		-0.245382	0.259016	-0.01363	10<P<100
Centrifugal	0	0	0	P<10	